New Jersey Institute of Technology
Digital Commons @ NJIT

Dissertations | Electronic Theses and Dissertations

Fall 1-31-2015

Inkjet printing multifunctional chromatic sensors and chromism study

Aide Wu
New Jersey Institute of Technology

Follow this and additional works at: https://digitalcommons.njit.edu/dissertations

 Part of the Materials Science and Engineering Commons

Recommended Citation

Wu, Aide, "Inkjet printing multifunctional chromatic sensors and chromism study" (2015). *Dissertations*. 112.
https://digitalcommons.njit.edu/dissertations/112

This Dissertation is brought to you for free and open access by the Electronic Theses and Dissertations at Digital Commons @ NJIT. It has been accepted for inclusion in Dissertations by an authorized administrator of Digital Commons @ NJIT. For more information, please contact digitalcommons@njit.edu.

Copyright Warning & Restrictions

The copyright law of the United States (Title 17, United States Code) governs the making of photocopies or other reproductions of copyrighted material.

Under certain conditions specified in the law, libraries and archives are authorized to furnish a photocopy or other reproduction. One of these specified conditions is that the photocopy or reproduction is not to be "used for any purpose other than private study, scholarship, or research." If a, user makes a request for, or later uses, a photocopy or reproduction for purposes in excess of "fair use" that user may be liable for copyright infringement,

This institution reserves the right to refuse to accept a copying order if, in its judgment, fulfillment of the order would involve violation of copyright law.

Please Note: The author retains the copyright while the New Jersey Institute of Technology reserves the right to distribute this thesis or dissertation

Printing note: If you do not wish to print this page, then select "Pages from: first page # to: last page #" on the print dialog screen

NJIT New Jersey's Science & Technology University

The Van Houten library has removed some of the personal information and all signatures from the approval page and biographical sketches of theses and dissertations in order to protect the identity of NJIT graduates and faculty.

ABSTRACT

INKJET PRINTING MULTIFUNCTIONAL CHROMATIC SENSORS AND CHROMISM STUDY

by
Aide Wu

The thermochromism and chemochromism of polydiacetylene (PDAs) and PDA/ZnO nano composites have been systematically studied by attentuated total reflection (ATR)-Fourier transform infrared (FTIR), temperature-dependent Raman, colorimetric (using optical densitometry) and differential scanning calorimetry (DSC). Reversibility of PDAs has been enhanced by the formation of chelation between the carboxylic groups on side chain of diacetylene and Zn ion. The thermochromatic transition temperature increases with the concentration of ZnO

Thin films of polydiacetylene (PDAs) and PDA/ZnO nanocomposites have been successfully fabricated by inkjet printing both solution type and suspension type ink. Results suggest that PDA monomers are well-aligned and closely packed following printing. By modifying the particle size of PDA monomers or the diacetylene/ZnO particle size, reversible PDA ink with wider range of ZnO concentration and longer shelf life could be obtained by using water based ink. Also, with inkjet printing technology, thin film of PDA and PDA/ZnO composites could be deposited on different substrate materials, such as paper, Kapton and Mylar film.

In order to further study alkyl side chain effect on the sensitivity of PDA, Density Function Theory (DFT) simulation is conducted, and the results show that the torsion of C-C bond is closely related to the length of the alkyl side chain.

INKJET PRINTING MULTIFUNCTIONAL CHROMATIC SENSORS AND CHROMISM STUDY

by
Aide Wu

A Dissertation
Submitted to the Faculty of
New Jersey Institute of Technology
in Partial Fulfillment of the Requirements for the Degree of
Doctor of Philosophy in Materials Science and Engineering

Interdisciplinary Program in Materials Science and Engineering

January 2015

Copyright © 2015 by Aide Wu

ALL RIGHTS RESERVED

.

APPROVAL PAGE

INKJET PRINTING MULTIFUNCTIONAL CHROMATIC SENSORS AND CHROMISM STUDY

Aide Wu

Dr. John F. Federici, Dissertation Co-Advisor Distinguished Professor of Physics, NJIT	Date
Dr. Zafar Iqbal, Dissertation Co-Advisor Research Professor of Chemistry and Environmental Science, NJIT	Date
Dr. Somenath Mitra, Committee Member Distinguished Professor of Chemistry and Environmental Science, NJIT	Date
Dr. Robert B. Barat, Committee Member Professor of Chemical Engineering, NJIT	Date
Dr. Cristiano L. Dias, Committee Member Assistant Professor of Physics, NJIT	Date

BIOGRAPHICAL SKETCH

Author: Aide Wu

Degree: Doctor of Philosophy

Date: January 2015

Undergraduate and Graduate Education:

- Doctor of Philosophy in Materials Science and Engineering,
  New Jersey Institute of Technology, Newark, NJ, 2015

- Master of Science in Materials Science and Engineering,
  Beijing General Research Institute for Nonferrous Metals, P. R. China, 2010

- Bachelor of Science in Materials Science and Engineering,
  Beijing University of Technology, Shanghai, P. R. China, 2007

Major: Materials Science and Engineering

Publications and Patents:

Wu, A.; Beck, C.; Ying, Y.; Federici, J.; Iqbal, Z. Thermochromism in Polydiacetylene–ZnO Nanocomposites. *The Journal of Physical Chemistry C* **2013**, *117*, 19593-19600.

Wu, A.; Gu, Y.; Beck, C.; Iqbal, Z.; Federici, J. F. Reversible Chromatic Sensor Fabricated by Inkjet Printing TCDA-ZnO on a Paper Substrate. *Sens. Actuators B* **2014**, *193*, 10-18.

Wu, A.; Gu, Y.; Stavrou, C.; Kazerani, H.; Federici, J. F.; Iqbal, Z. Inkjet printing colorimetric controllable and reversible poly-PCDA/ZnO composites. *Sens. Actuators B* **2014**, *203*, 320-326.

Wu, A., Gu, Y.; Tian, H.; Federici, J. F.; Iqbal, Z. Effect of Alkyl Chain Length on Chemical Sensing of Polydiacetylene and Polydiacetylene/ZnO Nanocomposites. *J. Colloid Polym. Sci.* **2014**, DOI: 10.1007/s00396-014-3365-y.

Wu, A.; Gu, Y. Study on electrochemical performance of carbon-coated LiFePO 4. *Emerg. Mater. Res.* **2013**, *2(3)*, 133-137.

Gu, Y.; Zhang, X.; Lu, S.; Zhao, T.; Jiang, D.; Yang, R.; Wu, A. LiFePO4/C via Fluoride Doping. Rare Metals **2012**, *31(6)*, 573-577.

Patents:

Wu, A; Federici, J; Iqbal, Z. "PCDA/Zinc Oxide Nanocomposites and Film Sensors", 2014

Wu, A; Federici, J; Iqbal, Z. "Polydiacetylene and Polydiacetylene/ZnO Nanocomposite Chemical Sensors", 2014

Wu, A; Gu, Y; Federici, J. "Systems and Method for Environmentally Friendly Inkjet Printing of Lithium Battery Cathode with Aqueous Binder"

自幼曾攻經史
長成亦有權謀
恰如猛虎卧荒丘
潛伏不showing忍受
不幸剌文嫂賴
那堪配在江州
他年若得報冤仇
血染潯陽江口
心在山東身在吳
飄蓬江海漫嗟吁
他時若遂凌雲志
敢笑黃巢不丈夫

This dissertation is dedicated to my parents and my wife

此論文獻給我的爸爸媽媽還有我的老婆

感謝你們這麼多年的無私傳出和支持

ACKNOWLEDGMENT

I would like to thank my dissertation co-advisors, Dr. John F. Federici and Dr. Zafar Iqbal, for their enduring support and supervision throughout my research. Also, I would like to thank Dr. Somenath Mitra, Dr. Robert B Barat and Dr. Cristiano L. Dias for their contributions to my research with their constructive suggestions.

I would like to acknowledge the US Army Armament Research, Development and Engineering Center (ARDEC) at Picatinny Arsenal, NJ for supporting this work financially through Mr. James Zunino.

Lastly, I would like to thank my parents and my wife for their infinite care and support.

TABLE OF CONTENTS

TABLE OF CONTENTS
(Continued)

TABLE OF CONTENTS
(Continued)

Chapter **Page**

TABLE OF CONTENTS
(Continued)

Chapter **Page**

LIST OF TABLES

LIST OF FIGURES

LIST OF FIGURES
(Continued)

LIST OF FIGURES
(Continued)

LIST OF FIGURES
(Continued)

LIST OF FIGURES
(Continued)

Figure **Page**

CHAPTER 1

INTRODUCTION

1.1 Motivation of Polydiacetylene (PDA) Based Chromatic Sensors Development

Chromatic sensors play a very important role in sensing. The main advantage of chromatic sensor is that they provide a visual color indication of sensing results without the need to convert the sensing results to an electronic or numeric signal for further processing[1]. Essentially, a visible color change in the sensing material, due to some external stimulus such as temperature, is readily recognized. As a chromatic sensor material, polydiacetylenes have been widely studied and used, because they can respond to different stimuli, such as mechanical stress, thermal stress, chemical stress, and so on[2-6]. However, there are two main problems with directly depositing uniform and functionalized layers of PDA aggregates during the coating process:

(a) The PDA coating has a lower density if it is directly coated onto a substrate. This is a consequence of PDA's long chain structure and lack of chain orientation.

(b) PDA is not soluble in most solvents and PDA aggregates are very hard to disperse. Those two factors cause PDA to distribute unevenly on substrates resulting in a rough coating surface.

The poor coating quality with PDA aggregates has limited the application of PDAs. The advent of topochemical methods in synthesis of PDA has not only successfully solved the aggregation problem, but also has made PDA designable for different applications[7-10]. With different pendent site groups, PDA can be formulated for different sensitivity ranges for a specific stimulus. With the help of solid state polymerization methods, nano-sized and PDA/inorganic composites have been synthesized and reported [11-16]. Methods that have been used for fabrication of thin polymer films are spin coating, self-assembly and

Langmuir-Blodgett (LB) or Langmuir–Schaefer methods. Inkjet printing method has been given more attention in polymer thin film fabrication[17-20].

1.2 Conjugated Polymers

Polymers containing alternating saturated/unsaturated bond and delocalized π- electrons through their backbones, are often referred as a conjugated polymer (CP) or conducting polymers. Conjugated polymers are very unique polymers because of their extended π-conjugated system on the backbone. The extended π-bonds contain continuous delocalized electrons which give rise to the unique optical and electronic properties. As a result, these electro-active polymers are used in a variety of applications including field-effect transistors, polymer actuators, light-emitting materials, sensors and solar cells. The practical value of conjugated polymers was recognized by Nobel Prize in chemistry in 2000. Numerous CPs have been investigated and some examples of typical CPs are represented in Figure 1.1. Conjugated polymer (CP) systems are very attractive in a sensor design because their absorption and emission properties are very sensitive to environmental perturbations[15,21-25]. CPs-based sensor systems typically compared to conventional small molecular sensors systems by their potentials for signal amplification when subjected to external stimuli[26-28]. Accordignly, a variety of conjugated polymers such as polythiophenes[29], polyanilines[30,31], poly(phenylene ethynylenes)[32,33], polyacetylenes[34], and polydiacetylenes[35], have been studied as sensor matrices.

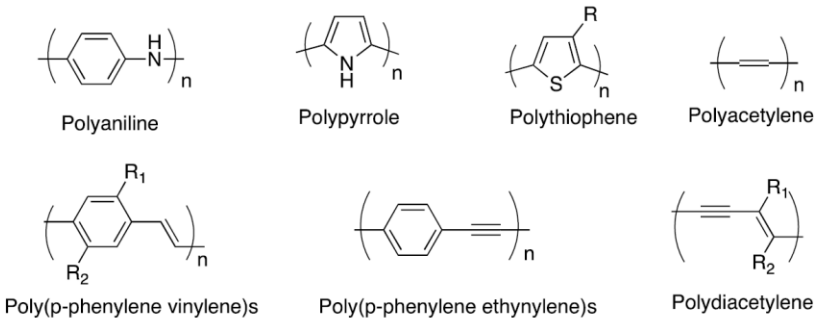

Figure 1.1 Chemical structures of various conjugated polymers.

1.3 Polydiacetylene Polymer

Since the first reports on polydiacetylene (PDA) synthesis appeared at the end of the 1960s by Wegner et al.[36,37], these molecules have captured the imagination of scientists and technologists alike due to their unique chromatic properties. Specifically, it has been shown that certain diacetylene monomers can be aligned in solutions and polymerized through ultraviolet (UV) irradiation, producing a conjugated PDA network[38,39] (Figure 1.2). The unique feature of PDA systems has been the observation that the conjugated PDA networks often absorb light in the visible spectral region, thereby exhibiting color, in most cases blue[40,41]. Moreover, conjugated PDA can undergo phase changes, induced by varied environmental stimuli, leading to dramatic colorimetric transformations that are visible to the naked eye. Another attractive feature of PDA systems in the context of sensing applications has been the fluorescence properties; blue phase PDA is non-fluorescence while the red-phase configuration exhibits high fluorescence with minimal bleaching[42-44].

Beside the intriguing chromatic properties of PDA, the diverse physical configurations of the PDA have attracted broad research interest. PDA systems have been shown to organize in vesicles[45,46], Langmuir monolayers[47-49], self-assembled films[50,51], and single crystals[52,53]. PDA has been also assembled as components within other "host"

matrixes, including inorganic matrixes[54-56], other polymers[57,58], and even living cells[59]. Remarkably, it has been shown that PDA generally retains its chromatic properties in these configurations, thus opening the way to construction of varied sensing assemblies.

Basic Molecular Properties of PDAs

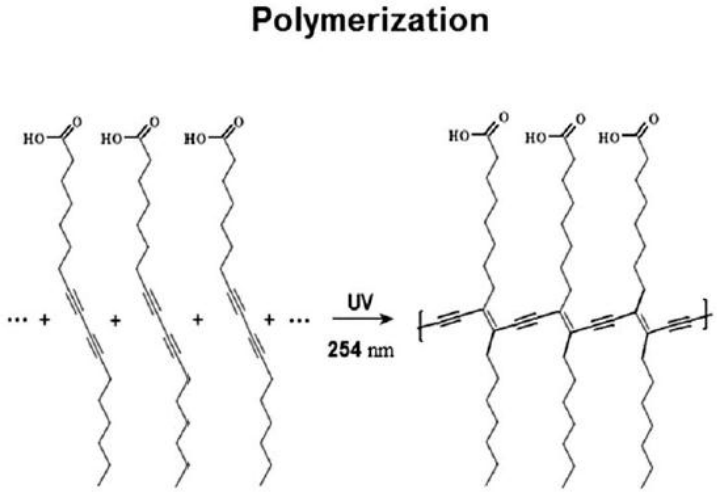

Figure 1.2 Schematic of the topological polymerization of diacetylene under UV radiation.

The unique chromatic properties of PDA systems arise from the molecular properties of the polymer. PDA is formed through 1,4 addition of aligned diacetylenic monomers, initiated by ultraviolet (UV) irradiation (Figure 1.2). The diacetylene monomers do not absorb light in the visible region, while polydiacetylene appears intense blue (absorption peak at around 650 nm) due to electron delocalization within the linear p-conjugated framework, and corresponding to a π–π* transition.

As indicated above, the colorimetric transformations of PDA, induced by a variety of external stimuli, have likely been the most interesting and technologically-attractive feature of PDA systems. The significant shift of the absorption peak from around 640 nm

(the blue phase) to around 500 nm (the red phase) is ascribed to disruption of the conjugated network, resulting in shorter electronic delocalization lengths. The red phase of PDA is accompanied by intense fluorescence, which further exhibits negligible bleaching, contributing to utilization of the fluorescence properties in varied sensing applications. Despite decades of studies, elucidating the exact mechanisms responsible for the chromatic transformations of PDA has not been fully accomplished. It has been recognized that the shifts in spectral absorbance are closely linked to structural modifications of the conjugated polymer framework[49]. Early models accounting for the spectral/structural modulations proposed transformation of the polymer backbone from the ene–yne to a butatriene conformation[60]. Recent crystallographic and theoretical investigations have illuminated intimate structural aspects pertaining to the chromatic properties. In particular, it has been established that the pendant side-chains of PDA play a prominent role in affecting the chromatic transformations. The interactions between the functional groups of the side-chains are believed to significantly affect the overall conformation of the polymer chain, primarily rotations around the C–C bonds affecting the planarity of the backbone and concomitant overlap between adjacent π orbitals [49]. Indeed, theoretical calculations suggested that even rotation of a few degrees of the side-groups around the C–C bond would give rise to a significant change of the π-orbital overlap and resultant blue-red transition[61].

The realization that PDA side-chains exhibit significant effects upon the chromatic properties of the polymer has led to intense research aiming to modulate PDA spectral response through synthetic modifications of side-chain functional groups. Efforts have been directed, for example, to alter the crystal packing of the individual monomers (the

essential precondition to photo-polymerization) and the resultant linear polymer chains (via side-chain modification). A notable consequence of the close links between crystal packing and pendant side-chain orientation is the achievement of color reversibility. While most of the early work on supramolecular PDA assemblies demonstrated irreversible color transformations, there have been an increasing number of reports depicting color-change reversibility via chemical modification of the PDA side-chains[62-64], thus altering the molecular packing and topochemical transformations within the polymer modules[65,66].

Synthetic pathway to PDAs

Early work in the field has mostly focused upon the "standard" diacetylene monomers 10,12-tricosadynoic acid and 5,7-pentacosadiynoic acid. These monomers, currently commercially available, can be aligned in aqueous solutions and the hydrogen bond network maintained among the carboxylic headgroups enable the occurrence of ene–yne transformations and formation of the polymerized conjugated backbone system [67].

Recent years have witnessed a proliferation of synthesis schemes producing novel diacetylene monomeric units. For example, peptide–diacetylene monomers in which the diacetylene backbone is flanked by peptide moieties have been reported[68]. And the PDA–peptide conjugates have been synthesized, bestowing interesting properties to the resultant materials[1,69-71]. Vesicles comprising a PDA–histidine derivative and PDA–pentalysine which further contained a fluorescent moiety, constituted vehicles for binding and detection of lipopolysaccharides (LPS) – the prominent recognition units displayed on bacterial surfaces[72]. Specifically, the organized positively-charged amino residues in the synthetically-modulated PDA vesicles mimicked the recognition surface of polymyxin-B,

a natural antibiotic which specifically binds to LPS primarily through electrostatic attraction[73].

Monomeric diacetylene units have also been derivatized with non-peptidic residues. An assembly of porous "molecular columns" enabled through the polymerization process "diacetylene macrocycle" units have been reported [74]. In essence, the polymerized diacetylene network in this case provided the "scaffolding" for the columns, rather than the means for optical/spectroscopic transformations. A systematic study has recently investigated the crystalline organizations of diacetylene monomers functionalized with different phenyl-containing units[75], revealing that despite the bulky phenyl-substituted headgroups, aromatic perfluorophenyl–phenyl interactions facilitated efficient polymerization and formation of the conjugated PDA backbone. Indeed, while diacetylene monomers can be readily manipulated via diverse synthetic routes, in many cases the resultant molecules do not undergo topotactic polymerization to the polymer phase since the structural modifications disrupt the monomer alignment essential for the ene–yne transformation[76,77].

Attaining reversibility of PDA chromatic changes has been among the most remarkable achievements in this field. In that regard, synthetic progress has often gone beyond establishing a firm understanding of the molecular mechanisms pertaining to color reversibility in PDA systems. It is generally accepted that reorganization of the hydrogen bond network through synthetic manipulations of the diacetylene headgroups is the core factor making possible reversible blue-red transformations of PDA. Accordingly, most reversible PDA systems have employed varied schemes for manipulating the polar head-groups of the polymer.

Almost all examples of reversible PDA-based systems have focused upon thermally-induced transformations, i.e. blue-red changes brought about by heating, while the reversible red blue transformation occurring following cooling. Among the diacetylene units shown to affect color reversibility following polymerization were monomers displaying 2,2,2- trifluoro-N-(4-hydroxyphenyl) acetamide[78], 3-carboxypropylpentacosa-10,12-diynamide[79], azo chromophore-functionalized diacetylene[80], secondary amine salts[81], naphthylmethylammonium carboxylate and non-polar benzyl moieties[82, 83].

Intriguing reversible thermochromism has been demonstrated in a supramolecular system in which PDA was not derivatized (i.e. the conventional 10,12-pentacosadiynoic acid has been used)[84]. In that system, temperature-induced reversible color transitions were traced to a hierarchical organization in which the PDA domains were encapsulated within a poly (vinylpyrolidone) (PVP) matrix. The intercalation of PVP domains within the PDA framework was the likely factor enabling reorientation of the PDA head groups affecting reversibility of the conjugated polymer network length (and consequent reversible chromatic transitions).

PDA-based composite materials

Composite materials comprising PDA mixed with or coupled to other molecular species have been pursued, yielding in many cases advanced materials exhibiting interesting properties. PDA–carbon nanotubes (CNTs) are a case in point[85,86]. In such systems, the surfaces of single-walled CNTs (SWCNTs) have been used as a "template" upon which organization and polymerization of the diacetylene units occurred. The resultant composite materials exhibited intriguing properties. Through interactions with the pendant side-chains of the polymer "ring-shaped" polydiacetylene structures formed upon the

SWCNT surface were capable of solubilizing and stabilizing highly hydrophobic substances, such as membrane proteins and dyes[85]. Accordingly, such PDA–SWCNT constructs might find uses as "smart detergents" in cosmetics, membrane proteins structure determination, and others. Also, it has been noticed that CNTs not only provided a physical framework upon which polymerization could be carried out, but also constituted a source of fluorescent energy[87], enable the application of this PDA composite in cellular imaging applications. A conceptually-similar PDA–nanostructure system has utilized magnetic nanoparticles (NPs) as a template for assembly of the chromatic polymer[88], the magnetic particles not only enabled the topotactic polymerization of the monomers into the extended polymer network, but also enable the blue-red transformation could be induced by a magnetic field.

Another major route in PDA technology development is conjugation of PDA with inorganic, porous materials. In general, porous materials constitute attractive targets for practical applications involving PDA. This is due to the large (internal) surface areas of porous matrixes useful for immobilization of high polymer concentration, and transparency – making possible exploiting the optical/spectroscopic properties of PDA within the inorganic framework[89]. Also, modulation of the diacetylene headgroups should not be ignored, and it has led to preparation of self-assembled species displaying remarkable structural and functional properties, realizing more PDA composite materials. By modifying the headgroup of PDA, PDA could be endowed with useful biological imaging functionalities[90].

1.4 Inkjet Printing Technology

Inkjet printing is one kind of fabrication method that enables deposition of materials into various patterns on different types of substrate and it has been widely applied to thin film fabrication. Metallic, polymer and bio materials are examples of materials that have been printed by inkjet printing methods. Because of its drop-on-demand feature, inkjet printing has evolved from text and graphic processing to its adaptation as a rapid manufacturing technique. Compared with other fabrication methods such as photolithography in fabricating micro and nano electronic devices, inkjet printing has the following advantages[91-93]:

- Non-contact and low cost method of fabrication
- Ability to deposit precise amount of materials in a rapid way
- Ability to print on specific locations which is controlled by computer
- Low temperature processing with no need for a vacuum
- Compatibility with various substrates
- Multilayer structured design

1.5 Inkjet Printing of PDA or PDA Monomers

Due to the features of inkjet printing, materials used for inkjet printing either have to be soluble or the particle size must be much smaller than the nozzle openings of the printing heads. So far, there is no report on directly inkjet printing PDAs. However, this is not surprising because the aggregate of PDAs is too big to fit through the nozzles of printing head.

PDA monomers rather than PDA aggregates are possible for inkjet printing, because with proper processing and treatment the monomer sizes will be smaller than the nozzle openings. However, inkjet printing of PDA monomers has rarely been reported. There is only a few reports on fabrication of PDA films by using inkjet printing. Yoon et al. used the inkjet printing method to print PCDA with different pendant site groups (PCDA, PCDA-AEE, and PCDA-mBzA). By adding nonionic surfactant Brij78, the polymerized PCDA-mBzA shows very good thermal response. Thermal stimulus caused color-change reversibility and can respond to electrical stimulus as well [94]. In addition, PCDA-mBzA/ Brij78 has be reported by U. Zschieschang et al. as a counterfeit-proof ink for banknotes [95].

1.6 Significance and Benefits

There are many scientific papers reported utilizing Polydiactylene (PDA) as a chromatic sensor by fabrication methods such as spin-coating, nano-assembly, and other methods, but only a few report sensor fabrication by inkjet printing. Also, only inkjet printing of PCDA based suspension has been reported. Ink-jet printing of other PDA monomers has not been reported. In addition, synthesizing PDA/ZnO composites by using inkjet printing is novel and promising.

The major benefits of proposed work are as follow:

- Chromatic sensors, by their very nature of indicating a change in a stimulus (such as temperature) through a visible color change, enable quick and visual interpretations of the sensor's state.
- The ability to ink-jet print chromatic sensor interjects a low cost method and simplicity of fabrication on multiple and potentially flexible substrates.

Because PDA can change color in response to thermal, chemical, mechanical stimulus, PDA based chromatic sensors can be used as temperature indicators, chemical

agent detectors, and/or circuit protection devices. For some specific practical applications of a PDA film sensor, it could be inkjet printed onto a decal which could then be attached to an ammunition box to indicate the temperature. It is a well-known issue with the storage of explosives that the explosives will decompose during storage at elevated temperatures. Another simple example is a PDA sensor printed on conventional paper substrate which could be used as a disposal chemical sensor in food inspections.

CHAPTER 2

THERMOCHROMISM IN POLYDIACETYLENE-ZINC OXIDE NANOCOMPOSITES

2.1 Introduction

Chromatic sensors play an important role in different types of sensing. The main advantage of a chromatic sensor is that it provides visual color indication without the need to convert to a digital signal [96]. Polydiacetylenes (PDAs), have been widely studied as a chromatic sensor material because they can respond to mechanical, temperature and chemical stimuli [2-6]. Solid state topotactic photo-polymerization of diacetylene monomers by exposure to UV or γ-radiation and subsequent thermochromism in closely packed and uniformly ordered thin films of various PDAs are well known [97] and have been widely studied for temperature-sensing applications.

PDAs have a one-dimensional conjugated backbone with a strong π to π^* absorption band in the red spectral region of the optical spectrum which gives rise to an intense blue color in the polymer. The blue phase undergoes a heat-induced thermochromic transition observed in many PDAs to a red phase. The blue to red chromatic transition is either irreversible or reversible under heating and cooling cycles depending on the chemical structure and interactions on the side chains of the PDA. In the blue phase, the strain induced by hydrogen bonding at the head groups leads to an increase in π- electron conjugation length. However, when hydrogen bonding interactions are disrupted by heat, the side group strain is released leading to twisting of the π- electron orbitals, decrease of π-electron conjugation[98] and concomitant transition to a red phase. The red phase can rapidly reverse back to the blue phase on cooling when interactions due to: (a) Strong head

aromatic groups [99], (b) Ionic moieties [100], and (c) Covalent bond [54,101], enhanced hydrogen [84,102-106] and multibonding bonding at the head groups [107-109] are present in the PDA structures. The red phase is irreversible when the head group interactions cannot be restored on cooling. These PDAs are therefore either irreversible or reversible sensors.

PDAs prepared from 10, 12-pentacosadiynoic acid (PCDA) and 10,12-docosadiynedioic acid (DCDA) have been widely investigated [110-112], but little attention has been given to the related but important monomer with a shorter hydrocarbon side chain, $CH_3(CH2)_9$-C≡C-C≡C-$(CH_2)_7CH_2COOH$ (10, 12-tricosadiynoic acid, TCDA). Previous work performed in this group (Patlolla et al [113]) on poly-PCDA-metal oxide nanocomposites provided a broad understanding of the changes in chromatic properties of the nanocomposites relative to those of pure PCDA. Here a more detailed investigation is carried out using Raman spectroscopy, DSC and colorimetry using optical densitometry as a function of temperature on poly-TCDA and poly-TCDA/ZnO nanocomposites, together with an ATR-FTIR study at ambient temperature to extract a molecular level understanding of poly-TCDA/ZnO nanocomposite formation.

2.2 Experimental Section

2.2.1 Materials

TCDA was purchased from GFS Chemicals and nanocrystalline ZnO (<100 nm diameter) was purchased from Sigma-Aldrich. Analytical grade chloroform was purchased from Sigma-Aldrich and used without further purification.

2.2.2 Synthesis of Poly-TCDA-ZnO Nanocomposites

Poly-TCDA/ZnO suspensions were prepared by suspending different amounts of ZnO (5 wt%, 10 wt%, 15 wt%) in solution of the TCDA monomer (1 mM) in chloroform. The suspension contained in a beaker was sonicated in a water bath at room temperature for 30 min and dried at 40 °C with magnetic stirring for 8 hours. The magnetic stirring was stopped after the liposome state was achieved. The pure TCDA and TCDA composites were polymerized to the blue phase of poly-TCDA and poly-PCDA-ZnO composite by irradiating with a 254 nm wavelength UV source. Powders of the blue phase composite were obtained by scraping from the beaker and grinding into a fine powder. Red phase composite powders and films were similarly produced after heating the blue phase to above the thermochromic transition temperature.

2.2.3 Raman Spectroscopy

Raman spectra at room temperature were obtained primarily using a Mesophotonics Raman spectrometer with 785 nm laser excitation. Temperature-dependent Raman measurements were carried out with an EZRaman LE Raman Analyzer system from Optronics using 785 nm laser excitation coupled to a Leica optical microscope. The spectrometer was calibrated using silicon wafer and diamond powder standards to a frequency accuracy of 1 cm^{-1}. The variable temperature optical stage used is from Linkam Scientific Instruments Ltd. Thick films for the Raman measurements were prepared by mixing suspensions of TCDA with certain amount of ZnO, using chloroform as the suspension medium. After drying and 254 nm uv-radiation, the polymerized dry powder of poly-TCDA and poly-TCDA/ZnO were measured on a silicon wafer substrate.

2.2.4 ATR-FTIR Spectroscopy

Fourier Transform Infrared (FTIR) was carried out using a Nicolet ThermoElectron FTIR 560 spectrometer with a MIRacle attenuated total reflectance (ATR) platform assembly and a Ge plate.

2.2.5 Optical Densitometry

Chromaticity, which is a quantitative measure of the vividness or dullness of a color (or how close the color is to either the gray or pure hue) was measured directly on thin film and coated samples using an X-Rite 518 optical densitometer as the samples were heated on a temperature-controlled hot plate.

2.2.6 Differential Scanning Calorimetry (DSC)

A Mettler Toledo DSC instrument (Mettle-Toledo Inc. Columbus, OH, USA) with a FP90 central processor was used to obtain the DSC data of 10 mg of precursor, polymer and composite samples wrapped in a small disk with aluminum foil using heating/cooling/heating cycles in the temperature range from 25°C to 300 °C at a rate of 10°C min^{-1}.

2.3 Results and Discussion

Attentuated Total Reflection (ATR)-Fourier Transform Infrared (FTIR) spectroscopy at room temperature in both the red and blue phases for pure poly-TCDA and for the blue phase in poly-TCDA/ZnO together with Raman spectroscopy as a function of temperature for poly-TCDA and poly-TCDA/ZnO provide details about the molecular structural changes around the chromatic transition and molecular interactions on nanocomposite

formation. The thermal and colorimetric changes as a function of temperature at these transitions are investigated further by DSC and optical densitometry, respectively.

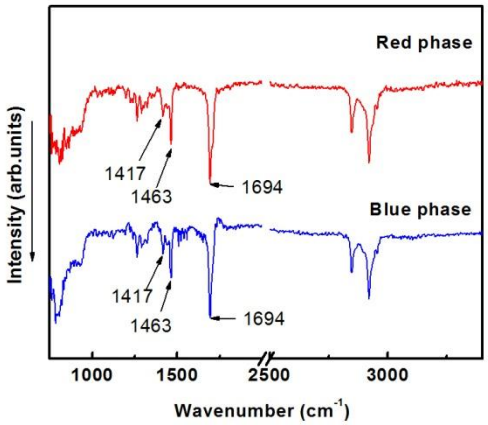

(a)

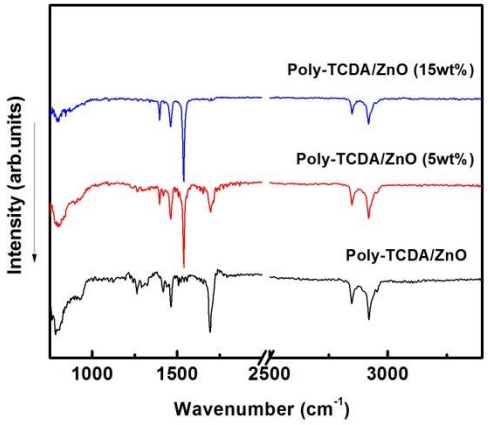

(b)

Figure 2.1 ATR-FTIR spectra at room temperature of: (a) Pure poly-TCDA in the blue and red phases; (b) Poly-TCDA and poly-TCDA/ZnO in the blue phase for two concentrations of ZnO between 700 and 3300 cm^{-1} spectral range, respectively.

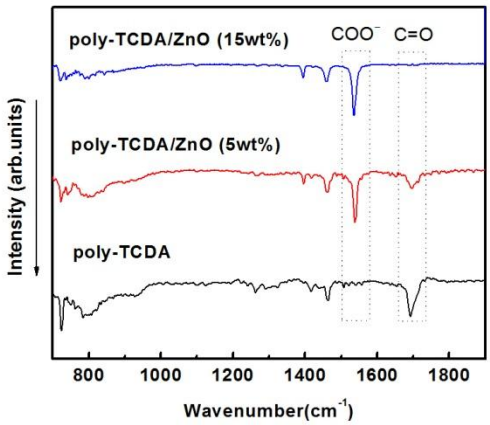

(c)

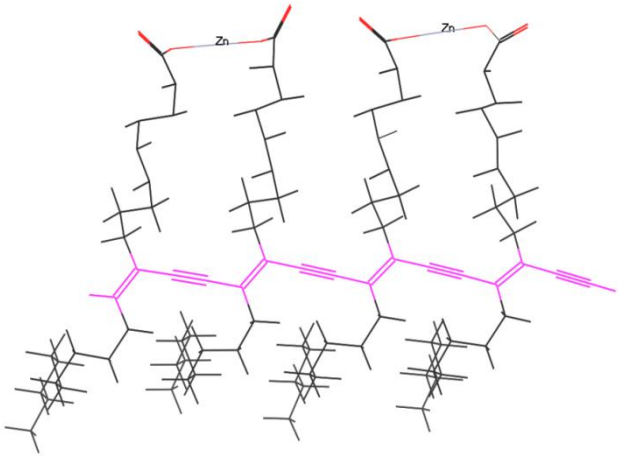

(d)

Figure 2.1 ATR-FTIR spectra at room temperature of: (c) Poly-TCDA and poly-TCDA/ZnO in the blue phase for two concentrations of ZnO expanded in the 750 and 1800 cm^{-1} spectral range, respectively; Panel (d) shows a computer-generated approximate model of the chelate proposed. (Continued)

Figure 2.1a shows the ATR-FTIR spectra of poly-TCDA in its blue and red phases, and Figures 2.1b and 1c show the spectra of poly-TCDA and poly-TCDA/ZnO in the 700 to 3500 cm^{-1} and expanded in the 700 to 1900 cm^{-1} regions, respectively. Lines at 2920 and 2847cm^{-1} are assigned to the asymmetric and symmetric stretching vibrations, respectively, of the CH_2 groups on the side chains, and those at 1463, 1417 and 1694 cm^{-1} can be attributed to the CH_2 scissoring and hydrogen-bonded carbonyl C=O stretching vibrations, respectively. On comparing the FTIR spectra of pure poly-TCDA with that of poly-TCDA/ZnO shown in Figures 2.1b and 2.1c, it is observed that a relatively strong new line appears at 1540 cm^{-1} in the spectrum of poly-TCDA/ZnO together with a concomitant decrease in intensity of the C=O stretching line at 1694 cm^{-1}. The 1540 cm^{-1} line can be assigned to an asymmetric COO^{-} stretching vibration and its presence in the spectra together with a corresponding decrease in the intensity of the C=O line suggests that a chelate between neighboring side chain -COOH head groups of poly-TCDA and Zn^{2+} ions from ZnO is formed (see computer-generated approximate model in Figure 2.1d). This chemical interaction between ZnO and poly-TCDA, dependent on the ionicity of the Zn-O bond is likely to cause the high temperature red phase to reverse back to the blue phase on cooling [114] in poly-TCDA/ZnO composites.

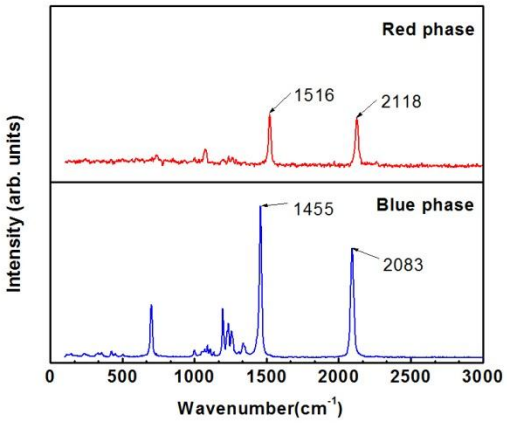

(a)

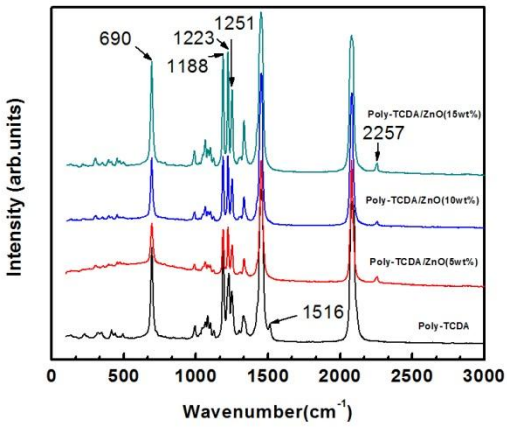

(b)

Figure 2.2 785 nm laser-excited Raman spectra of: (a) blue and red phases of poly-TCDA at room temperature; (b) blue phase of poly-TCDA and poly-TCDA/ZnO composites with three different ZnO concentrations at ambient temperature.

Raman scattering due to the molecular vibrational modes of the conjugated polymer backbone are expected to be primarily resonance-enhanced for excitation using 780 nm laser radiation. From the Raman spectra in Figure 2.2a for pure poly-TCDA, two intense lines at 2083 cm^{-1} and 1455 cm^{-1} are observed at room temperature in the blue

phase, which can be definitively assigned to the C≡C and C=C stretching modes of the polymer backbone, respectively. Note that the C=C stretching mode is close in frequency to a line at 1463 cm^{-1} assigned to a side chain CH_2 deformation mode observed in the ATR-FTIR spectra in Figure 2.1. In the red phase the room temperature C≡C and C=C stretching vibration frequencies at 2114 cm^{-1} and 1516 cm^{-1}, respectively, increase due to the irreversible stress on the polymer backbone due to dissociation of the head group hydrogen bonds in the red phase. The line intensities in the red phase are lower because of decreased resonance interaction with the polymer backbone. This decrease in resonance interaction with the polymer backbone in the red phase was not evident in the Raman spectrum of the red phase of PCDA[25] and is likely to be due to the fact that the hydrocarbon side chain is longer in PCDA. The Raman lines at frequencies below that of the C=C stretching mode can be assigned to Raman-active deformation and C-C stretching motions of the conjugated polymer backbone mixed with hydrocarbon chain deformation modes. The triplet of lines around 1250 cm^{-1} and the line at 690 cm^{-1} in the blue phase are relatively intense as a result of resonance enhancement due to mixing of the backbone C-C stretching and deformation modes.

Figure 2.2b shows the Raman spectrum of pure poly-TCDA in the blue phase compared with the blue phase spectra of poly-TCDA/ZnO composites. From Figure 2.2b, it is evident that a very weak line at 2257 cm^{-1} in the C≡C stretching mode region of poly-TCDA increases in intensity in the composite. By contrast, a relatively weak line in the C=C region at 1516 cm^{-1} in the blue phase due to a red phase impurity disappears on composite formation. The line at 2257 cm^{-1} can be assigned to a diyne defect formed on the backbone due to the chemical interaction between TCDA and ZnO [114]. However, the

intensity of this line appears to saturate at low ZnO concentration and does not increase with increasing ZnO. Another interesting feature in Figure 2.2b which is consistent with the chemical interaction of poly-TCDA with ZnO is that the line at 690 cm^{-1} and the triplet of lines at 1250 cm^{-1} assigned above to largely polymer backbone modes, show substantial increase in intensity in the composite phase.

Raman spectra under heating and cooling cycles in the 25 °C to 150 °C temperature range for poly-TCDA and poly-TCDA/ZnO at different ZnO concentrations are shown in Figures 2.3-2.5. The Raman data were taken in steps of 10°C from 30 °C to 150 °C and also recorded in 10 °C steps during the cool down to room temperature. Figure 2.3 displays the Raman spectra of poly-TCDA with increasing temperature to 150 °C followed by cooling from 140 °C to 30 °C. From the heat-up spectra in Figure 2.3a, it is can be observed that the backbone stretching and deformation lines in the blue phase decrease in intensity with increasing temperature as the sample goes to the red phase consistent with the fact that resonance-enhancement is weaker in the red phase as discussed above. The weak line at 1516 cm^{-1} assigned to a red phase impurity in the blue phase grows in intensity and becomes the predominant C=C backbone stretching mode in the red phase. From Figure 2.3b it is evident that the spectrum remains essentially unchanged on cooling consistent with the irreversibility of the red phase of poly-TCDA.

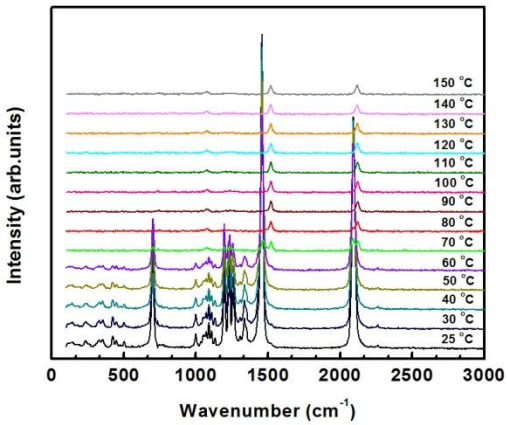

(a)

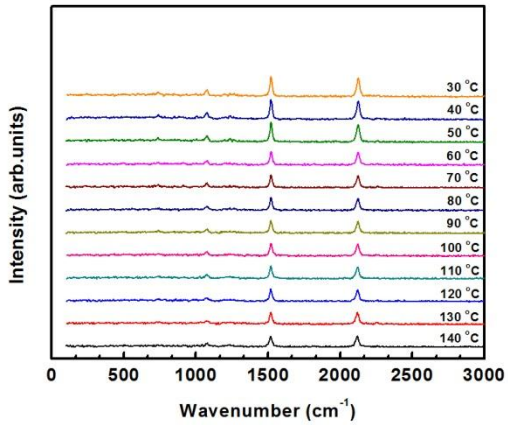

(b)

Figure 2.3 785 nm laser excited Raman spectra of pure poly-TCDA as a function of: (a) Increasing temperature, and (b) Decreasing temperature.

The heating and cooling Raman spectra of poly-TCDA/ZnO with the ZnO content at 5 wt% are shown in Figure 2.4. By contrast with the variable temperature spectra for pure poly-TCDA, in Figure 2.4a, a broad scattering band centered near 690 cm^{-1} appears reproducibly in the spectra with increasing intensity as the temperature approaches and goes above the ca. 120 °C melting transition of the ZnO composites observed in the DSC data (see discussion below and Figure 2.7). Note that the broad scattering feature appears

below the melting transition temperature and increases in intensity above 120 °C. It can be tentatively assigned to light scattering from an amorphous network of the the poly-TCDA/ZnO complex. The scattering is not seen at higher ZnO concentrations as discussed below and it is also not observed in poly-PCDA/ZnO[113] at all concentrations of ZnO probably because the diffusional motions of the longer hydrocarbon side chain in poly-PCDA compared with poly-TCDA prevents the formation of the amorphous network. The intensity from the amorphous network shows a small decrease on cooling through the melting temperature down to room temperature in Figure 2.4b. Moreover, the features of the spectra in Figure 2.4b show that the red phase of the composite with 5% by weight of ZnO converts only partially back to the blue phase on cooling.

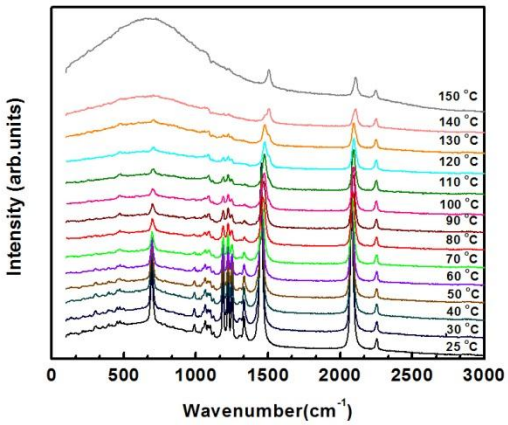

(a)

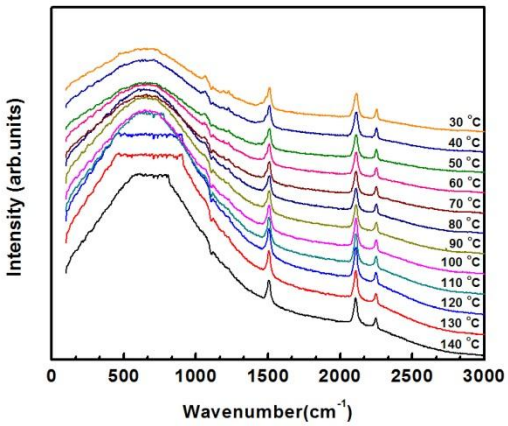

(b)

Figure 2.4 785 nm laser excited Raman spectra of poly-TCDA/ZnO (5 wt%) as a function of: (a) Increasing temperature, and (b) Decreasing temperature.

Figure 2.5 shows the heating and cooling Raman spectra of poly-TCDA/ZnO (15 wt%). Similar heating and cooling Raman spectra (not shown here) were observed for poly-TCDA/ZnO (10 wt%). Broad scattering due to amorphous poly-TCDA/ZnO at these higher ZnO concentrations are not observed (Figures 2.5a and 2.5b). Also, the red phase spectrum changes rapidly back to that of the blue phase on cooling. The Raman frequencies

of the C≡C and C=C backbone stretching vibrations of pure poly-TCDA, poly-TCDA with 5wt%, 10 wt% and15 wt % of ZnO below 100 nm in size as a function of heating and cooling cycles are plotted as a function of temperature in Figure 2.6. Note that the frequency upshift in the red phase decreases with increasing ZnO content suggesting that the stress on the polymer backbone is lowered due to chelation of ZnO with the head group of poly-TCDA to make the chromatic transition reversible. The plots in Figure 2.6 of the Raman-active C≡C and C=C backbone stretching frequencies as a function of temperature cycling indicate increases in frequencies at the chromatic blue to red transition at 70 °C on heating for pure poly-TCDA and near 120 °C for the poly-TCDA/ZnO composites. For poly-TCDA/ZnO (5 wt%), the slight upshift of frequency of the C=C and C≡C modes at 70°C could be due to non-chelated TCDA monomer. The frequency upshift at 130 °C in the composites is due to chelate formation between TCDA and ZnO.

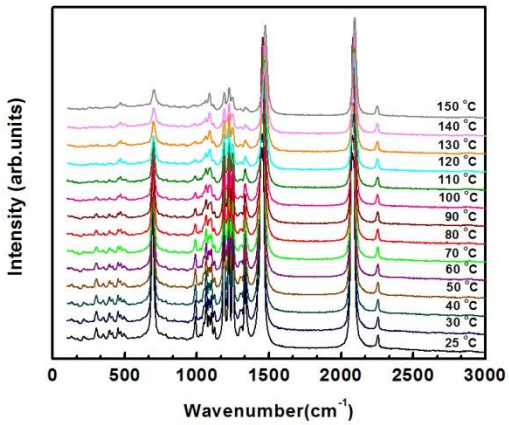

(a)

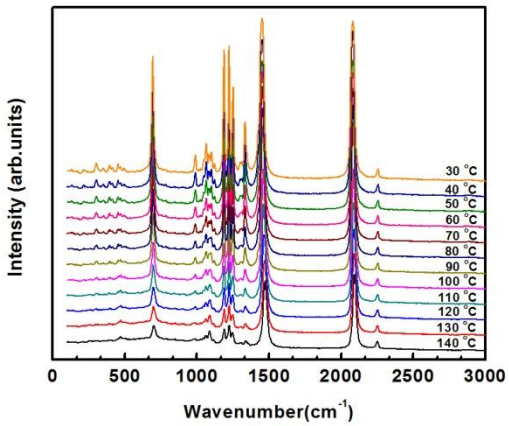

(b)

Figure 2.5 785 nm laser excited Raman spectra of poly-TCDA/ZnO (15 wt%) as a function of: (a) Increasing temperature, and (b) Decreasing temperature.

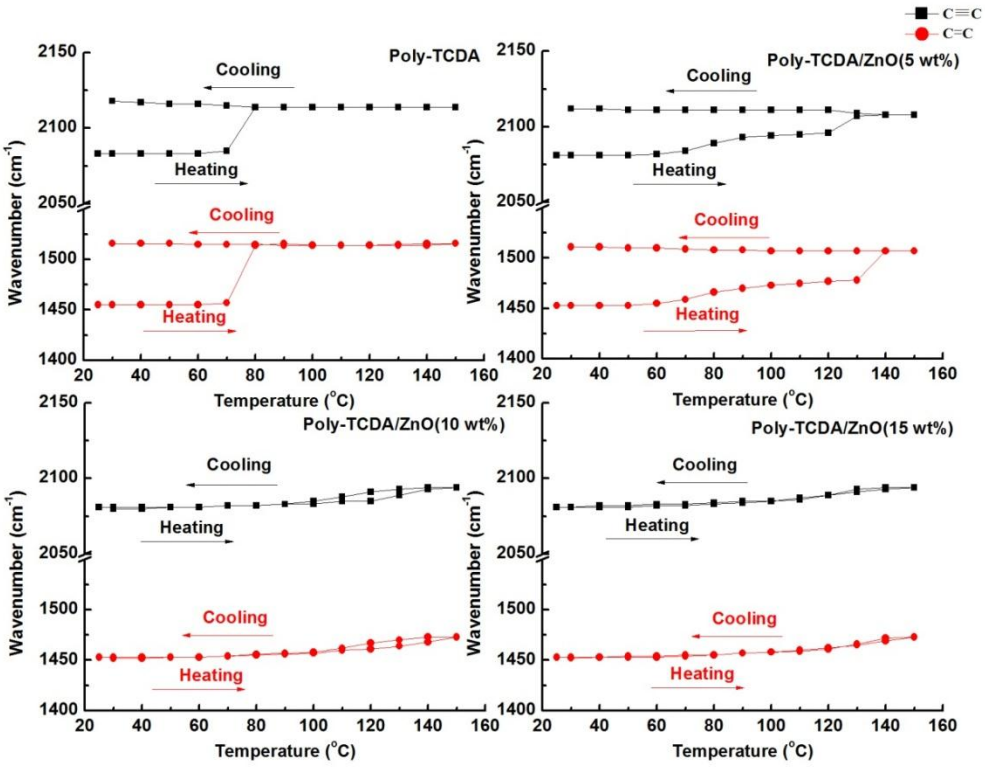

Figure 2.6 Temperature dependence on heating and cooling of the polymer backbone C≡C and C=C stretching mode frequencies of poly-TCDA and poly-TCDA/ZnO composites with different ZnO contents.

Differential scanning calorimetry (DSC) measurements provide further understanding of the nature of TCDA/ poly-TCDA/ZnO interactions. DSC data were obtained for pure TCDA monomer, poly-TCDA, and poly-TCDA/ZnO, at heating and cooling rates of 10 °C min^{-1} between 25 °C and 300 °C. The heating scan for pure TCDA in Figure 2.7a shows an endothermic peak at 61 °C due to melting. On cooling (scan not shown here) down-shifted exothermic crystallization peaks at 59 °C due to hysteresis are observed. The heating scan for poly-TCDA in Figure 2.7b shows an endothermic peak at 61 °C due to melting of the unpolymerized monomer. A broad endotherm with a shoulder at 154 °C and a peak at 190 °C are assigned to the melting of poly-TCDA. On cooling (scan

not shown), polymer crystallization is indicated by broad exothermic features at 159 °C and 194 °C which are upshifted due to hysteresis relative to the corresponding endothermic melting peaks. Crystallization of unpolymerized monomer is not observed during the cooling cycle probably due to loss of the monomer by sublimation during thermal cycling. The heating scans for TCDA-ZnO nanocomposites in Figure 2.7d show endotherm around 57 °C due to unpolymerized monomer and a new endothermic feature at around 137 °C due to melting of the monomer modified by chelate formation with ZnO discussed above, which coincides that fact that no endothermic feature of ZnO (Figure 2.7c) is observed in the DCS data of composites. It is also seen from Figure 2.7d that with the increase of ZnO content, the endotherm due to TCDA becomes weaker and the peak shifts to higher temperature indicating that the chelate between ZnO and head group –COOH becomes stronger because more chelate formation can occur with increasing ZnO content. This is consistent with the FTIR, Raman and DSC data discussed above suggesting an interaction of ZnO particles with the head group of the polymer side-chain to form a chelate which can be schematically written as: $Zn^{2+}(COO^{-})^{2}$. In pure poly-TCDA, heating causes an irreversible stress on the polymer backbone due to the dissociation of hydrogen bonds between the side chain head groups to form the red phase. In the presence of ZnO, chelate formation results in release of strain on cooling and reversal back to the blue phase.

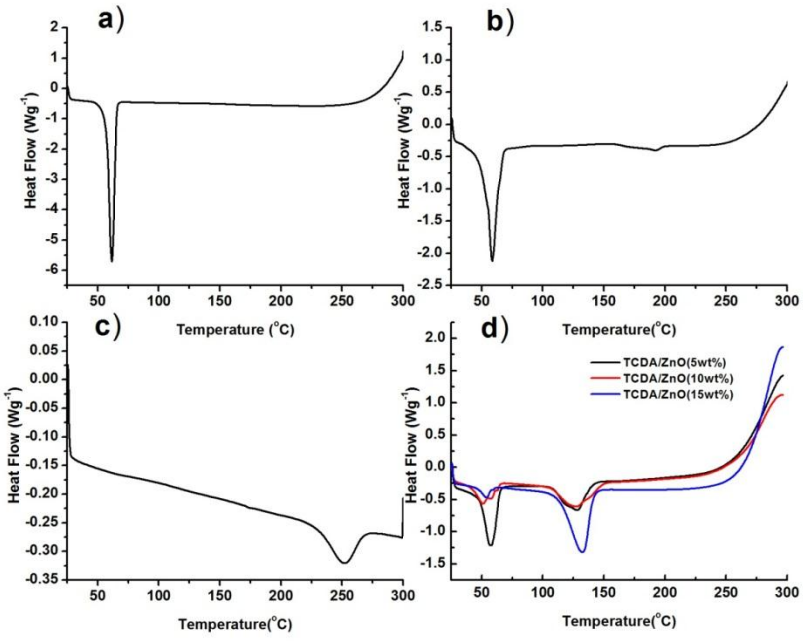

Figure 2.7 Heating DSC scans for: (a) TCDA monomer; (b) poly-TCDA; (c) ZnO nanopowder (<100 nm); (d) TCDA monomer/ZnO nanocomposites of three different compositions. The slightly broadened transition in (b) is due to unpolymerized monomer.

Chroma describes the vividness or dullness of a color, in other words, how close the color is to either gray or the pure hue (Figure 2.8a). The changes in chromaticity for different samples shown in Figure 2.8b as a function of temperature further verified the interaction between poly-TCDA and ZnO with increase of ZnO content from 5 wt% to 15 wt%. The rapid increase followed by a drop of the chromaticity of poly-TCDA is caused by the chromatic transition near 70 ℃. 5 wt% ZnO increases the chromatic transition to 120 ℃ consistent with the Raman data. The poly-TCDA/ZnO composites with 10 wt% and 15 wt% have almost the same correlation of chromaticity and temperature which indicates that there is a critical ZnO content to form the chelate between TCDA and ZnO. Figures 2.8c and 2.8d show fairly good reversibility in chromaticity as a function of number of

cycles from 25 ℃ to 80 ℃ and from 25 ℃ to 150 ℃ indicating that the nanocomposite can function as a very reproducible thermal sensor.

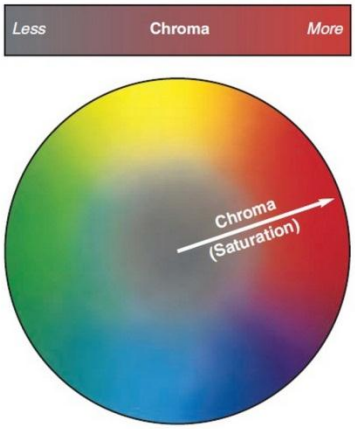

(a)

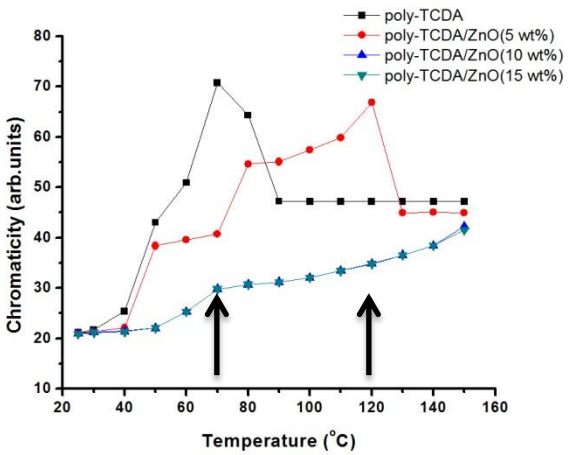

(b)

Figure 2.8 (a) Schematic showing chromaticity (chroma) distribution from gray (dull) color at the center to saturated (vivid) color at the perimeter (arrows indicate chromatic transition temperatures discussed in the text); (b) Chromaticity versus temperature plots for poly-TCDA and poly-TCDA/ZnO composites of three different compositions.

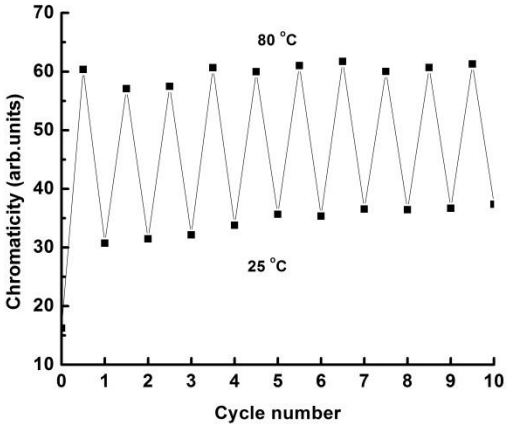

(c)

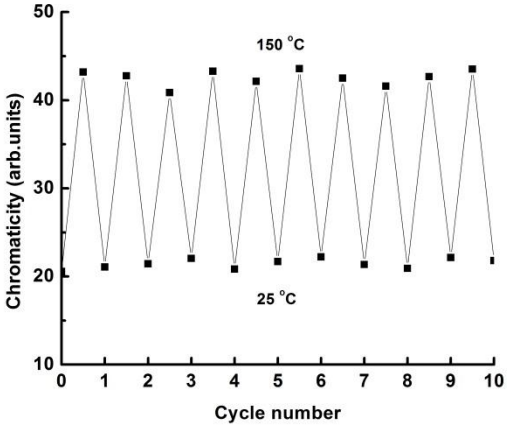

(d)

Figure 2.8 (c) Chromaticity of poly-TCDA/ZnO (5wt%) as a function of thermal cycle; **(**d) Chromaticity of poly-TCDA/ZnO (15wt%) as a function of thermal cycle. (Continued)

2.4 Conclusions

Raman, FTIR, DSC and colorimetric measurements have been used to understand the thermochromic reversibility introduced by composite formation of poly-TCDA with ZnO in the particle size range below 100 nm. Raman frequency upshifts occur at 70 ℃ and 120 ℃ in pure poly-TCDA and poly-TCDA/ZnO composites, respectively, corresponding to chromatic transitions. The peak shifts of the Raman-active υ(C≡C) and υ(C=C) vibration peaks increase with increase of ZnO content. Poly-TCDA/5 wt% ZnO shows only partially reversible color change, whereas poly-TCDA/10 wt% ZnO and poly-TCDA/15 wt% ZnO change color reversibly and have similar thermochromic responses. The Raman data indicate the irreversible formation of an amorphous poly-TCDA phase in poly-TCDA/5 wt% ZnO but not in poly-TCDA composites with 10 wt% and 15 wt% ZnO. Chelate formation between ZnO and neigboring side chain -COOH head groups is proposed which leads to reversibility of the chromatic transition and increase of the chromatic transition temperature. Compared with the results of previous study on PCDA, the amorphous feature can be found in poly-TCDA with low concentration of ZnO exclusively, which probably results from the fact that the carbon chain in TCDA is shorter than that in PCDA. Excellent reversibility in chromaticity as a function of number of cycles from 25 ℃ to 80 ℃ and from 25 ℃ to 150 ℃ is observed indicating that the poly-TCDA/ZnO nanocomposites can function as a temperature sensor.

CHAPTER 3

REVERSIBLE CHROMATIC SENSOR FABRICATED BY INKJET PRINTING TCDA-ZINC OXIDE ON A PAPER SUBSTRATE

3.1 Introduction

Recently, great attention has been drawn to printing and deposition of functional materials on paper substrates because the features of paper substrates could enable their use in flexible, light-weight and disposable devices[115,116]. Various organic and inorganic conducting, semiconducting, and dielectric materials for applications in displays, sensors, energy storage materials, and memory devices on paper substrates have been successfully prepared and widely reported[95,117-121]. Among the patterning methods employed for deposition of functional materials on paper substrates, the inkjet printing method[122] is of great interest due to the method's well-known attributes[91-93] which are mentioned before.

As far as sensing materials are concerned, polydiacetylenes (PDAs) have been widely studied as a chromatic sensor material because they can respond to a variety of signals, such as mechanical, temperature and chemical stimuli[2-6]. Solid state topotactic photo-polymerization of diacetylene monomers by exposure to UV- or γ-radiation and subsequent thermochromism in closely packed and uniformly ordered thin films of various PDAs are well known[123] and have been widely studied for temperature-sensing applications.

PDAs have a one-dimensional conjugated backbone with a strong π to π^* absorption band in the red spectral region of the optical spectrum which gives rise to an intense blue color in the polymer. The blue phase undergoes a temperature-induced or thermochromic transition observed in many PDAs to a red phase on heating. The blue to

red chromatic transition is either irreversible or reversible under heating and cooling cycles depending on the chemical structure and interactions on the side chains of the PDA.

PDAs prepared from 10, 12-pentacosadiynoic acid (PCDA) and 10, 12-docosadiynedioic acid (DCDA) have been widely investigated[110,124,125], and a PCDA-based ink has been inkjet printed by Bora Yoon et al[94]. Yoon's aqueous PCDA requires a surfactant to maintain an acceptable concentration for inkjet printing without aggregation. Belonging to the same group of PDA monomers and sharing a similar molecular structure but smaller molecular weight as PCDA, TCDA has not been given as much attention for chromatic sensor or for inkjet printing applications. Also, according to the work done by Patlolla et al[113], PCDA-metal oxide nanocomposites has shown the effect of nanoscale metal oxides on changing the chromatic properties of poly-PCDA. Inkjet printing would provide another fast method in ionic bond strengthened PDA thin film fabrication. In this paper attention is given to: (a) Inkjet printing of relatively high concentration TCDA-ZnO suspension without using surfactant on a paper substrate, and (b) The thermochromic properties of materials fabricated by inkjet printing.

3.2 Experimental Section

3.2.1 Materials

TCDA was purchased from GFS Chemicals and nanocrystalline ZnO (<100 nm diameter) was purchased from Sigma-Aldrich. Analytical grade chloroform (>99%) was purchased from Sigma-Aldrich and used without further purification.

3.2.2 Preparation of TCDA and TCDA-ZnO Composites Ink

TCDA was purified by dissolving and removing the polymerized solid. TCDA composite inks were prepared by suspending a nominal amount of 5wt% ZnO in TCDA/chloroform solution with the ratio of TCDA/chloroform equal to 0.1mol/50ml. The suspension was sonicated in a water bath at room temperature for 15 min and then allowed to stand for 1 hour to enable removal of unsuspended ZnO. It was estimated that the final suspension contained approximately 2.5 wt% ZnO in TCDA.

3.2.3 Design and Fabrication of Poly-TCDA Based Chromatic Sensor

The design and fabrication the poly-TCDA based sensor is conducted using a Fujifilm Dimatix printer model DMP-2800, which is based on piezoelectric inkjet technology. The cartridge with a nozzle pore size of ca. 20 μm in diameter was filled with a TCDA/chloroform solution or suspension of the TCDA/ZnO in chloroform and the ink was printed on unmodified A4-sized paper. Both TCDA and TCDA/ZnO were inkjet printed with 20 volts applied on nozzle pores, the nozzle cleaning was carried after every 5 bands of printing. After inkjet printing either TCDA or TCDA/ZnO composite suspensions on flexible substrates, the printed images were formed following solvent evaporation at 40 ℃. The patterns for Raman and optical densitometry measurements were in 5mm × 5 mm square shapes.

3.2.4 Synthesis of Poly-TCDA-ZnO Nanocomposites

The TCDA and TCDA/ZnO composites inkjet printed on substrates were polymerized to the blue phase of poly-PCDA composites by irradiating with a 254 nm wavelength UV source after inkjet printing. Figure 3.1 illustrates the polymerization reaction of TCDA

under UV exposure. Red phase poly-TCDA was prepared by heating up the inkjet printed pattern to the chromatic transition temperature.

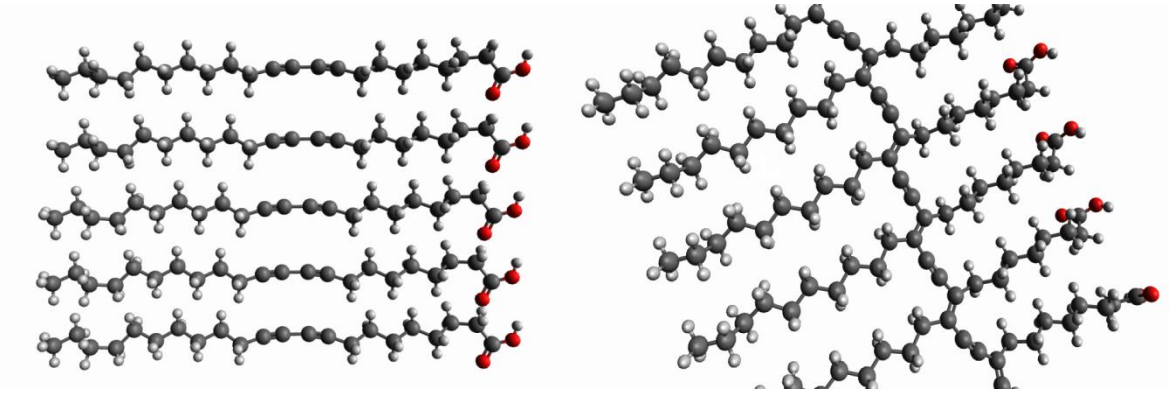

Figure 3.1 Structure of TCDA (left) and poly-TCDA after UV-irradiation (right).

3.2.5 Material Characterization Techniques

Room temperature Raman spectra of thin films fabricated by inkjet printing were obtained primarily by using a Mesophotonics Raman spectrometer with 785 nm laser excitation. Temperature-dependent Raman measurements for the inkjet printed patterns were carried out with an EZ Raman-L system (LE-178155, Enwave Optronics, Inc) coupled to a Leica optical microscope. The spectrometer was calibrated using silicon wafer and diamond powder standards to a frequency accuracy of 1 cm^{-1}. The variable temperature optical stage used is from Linkam Scientific Instruments Ltd. Thin films for the Raman measurements were prepared by 5-layer inkjet printing the suspensions of TCDA/ZnO in chloroform on a silicon wafer. After 254 nm uv-radiation, the polymerized TCDA and poly-TCDA-ZnO were measured directly.

Fourier Transform Infrared (FTIR) was carried out using a Nicolet ThermoElectron FTIR 560 spectrometer with a MIRacle attenuated total reflectance (ATR) platform

assembly and a Ge plate. Poly-TCDA powder was obtained by scratching off the inkjet printed poly-TCDA/composites on a Kapton film. The inkjet printing parameters on Kapton were the same as that for inkjet printing on paper substrates.

Chromaticity, which is a quantitative measure of the vividness or dullness of a color (or how close the color is to either the gray or pure hue) was measured directly on printed films using an X-Rite 518 optical densitometer as the film was heated on a temperature-controlled hot plate.

A Mettler Toledo DSC instrument with a FP90 central processor was used to obtain the DSC data of inkjet printed precursor, polymer and composites. Measurements were made on 10 mg powder wrapped in a small disk with aluminum foil under heating/cooling/heating cycles in the temperature range from 25 ℃ to 300 ℃ at a rate of 10 ℃ min^{-1}.

3.3 Results and Discussion

In our previous work[126], we studied the poly-TCDA and poly-TCDA/ZnO powders by using Raman, ATR-FTIR, DSC methods. The main conclusion from that work was that ZnO can form a chelate with neighboring side chain -COOH head groups of poly-TCDA, which resulted in reversible chromatic transition and increase of the chromatic transition temperature[126]. In this work, we characterize the solid phase of inkjet printed films. The major goal of the characterization of inkjet printed films is to confirm that the printing process does not change the functionality of the poly-TCDA and poly-TCDA-ZnO films.

3.3.1 Feasibility of Inkjet Printing TCDA and TCDA-ZnO Composites

Figure 3.2 demonstrates that, in actuality, the ink is not visible when it is in the monomer state because TCDA does not absorb visible light (Figure 3.2a). However, the polymerization of TCDA initiated by UV-irradiation (254 nm, 1 mW/cm 2, 30 s) results in the formation of blue image patterns (Figure 3.2b). This observation supports the proposal that PDA monomers are well-aligned and closely packed following printing and that PDAs are indeed generated on the paper substrate. This is an important result because if the closely packed alignment of the PDA monomers were disrupted during the printing and fixing steps, polymerization would not proceed.

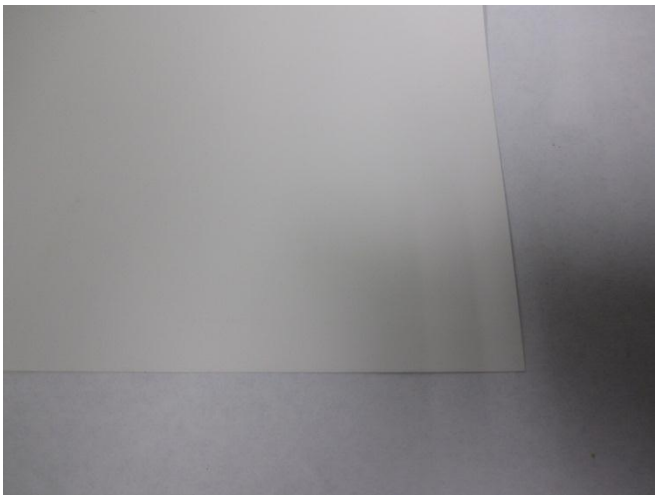

(a)

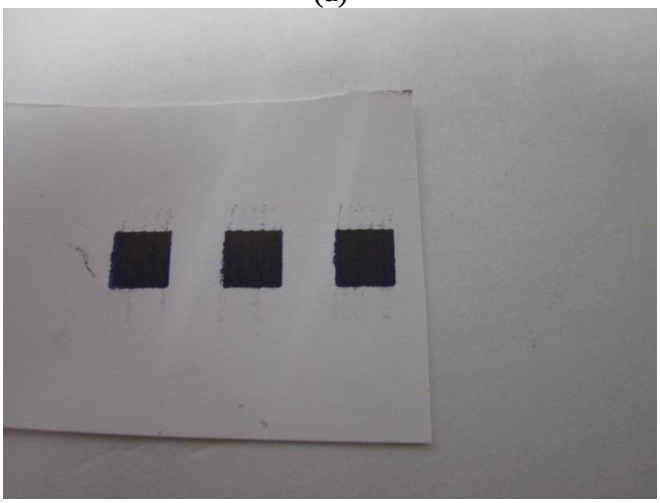

(b)

Figure 3.2 Digital photographs of inkjet printed TCDA: (a) TCDA monomer before UV radiation; (b) TCDA after UV radiation.

3.3.2 Raman and ATR-FTIR Spectroscopy of Poly-TCDA and Poly-TCDA-ZnO Composites

The molecular structural changes of the chromatic transition and molecular interactions on nanocomposite formation were studied by ATR-FTIR and Raman spectroscopy at room temperature in both the red and blue phases for pure poly-TCDA and for the blue phase in poly-TCDA-ZnO.

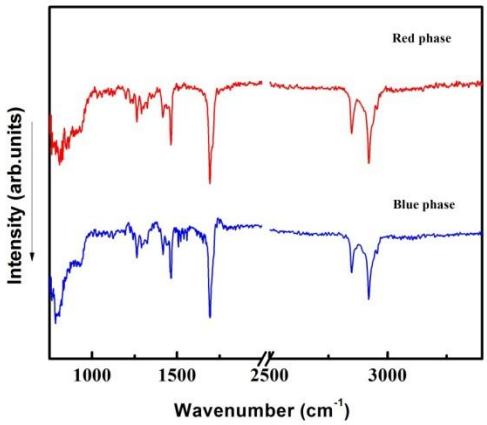

(a)

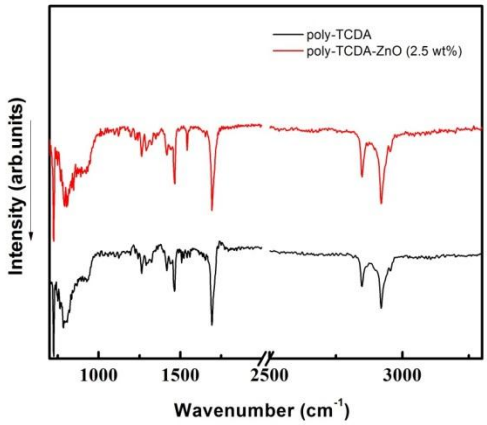

(b)

Figure 3.3 ATR-FTIR spectra at room temperature of: (a) Pure poly-TCDA in the blue and red phases; (b) Poly-TCDA and poly-TCDA-ZnO in the blue phase between 700 and 3300 cm^{-1}.

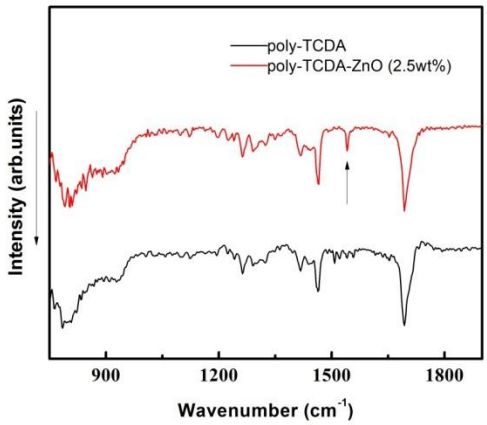

(c)

Figure 3.3 ATR-FTIR spectra of: (c) Poly-TCDA and poly-TCDA-ZnO in the blue phase expanded in the 750 and 1900 cm^{-1} spectral range. (Continued)

Figure 3.3a shows the ATR-FTIR spectra of poly-TCDA in its blue and red phases, and Figure 3.3b and 3c show the spectra of poly-TCDA and poly-TCDA-ZnO in the frequency region from 700 to 3300 cm^{-1}, and in the expanded range from 750 to 1900 cm^{-1}, respectively. As in our previous work [126], lines at 2920 and 2847cm^{-1} are assigned to the asymmetric and symmetric stretching vibrations, respectively, of the CH_2 groups of the hydrocarbon side chains on poly-TCDA, and those at 1463, 1417 and 1694 cm^{-1} can be attributed to the CH_2 scissoring and hydrogen-bonded carbonyl C=O stretching vibrations, respectively. On comparing the FTIR spectra of pure poly-TCDA with that of poly-TCDA-ZnO shown in Figure 3.3b and 3.3c, it is observed that a relatively strong line appears at 1540 cm^{-1} in the spectrum of poly-TCDA-ZnO together with a decrease in intensity of the C=O stretching line at 1694 cm^{-1}. The 1540 cm^{-1} line (indicated by an arrow in Figure 3.3c) can be assigned to an asymmetric COO^- vibration and its presence in the

spectra indicates the formation of a chelate between the side chain -COOH head groups of poly-TCDA and Zn^{2+} from ZnO, which is similar to the result reported by Patlolla et al[113].

785nm laser excited Raman spectra are obtained to probe the resonance-enhanced molecular vibrational modes of the conjugated polymer backbone. From the Raman spectra in Figure 3.4 and Table 3.1 for pure poly-TCDA, two primary lines at 2083 cm^{-1} and 1455 cm^{-1} are observed at room temperature in the blue phase, which can be clearly assigned to the C≡C and C=C stretching modes of the polymer backbone, respectively. In the red phase at 25 °C, the C≡C and C=C stretching vibration frequencies occur at 2118 cm^{-1} and 1516 cm^{-1}, respectively. Compared with those in blue phase, the upshift in frequency is due to the irreversible stress on the polymer backbone caused by the breakup of the head group hydrogen bonds in the red phase.

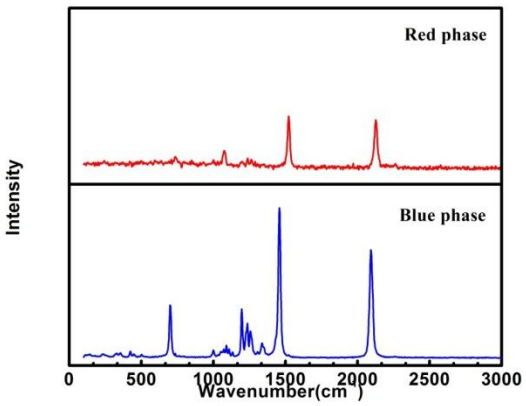

Figure 3.4 785 nm laser-excited Raman spectra of the inkjet printed blue (bottom) and red (top) phases of poly-TCDA at room temperature.

Figure 3.5 shows the Raman spectrum of pure poly-TCDA in the blue phase compared with the blue phase spectra of poly-TCDA-ZnO composites prepared by the inkjet printing method. From Figure 3.5, it is evident that a very weak line at 2257 cm^{-1} in

the C≡C stretching mode region of poly-TCDA shows up in the Raman spectra of poly-TCDA-ZnO, which can be assigned to a diyne formed as a defect on the backbone due to the interaction between TCDA and ZnO [114]. Similar to the poly-TCDA prepared by the conventional method in previous work, the line at 1516 cm^{-1} shows up in pure poly-TCDA fabricated by inkjet printing, which can be attributed to the presence of a red phase impurity in the majority blue phase. Another feature which is similar to the previous work [126] in Figure 3.5 is that the line at 690 cm^{-1} and the triplet of lines at 1250 cm^{-1} assigned above to polymer backbone modes, show substantial decrease in intensity with composite formation; meanwhile a broad diffuse scattering appears around the line at 690 cm^{-1}. These spectral effects above could be due to the increase of the degree of long-range disorder caused by the formation of a chelate between ZnO and C=O groups, and the disordered molecular arrangement reduces resonance interaction with the polymer backbone. By comparison with poly-TCDA (see Table 3.1), the Raman frequency upshift of the C≡C and C=C backbone stretching vibrations in red phase decreases in the presence of ZnO, which suggests that the backbone stress is lowered due to the interaction of ZnO with poly-TCDA.

Table 3.1 C≡C and C=C Raman Peak Frequencies in Pure Poly-TCDA and in Poly-TCDA-ZnO Nanocomposites in the Blue and Red Phases

Phase	Poly-TCDA, 25 ℃		Poly-TCDA/ZnO (2.5 wt%) [Blue,25 ℃; Red, 150 ℃]	
	υ(C≡C) cm^{-1}	υ(C=C) cm^{-1}	υ(C≡C) cm^{-1}	υ(C=C) cm^{-1}
Blue	2083	1455	2081	1453
Red	2118	1516	2108	1507

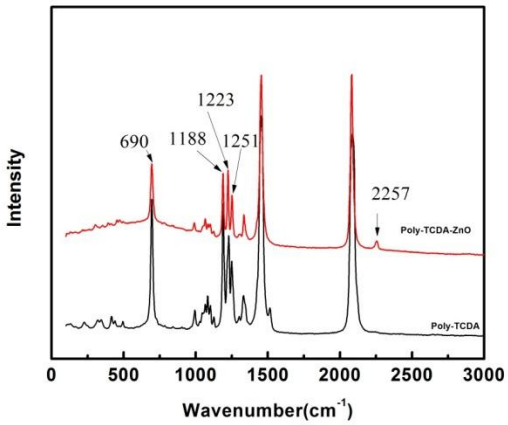

Figure 3.5 Raman spectra of pure poly-TCDA and poly-TCDA-ZnO thin film fabricated by inkjet printing.

The analysis of ATR-FTIR and Raman spectra further proves that inkjet printing does not affect the close packing alignment of the TCDA molecule and demonstrates the feasibility of polymerization after TCDA was inkjet printed on a paper substrate. Besides, ATR-FTIR and Raman spectra indicate the interaction between TCDA and ZnO. Compared with poly-TCDA and poly-TCDA-5 wt%ZnO powders prepared by the conventional method, no obvious spectral differences are observed.

3.3.3 Temperature-Dependent Raman Spectroscopy of Poly-TCDA and Poly-TCDA-ZnO Composites

Temperature-dependent Raman spectroscopy is used to further investigate the thermochromism of poly-TCDA or poly-TCDA-ZnO composites. Raman spectra under heating and cooling cycles in the 25 ℃ to 150 ℃ temperature range for poly-TCDA and poly-TCDA-ZnO are shown in Figures 3.6 and 3.7, respectively. The Raman data were taken in steps of 10 ℃ from 30 ℃ to 150 ℃ and also recorded in 10 ℃ steps during the cool down to room temperature.

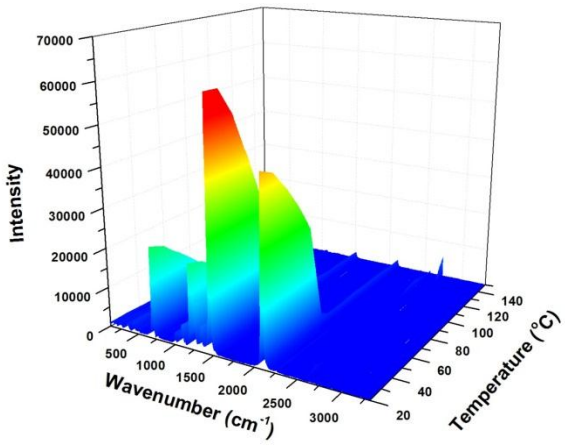

(a)

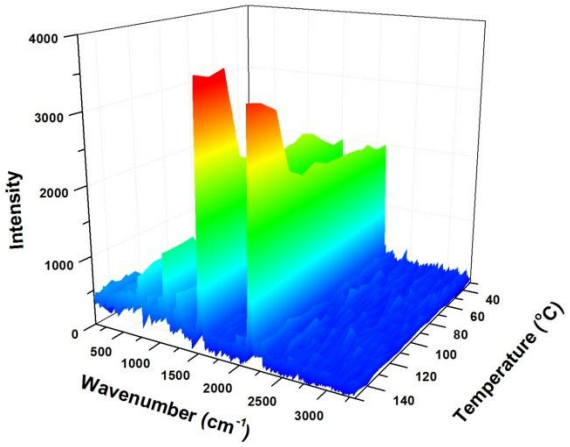

(b)

Figure 3.6 785 nm laser excited Raman spectra of pure poly-TCDA as a function of: (a) Increasing temperature, and (b) Decreasing temperature.

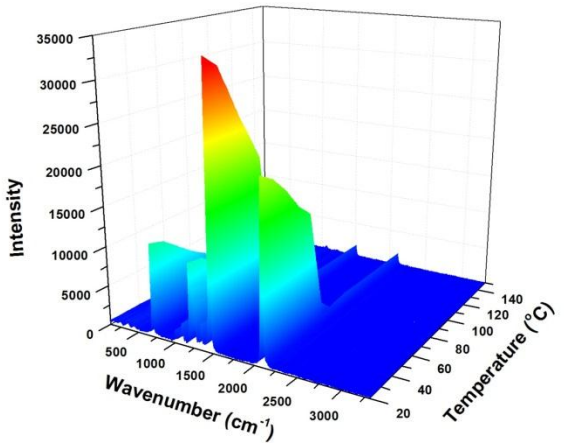

(a)

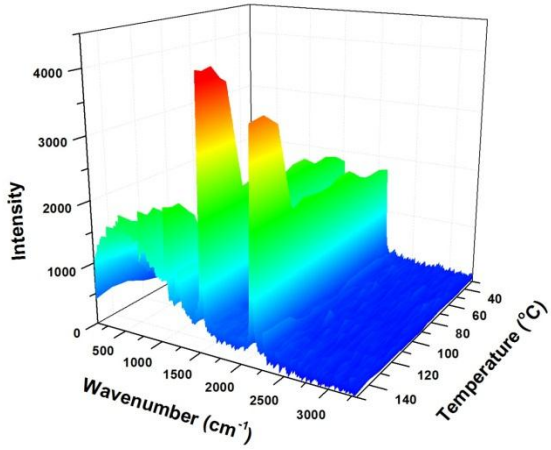

(b)

Figure 3.7 785 nm laser excited Raman spectra of poly-TCDA-ZnO (2.5 wt%) as a function of: (a) Increasing temperature, and (b) Decreasing temperature.

Figure 3.7 shows the variable temperature Raman spectra of poly-TCDA-ZnO (2.5 wt%). In contrast to the variable temperature spectra for pure poly-TCDA (Figure 3.6), a broad scattering band at 690 cm^{-1} appears in the spectra with increasing intensity as the temperature is raised to form the red phase. Together with the ATR-FTIR results, it could be due to the the C=O group of TCDA forming a COO^- ion with ZnO. The ionic bonding formed however is not strong enough to maintain the backbone structure of poly-TCDA

under thermal stress conditions. The irreversible property caused by lack of strong enough ionic bonding is supported by the fact that the variable temperature Raman spectra show the same intensity and no obvious wavenumber shifts for the C≡C and C=C modes on cooling, which is in agreement with the data for poly-TCDA-ZnO (5 wt%) reported previously[126]. The wavenumber changes for the C≡C and C=C modes as a function of temperature is shown in Figure 3.8.

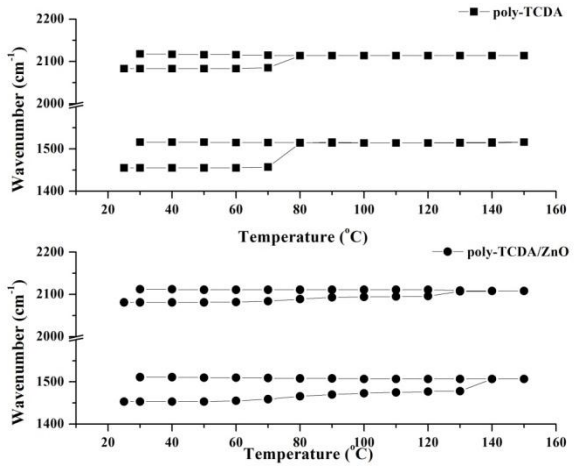

Figure 3.8 C≡C and C=C stretching mode frequencies versus temperature for inkjet printed poly-TCDA and poly-TCDA-ZnO as a function of temperature.

3.3.4 Differential Scanning Calorimetry (DSC) Measurements

DSC measurements were performed to provide further understanding of the nature of the interaction between TCDA/poly-TCDA and ZnO. DSC data were obtained for pure TCDA monomer, poly-TCDA, and poly-TCDA-ZnO, at heating and cooling rates of 10 ℃ min^{-1} between 25 ℃ and 300 ℃. The heating scan for pure TCDA in Figure 3.9a shows an endothermic peak at 61 ℃ due to melting. On cooling scan, a down-shifted exothermic crystallization peaks at 59 ℃ due to hysteresis is observed. The heating scan for poly-TCDA in Figure 3.9b shows an endothermic peak at 61 ℃ due to melting of the

unpolymerized monomer. A broad endotherm with a shoulder at 154 ℃ and a peak 190 ℃ are assigned to the melting of poly-TCDA. On cooling, polymer crystallization is indicated by broad exothermic features at 159 ℃ and 194 ℃ which are upshifted due to hysteresis relative to the corresponding endothermic melting peaks. Crystallization of unpolymerized monomer is not observed during the cooling cycle probably due to loss of the monomer by sublimation during thermal cycling. The heating scan for poly-TCDA-ZnO in Figure 3.9 shows an endotherm at around 57 ℃ due to unpolymerized monomer and a new endothermic feature at 132 ℃ due to melting of the monomer modified by the chelate formation discussed above, the broad exothermic features between 159 ℃ and 209 ℃ which could refer to that of poly-TCDA are assigned to the melting of poly-TCDA. The new endothermic peak in poly-TCDA-ZnO is consistent with the FTIR and temperature-dependent Raman spectra discussed above suggesting an interaction of ZnO particles with the head group of the polymer side-chain to form a chelate which can be schematically written as: $Zn^{2+}(COO^{-})_2$. The temperature dependent Raman and DSC results also suggest the inkjet printing does not affect the interaction between TCDA and ZnO. It was also observed that the ZnO particles are uniformly distributed after deposition on the substrates.

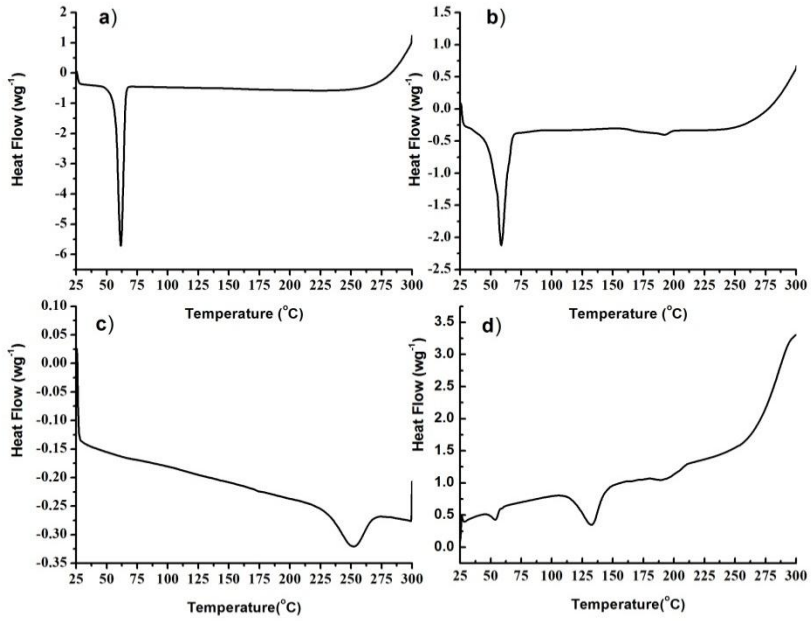

Figure 3.9 DSC heating scans for: a) TCDA, b) poly-TCDA, c) ZnO (<100nm) powder and d) poly-TCDA-ZnO.

3.3.5 Optical Densitometry

The changes in chromaticity as a function of temperature for inkjet printed poly-TCDA and poly-TCDA-ZnO (2.5 wt%) samples are shown in Figure 3.10. The rapid increase followed by a drop of the chromaticity of poly-TCDA is caused by the chromatic transition near 70 ℃. For poly-TCDA with 2.5 wt% ZnO, the chromatic transition temperature increases to 110 ℃ compared with the results of our previous work on conventionally prepared films [126] where poly-TCDA-ZnO (5 wt%) was used and the transition occurred at 120 ℃. It was also found that the chromatic behavior of the poly-TCDA film fabricated by inkjet printing is very similar to that of poly-TCDA prepared by the conventional method. The difference in transition temperature is probably caused by the smaller concentration of ZnO used to form the chelate. Because there is not enough ZnO to form the ionic bond

between Zn^{2+} and the head group of TCDA to assist in the thermal-stress release, reversible color change of poly-TCDA-ZnO could be limited at a particular temperature. According to the temperature-dependent Raman spectra and temperature-dependent chromaticity plots, 80 ℃ could be the suitable temperature for reversibility of the chromatic transition.

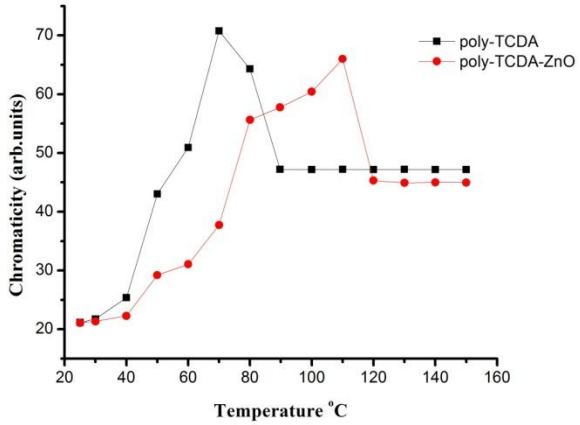

Figure 3.10 Chromaticity versus temperature plots for poly-TCDA and poly-TCDA-ZnO (2.5 wt%) composite inkjet printed films.

Differences of chromaticity of poly-TCDA in the blue phase and red phase after every 5 heating-cooling cycles are shown in Figure 3.11. It can be seen from the Figure 3.11 that poly-TCDA barely shows chromatic reversibility after the first five cycles by the naked eye, and after 20 cycles the difference of chromaticity at 80 ℃ and 25 ℃ cannot be differentiated by the optical densitometer. By contrast, poly-TCDA-ZnO demonstrates fairly good chromatic reversibility up to 40 thermal cycles.

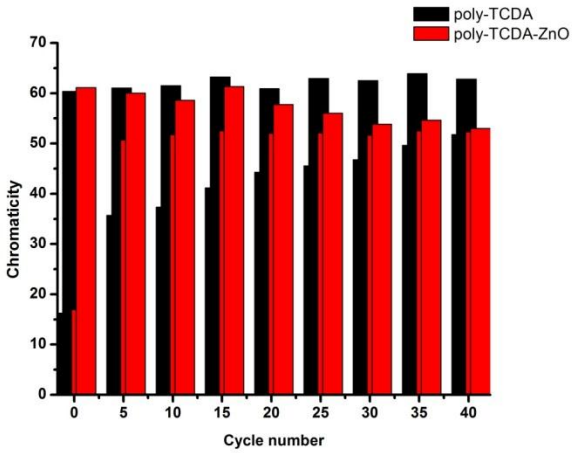

Figure 3.11 Differences in chromaticity for poly-TCDA and poly-TCDA-ZnO after every 5 heating-cooling cycles.

Figure 3.12 shows photographs of poly-TCDA/poly-TCDA-ZnO samples fabricated by inkjet printing on paper substrates which are used for the chromaticity measurement discussed above. Figures 3.12a and 3.12b, respectively illustrate the color of poly-TCDA-ZnO at room temperature and 80 ℃ (poly-TCDA is not shown). For poly-TCDA-ZnO (Figure 3.12c) at 25 ℃, after 40 cycles, a partial region in the printed sample is red (by the naked eye), which could be caused by the lack of ZnO to strengthen the poly-TCDA backbone. The red region could be responsible for the increase of chromaticity of poly-TCDA-ZnO at room temperature after a certain number of thermal cycles. Figure 3.12d shows inkjet printed poly-TCDA after five thermal cycles, where the small blue region could explain the chromaticity difference after five heating-cooling cycles in Figure 3.11.

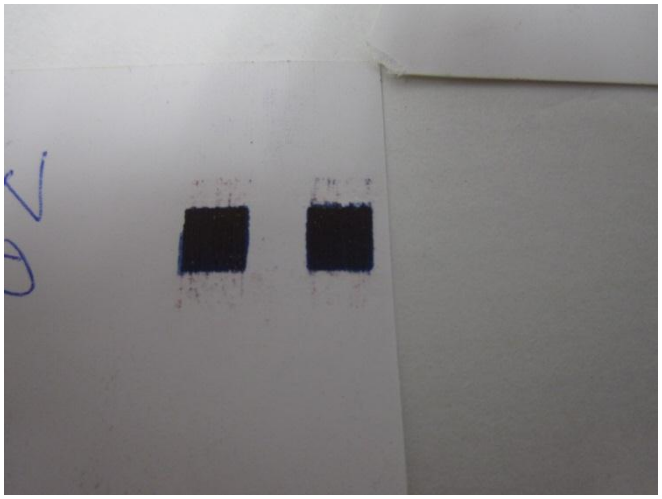

(a)

(b)

Figure 3.12 Photographs of 5mm×5mm square patterned poly-TCDA and poly-TCDA-ZnO fabricated by 5-layers inkjet printing: (a) poly-TCDA-ZnO at room temperature; (b) poly-TCDA-ZnO at 80 ℃

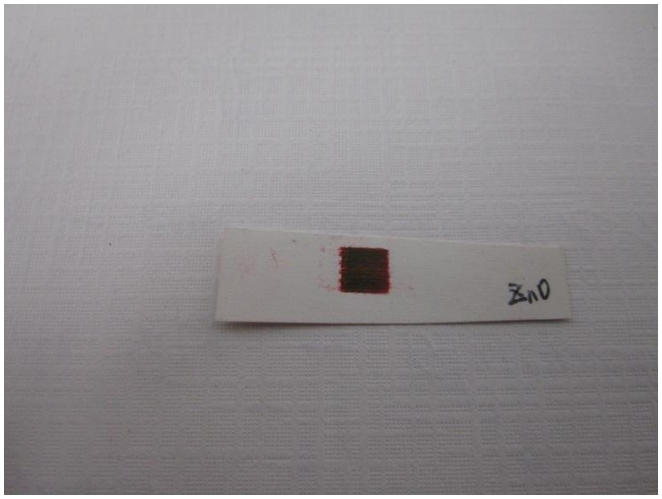

(c)

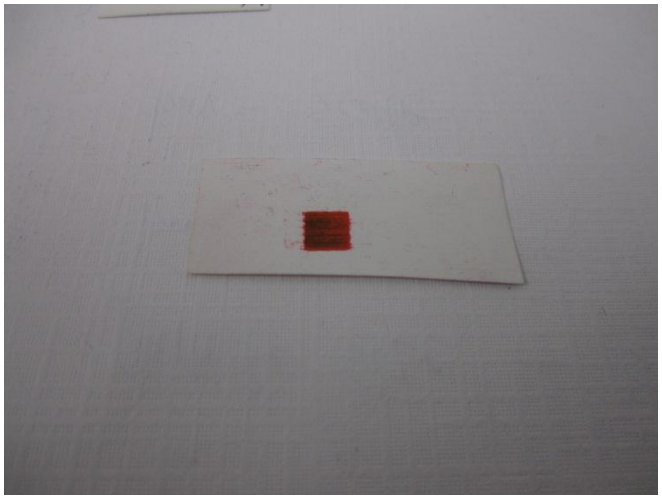

(d)

Figure 3.12 Photographs of 5mm×5mm square patterned poly-TCDA and poly-TCDA-ZnO fabricated by 5-layer inkjet printing: (c) poly-TCDA-ZnO at 25 ℃ after 40 cycles; (d) poly-TCDA at 25 ℃ after 5 cycles. (Continued)

The QR code is a type of matrix symbol, which was developed by the Japanese company Denson-Wave in 1994. Compared with a conventional bar code, a QR code has the following features [127]:

- Huge data capacity: QR code can store 7,089 numeric characters and 4,296 alphanumeric characters, and 1,817 kanji characters.

- Fast speed scanning: A mobile phone with camera function can get the content from a barcode quickly and easily.
- Small printout size: QR Codes carry data both horizontally and vertically, thus QR codes are better than 1D barcodes in data capacity.

- Advance error correcting: Even if 50% of the areas of a barcode are damaged, QR codes can still be recognized correctly.

- Freedom from directional scanning: The scanning direction of QR code is therefore arbitrary.

While QR codes have become a standard for tracking, sorting and cataloging inventory, the functionality and utility could be increased by incorporating a sensory capability within the QR code. In principle, one can print various sections of the QR code with chromatic inks to sense various stimuli, such as temperature, stress and presence of a chemical. As a simple demonstration, we fabricated a "Smart" QR code, for which a color sensitive QR code reader could not only recognize an information storage pattern but also some specific temperature. In this example, only a portion of the designed pattern would be printed out by poly-TCDA-ZnO composites or poly-TCDA as a thermal sensor. The rest of the pattern is printed out by black ink.

Figure 3.13 shows photographs of a thermal sensor type QR code, which is 1" × 1" on conventional printing paper. The QR code is capable of temperature sensing (from 25 ℃ to 80 ℃) and the chromatic transition is reversible (for poly-TCDA-ZnO composites). The irreversible color change type poly-TCDA QR code has also been successfully inkjet printed but is not shown here.

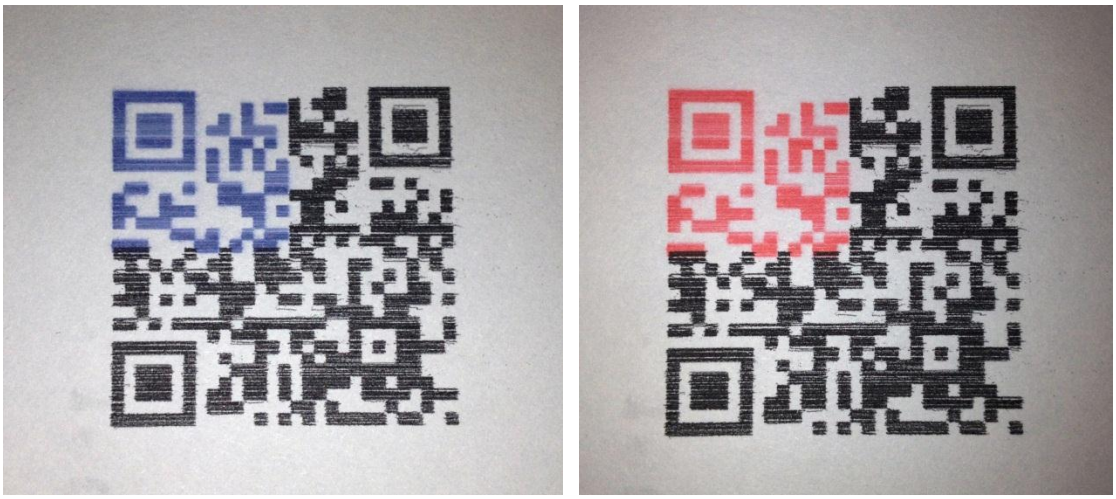

Figure 3.13 QR code with partial area of poly-TCDA/ZnO fabricated by inkjet printing methods.

3.4 Conclusions

Raman, FTIR and DSC measurements have been used to understand the thermochromic reversibility introduced by composite formation of poly-TCDA with ZnO in the size range below 100 nm. The results indicate that PDA monomers are well-aligned and closely packed following printing. For a TCDA/ZnO suspension, inkjet printing would not affect the interaction between ZnO and TCDA and the distribution of ZnO after the material is deposited on the substrate. The υ(C≡C) and υ(C=C) vibration peaks' shifting temperature increases with the addition of ZnO. From temperature-dependent Raman spectra, poly-TCDA-ZnO (2.5 wt%) does not show complete chromatic reversibility from 25 ℃ to 150 ℃; however, the chelate formed between ZnO and TCDA enables poly-TCDA-ZnO (2.5 wt%) to show a reversible chromatic transition from 25 ℃ to 80 ℃, which is not found in pure poly-TCDA. The poly-TCDA/poly-TCDA-ZnO (2.5 wt%) thin film has also been successfully fabricated by inkjet printing on conventional paper for use in a QR code as an information storage thermal sensor.

CHAPTER 4

INKJET PRINTING COLORIMETRIC CONTROLLABLE AND REVERSIBLE POLY-PCDA/ZINC OXIDE

4.1 Introduction

Polydiacetylenes (PDAs) have been widely studied as chromatic sensing materials due to their unique chromism property[128]. The dramatic blue to red color change is exhibited when PDAs are exposed to various stimuli such as temperature, chemical and mechanical stimuli, which broadens the application of PDAs as thermal sensors, chemosensors, biosensors and stress sensors[2-6]. Solid state topotactic photo-polymerization of diacetylene monomers by exposure to UV or γ-radiation and subsequent thermochromism in closely packed and uniformly ordered thin films of various PDAs are well known[97]. Previous study in this group by Patlolla et al. demonstrated the interaction between PCDA and ZnO nanoparticles, but the effect of ZnO concentration on the poly-PCDA network system was ignored[113].

Also, the application of chromatic sensor material has been limited by the material deposition technology of thin film fabrication. Among various economic material deposition methods such as spin coating, spray, stencil and screen printing, inkjet printing method[122] is of great interest, mainly due to: (a) ability to deposit precise amount of materials in a rapid way, (b) low temperature processing with no need for a vacuum, and (c) Compatibility with various substrates[91-93]. Various organic and inorganic conducting, semiconducting, and dielectric materials for applications in displays, sensors, energy storage materials, and memory devices have been successfully fabricated by inkjet printing method[95,117-121].

In this chapter, as a continuing study of previous research[113], a more detailed investigation on inkjet printing 10, 12-pentacosadiynoic acid (PCDA) and PCDA/ZnO composites was carried out using ATR-FTIR, temperature-dependent Raman spectroscopy, and colorimetry as a function of temperature on poly-PCDA and poly-PCDA/ZnO nanocomposites. By analyzing these results, we propose a new fast and convenient approach of deposition reversible PDA, of which chromatic transition properties could be varied by adjusting ZnO nano particle concentration.

4.2 Experimental Section

4.2.1 Materials

PCDA was purchased from GFS Chemicals and nanocrystalline ZnO (<100 nm diameter) was purchased from Sigma-Aldrich. Analytical grade chloroform was purchased from Sigma-Aldrich and used without further purification.

4.2.2 Preparation of PCDA and PCDA/ZnO Composites Ink

Different amounts of ZnO (5 wt%, 10 wt%, 15 wt%) are suspended in the solution of the PCDA monomer (4 mM) in chloroform. The suspension was sonicated in a water bath at 25 ℃ for 30 min and dried at 40 ℃ with magnetic stirring for 8 hours. The magnetic stirring was stopped after the chloroform evaporated. PCDA or PCDA/ZnO nanocomposites ink was prepared by probe sonicating 1mMol PCDA or PCDA/ZnO in 40ml deionized water (DI water) with certain amount (1.5 wt%) Sodium Dodecyl Sulfate (SDS) for 30 min. Constant temperature bath (25 ℃) was utilized to prevent the heat effect of the sonication.

4.2.3 Fabrication of Poly-PCDA and Poly-PCDA/ZnO Composites by Inkjet Printing

The design and fabrication the poly-PCDA based sensor was conducted using a Fujifilm Dimatix printer (Model DMP-2800), which is based on piezoelectric inkjet technology. The cartridge with a nozzle pore size of ca. 20 μm in diameter was filled with water-based PCDA or PCDA/ZnO suspension, which was printed on unmodified A4-sized paper. Both PCDA and PCDA/ZnO were inkjet printed with 25 volts applied on nozzle pores, the nozzle cleaning was carried after every 5 bands of printing and the platen temperature was 40 ℃ to evaporate the water. After inkjet printing either PCDA or PCDA/ZnO composites suspensions on flexible substrates, the printed images were formed by irradiating with a 254 nm wavelength UV source following solvent evaporation at 40 ℃. The patterns for Raman and optical densitometry measurements were in 5mm × 5 mm square shape.

4.2.4 Material Characterizations

A Mesophotonics Raman spectrometer with 785 nm laser excitation was used to collect the Raman spectra at room temperature. Temperature-dependent Raman measurements were carried out with an EZRaman LE Raman Analyzer system from Optronics using 785 nm laser excitation coupled to a Leica optical microscope. The spectrometer was calibrated using silicon wafer and diamond powder standards to a frequency accuracy of 1 cm^{-1}. The variable temperature optical stage used is from Linkam Scientific Instruments Ltd. Thin films for the Raman measurements were prepared by 5-layer inkjet printing the water-based PCDA or PCDA/ZnO suspension on a silicon wafer. After 254 nm uv-radiation, the polymerized PCDA and poly-PCDA/ZnO were measured directly.

Fourier Transform Infrared (FTIR) was carried out using a Nicolet ThermoElectron FTIR 560 spectrometer with a MIRacle attenuated total reflectance (ATR) platform

assembly and a Ge plate. Poly-PCDA/composites powder was obtained by scratching off the inkjet printed poly-PCDA/composites on a Kapton film. The inkjet printing parameters on Kapton were the same as that for inkjet printing on paper substrates

As a quantitative measure of the vividness or dullness of a color (or how close the color is to either the gray or pure hue), chromaticity of thin film and coated samples at different temperature during heating process was measured directly by an X-Rite 518 optical densitometer on a temperature-controlled hot plate.

4.3 Results and Discussion

4.3.1 Inkjet Printing of PCDA and PCDA/ZnO

The inkjet printing was conducted by using Fijifilm Dimatix (Model 2800) inkjet printer, due to the facts that the nozzles of 10-picoliter printing cartridge is ca.20 μm in diameter and the PCDA/ZnO composite inks are water based suspensions, sonication power and duration will be the primary factors that affect the feasibility of inkjet printing these materials.

For the sonication power factor, probe sonication and bath sonication methods were selected. By comparison between PCDA undergoing bath sonication and probe sonication (30 min) (Figure 4.1), it is clear that probe sonication is more preferable than bath sonication due to the high power input.

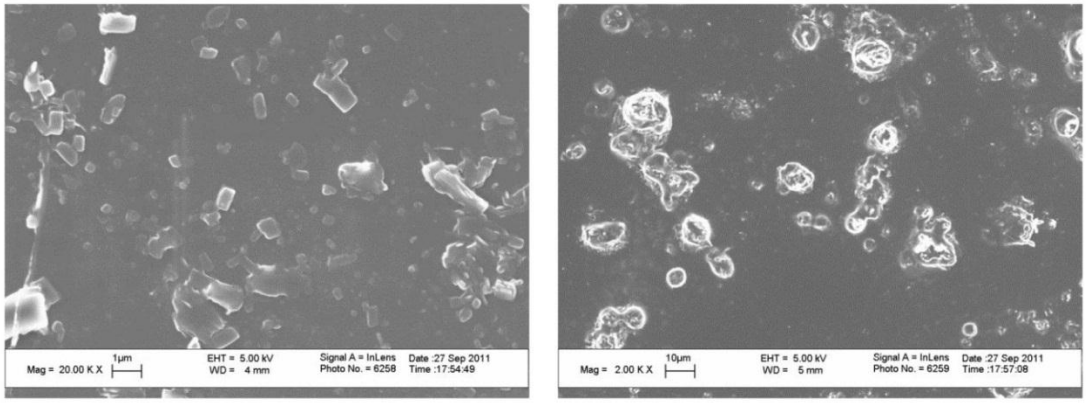

Figure 4.1 SEM images of PCDA after horn sonication (left) and bath sonication (right).

The particle size change trend of PCDA particle is shown in Figure 4.2, it can be seen that the particle size of PCDA dramatically decreases from millimeter scale to around 10 µm at the first 15 min, after that the particle size decreases slowly from ca. 10 µm to ca. 1 µm.

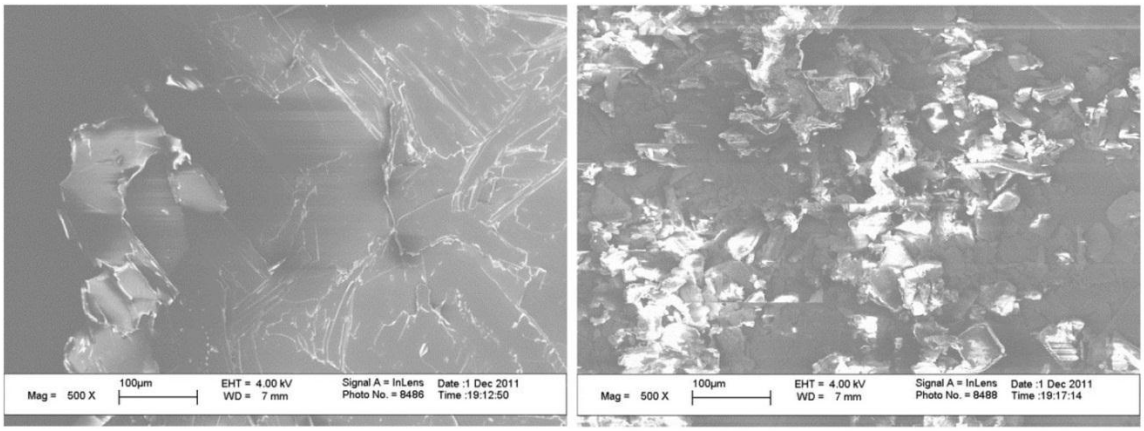

5min **10min**

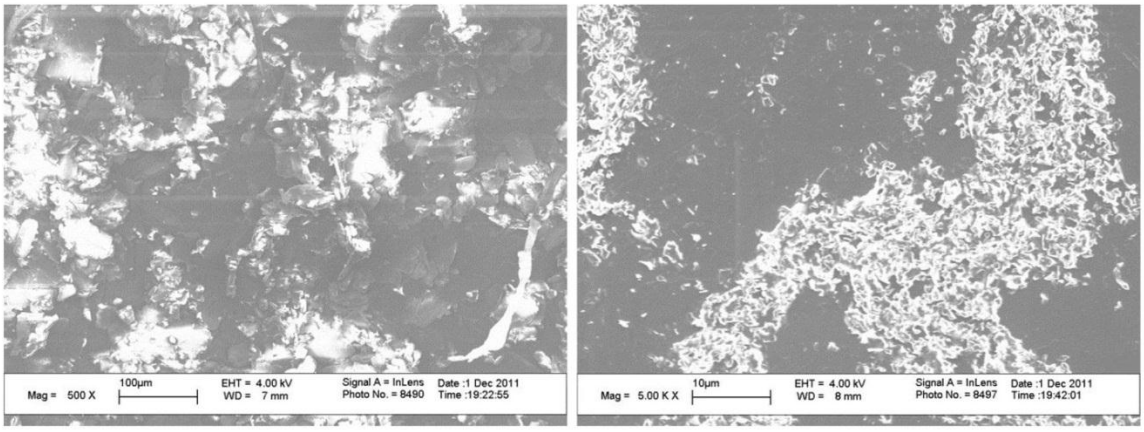

15min **20min**

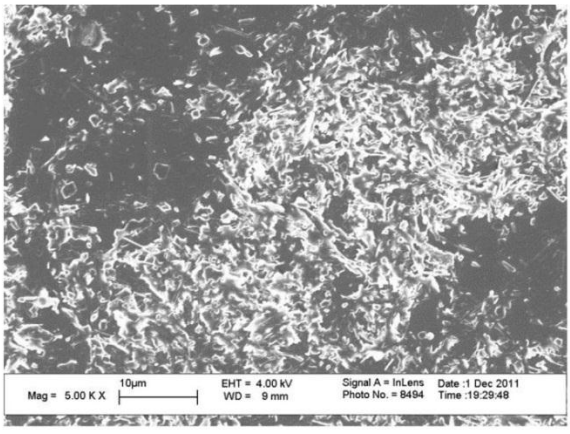

25min

Figure 4.2 SEM images of PCDA after different probe sonication durations.

Figure 4.3 demonstrates that the ink is not visible when it is in the monomer state because PCDA does not absorb visible light (Figure 4.3a), in order to increase the contrast the ink was jet printed on Kapton film (Figure 4.3b). However, the polymerization of PCDA initiated by UV-irradiation (254 nm, 1 mW/cm 2, 30 s) results in the formation of blue image patterns (Figure 4.3c). This phenomenon agrees with the result reported by Yoon et al. that PDA monomers are well-aligned and closely packed following printing and that PDAs are indeed generated on the paper substrate[94]. Also, Figures 4.3c and 4.3d demonstrate a naked-eye-detected reversible color change of poly-PCDA/ZnO.

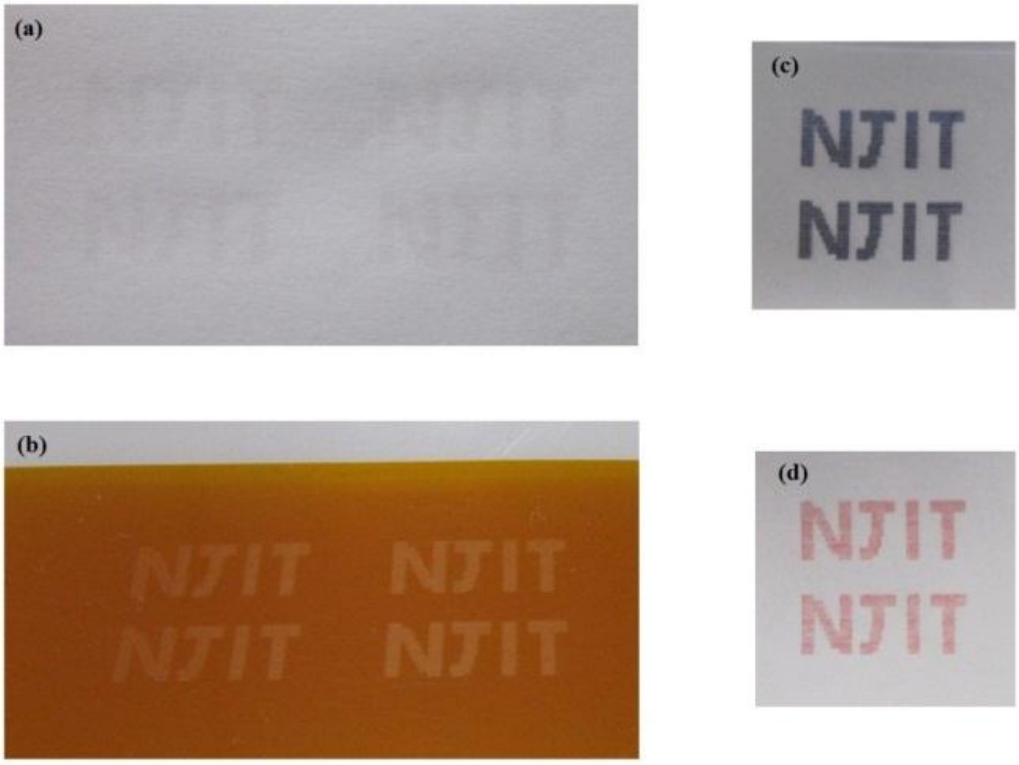

Figure 4.3 Digital photographs of: (a) Inkjet printed PCDA/ZnO composite on conventional paper substrate; (b) Inkjet printed PCDA/ZnO composite on Kapton film substrate; (c) Poly-PCDA/ZnO at 25 ℃ and (d) Poly-PCDA/ZnO at 150 ℃.

4.3.2 Thermochromism in Poly-PCDA/ZnO Composites Fabricated by Inkjet Printing

The molecular interaction upon the nanocomposite formation was studied by ATR-FTIR spectroscopy at room temperature in both the red and blue phases for poly-PCDA and in blue phase for poly-PCDA/ZnO composites fabricated by inkjet printing. The inkjet printed PCDA and PCDA/ZnO composites were investigated by Raman spectroscopy as well. Details about the molecular structural changes around the chromatic transition temperature were acquired by temperature-dependent Raman spectra of poly-PCDA and poly-PCDA/ZnO composites. The colorimetric changes as a function of temperature are investigated further by both optical densitometry and RGB measurement.

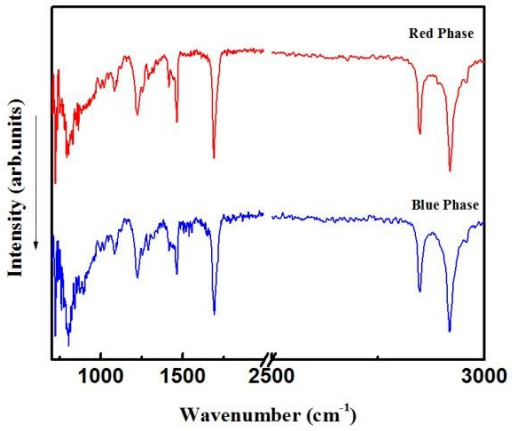

(a)

Figure 4.4 ATR-FTIR spectra at room temperature of: (a) Inkjet ptinted poly-PCDA in the blue and red phases.

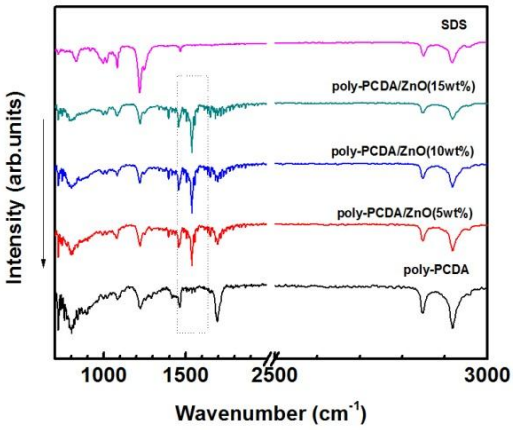

(b)

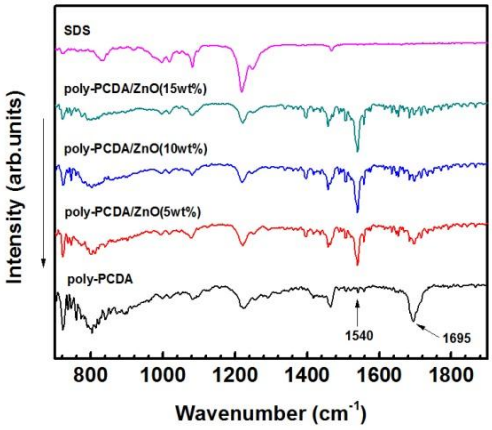

(c)

Figure 4.4 ATR-FTIR spectra at room temperature of: (b) and (c) Inkjet printed poly-PCDA and poly-PCDA/ZnO composites in the blue phase between 700 and 3000 cm^{-1} and expanded in the 700 and 1900 cm^{-1} spectral range. (Continued)

Figure 4.4a shows the ATR-FTIR spectra of inkjet printed poly-PCDA in its blue and red phases, and Figures 4.4b and 4.4c show the spectra of poly-PCDA and poly-PCDA/ZnO composites in the 700 to 3000 cm^{-1} and expanded in the 700 to 1900 cm^{-1} regions, respectively. For poly-PCDA and poly-PCDA/ZnO themselves, the asymmetric and symmetric stretching vibrations lines of the polydiacetylene side chains CH_2 groups at

ca. 2900 cm^{-1}, and the lines at 1465, 1420 and 1695 cm^{-1} are the same as those reported in the previous study[113]. Note that neither the interaction between SDS and poly-PCDA nor that between SDS and poly-PCDA/ZnO composites is observed from AFR-FTIR spectra. Compared with ATR-FTIR spectra of poly-PCDA in 4.4b and 4.4c, it is obvious that a relative strong new line shows up in the spectra of poly-PCDA/ZnO composites at 1540 cm^{-1}, meanwhile the C=O stretching line at 1695 cm^{-1} decreases in intensity with the increase the concentration of ZnO. The appearance of line at 1540 cm^{-1} well agrees with the previous work[113], which suggests the formation of a chelate between the neighboring side chain -COOH head groups of poly-PCDA and zinc ions from ZnO.

A series of 780 nm laser excited Raman spectra were obtained to investigate the resonance-enhanced molecular vibrational modes of the conjugated poly-PCDA backbone. From the Raman spectra in Figure 4.5a for inkjet printed poly-PCDA, two intense lines at 2086 cm^{-1} and 1457 cm^{-1} in the blue phase, and for the lines at 2124 cm^{-1} and 1520 cm^{-1}in the red phase are the same as previous work reported that they were assigned to C≡C and C=C stretching vibrations, respectively. It could be implied that the SDS does not affect the phase transition of poly-PCDA. By comparison, the upshift in frequency is due to the irreversible stress on the polymer backbone which could result from the dissociation of the head group hydrogen bonds in the red phase[129]. The Raman lines at frequencies below that of the C=C stretching mode can be assigned to Raman-active deformation and C-C stretching motions of the conjugated polymer backbone mixed with hydrocarbon chain deformation modes. The triplet of lines around 1250 cm^{-1} and the line at 700 cm^{-1} in the blue phase are relatively intense which is due to resonance enhancement caused by the mixing of the backbone C-C stretching and deformation modes.

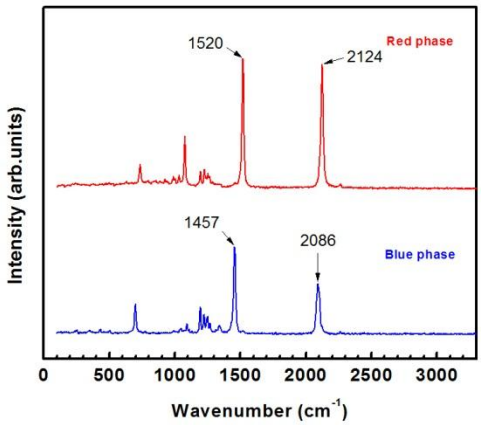

(a)

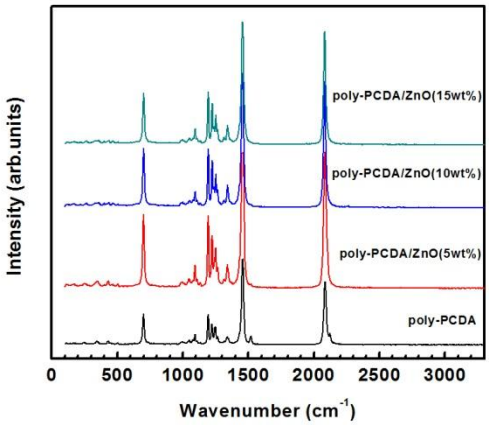

(b)

Figure 4.5 785 nm laser-excited Raman spectra of: (a) Blue (bottom) and red (top) phases of poly-PCDA at room temperature; (b) Blue phase of poly-PCDA and poly-PCDA/ZnO composites with three different ZnO concentrations at ambient temperature.

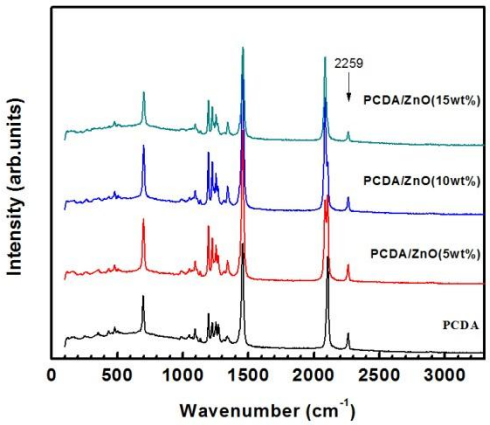

(c)

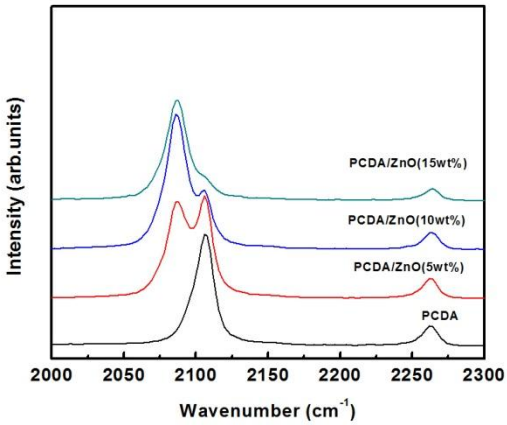

(d)

Figure 4.5 785 nm laser-excited Raman spectra of: (c) PCDA and PCDA/ZnO with three different ZnO concentrations; (d) Raman spectra expanded in 2000 and 2300 cm^{-1} spectral range. (Continued)

Figure 4.5b shows the Raman spectrum of the inkjet printed poly-PCDA in the blue phase compared with the blue phase spectra of poly-PCDA/ZnO composites fabricated by inkjet printing. No peak in the C≡C stretching mode region of poly-PCDA could not be found in both the spectrum of poly-PCDA and that of poly-PCDA/ZnO composites, which indicates no unconverted PCDA or formation of diyne exists in the polymer/polymer

composites[114]. By contrast, a relatively weak line in the C=C region at 1520 cm^{-1} in the blue phase due to a red phase impurity disappears on composite formation. In comparison with poly-PCDA, another interesting feature which is consistent with the chemical interaction of poly-PCDA with ZnO is that the line at 690 cm^{-1} and the triplet of lines at 1250 cm^{-1} assigned above to largely polymer backbone modes increases substantially in the composite phases. Together with ATR-FTIR results, it is clear that the SDS would not affect the functional group of poly-PCDA, and the chelation between ZnO and poly-PCDA.

Since no vibration intensity variation of COO^- and COOH for different ZnO concentrations was reported in work done by Patlolla[113], and the concentration of ZnO could affect the chromatic property of poly-PCDA, further investigation was carried out the study the effect of ZnO concentration on PCDA system. The obtained Raman spectra of inkjet printed PCDA and PCDA/ZnO composites are shown in Figure 4.5c. The line at 2259 cm^{-1} appearing in PCDA and PCDA/ZnO composites could be assign to the acetylene of PCDA, the line at 1457cm^{-1} and 2107cm^{-1} in PCDA could be due to the C=C and C≡C stretching modes, respectively, which are caused by the polymerized PCDA. The frequency discrepancies between polymerized PCDA in PCDA and poly-PCDA could be due to the low polymerization degree of PCDA which gives weaker conjugation effect. With the adding of ZnO, a new line shows up at 2086cm^{-1}. From Figure 4.5d, it can be observed that in the PCDA sample with 5wt% ZnO the line at 2086 cm^{-1} almost bears the same intensity of the one at 2107cm^{-1}, then it increases in intensity with the increase of ZnO concentration. By comparing with the Raman spectra of poly-PCDA and poly-PCDA/ZnO composites, the line at 2086cm^{-1} could be caused by the C≡C stretching

modes of poly-PCDA blue phase, and the one at 2107cm^{-1} could be assign to the stretching modes C≡C of poly-PCDA red phase. Based on the ATR-FTIR results, chelates formed between ZnO and PCDA. The interaction of carbonyl head group of PCDA with Zn ion of ZnO in acid environment could enhance the formation of the blue phase poly-PCDA, meanwhile inhibiting the formation of red phase poly-PCDA.

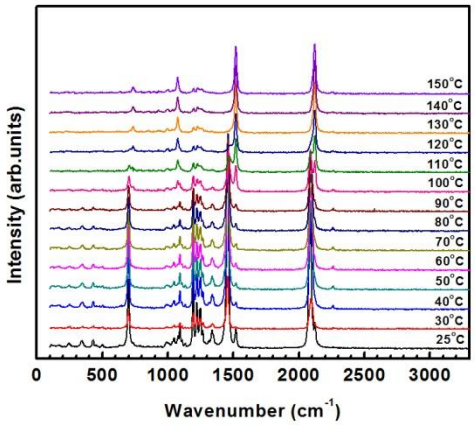

(a)

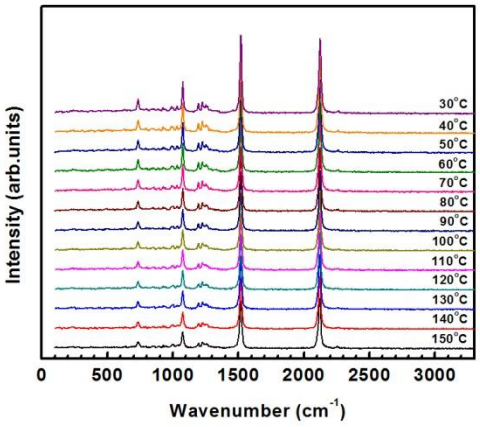

(b)

Figure 4.6 785 nm laser excited Raman spectra of pure poly-PCDA as a function of: (a) Increasing temperature, and (b) Decreasing temperature.

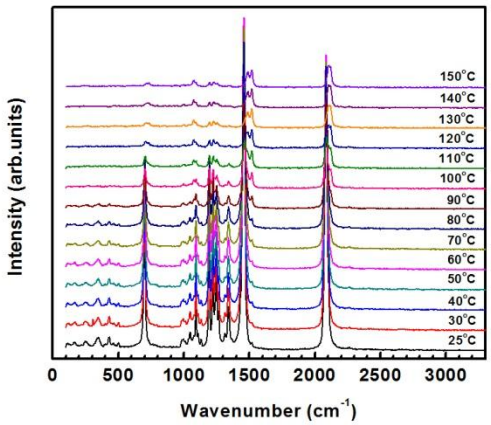

(a)

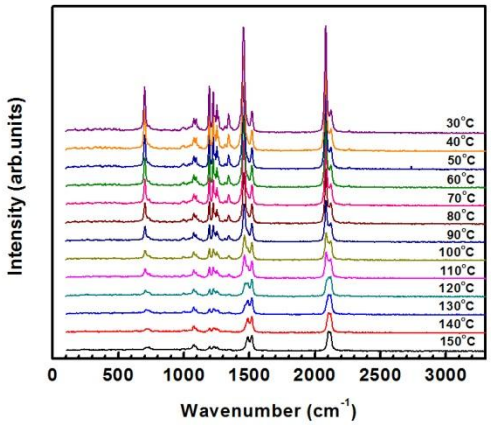

(b)

Figure 4.7 785 nm laser excited Raman spectra of pure poly-PCDA/ZnO (5 wt%) as a function of: (a) Increasing temperature, and (b) Decreasing temperature.

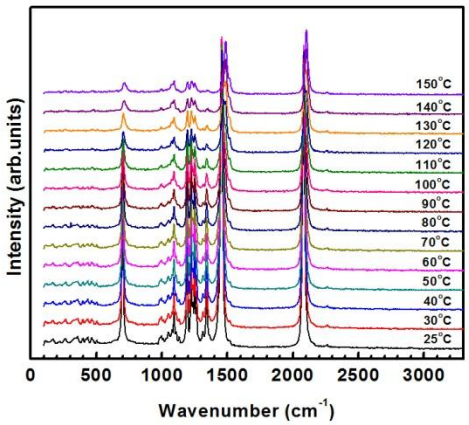

(a)

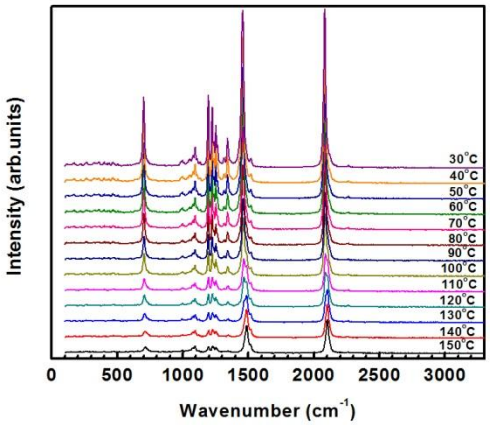

(b)

Figure 4.8 785 nm laser excited Raman spectra of pure poly-PCDA/ZnO (10 wt%) as a function of: (a) Increasing temperature, and (b) Decreasing temperature.

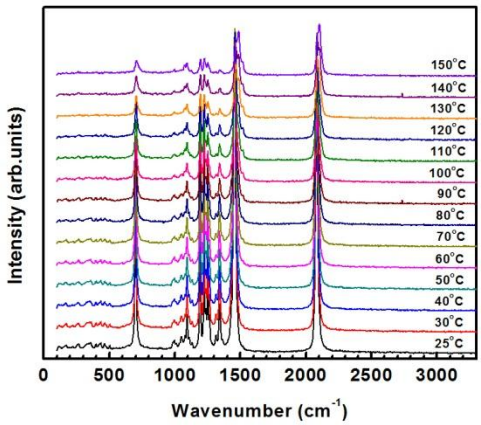

(a)

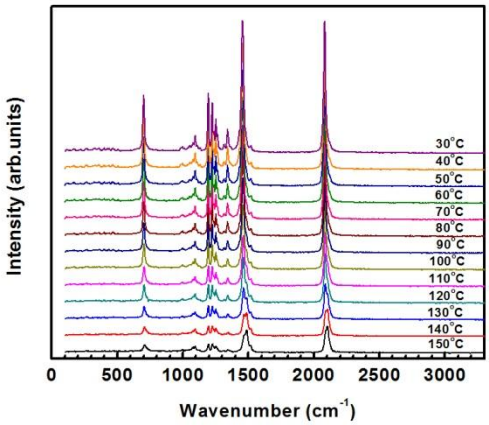

(b)

Figure 4.9 785 nm laser excited Raman spectra of pure poly-PCDA/ZnO (15 wt%) as a function of: (a) Increasing temperature, and (b) Decreasing temperature.

The effect of ZnO on the poly-PCDA is further investigated by temperature-dependent Raman spectra for poly-PCDA and poly-PCDA/ZnO composites, the spectra of which are shown in supplementary materials (Figure 4.6-4.9). The test temperature range is from 25 ℃ to 150 ℃ in increments of 10 ℃. After reaching 150 ℃, data was collected for the cool down process at the same temperature values as the heating

process. Since C≡C and C=C vibrations are the two major characteristic peaks to study the chromatic properties of PDA, the frequencies of stretching vibration for C≡C and C=C of poly-PCDA and poly-PCDA/ZnO composites as a function of temperature cycling are plotted in Figure 4.10. Note that the frequency upshift in the red phase decreases with increasing ZnO concentration suggesting that the stress on the polymer backbone is lowered due to chelation of ZnO with the head group of poly-PCDA to make the chromatic transition reversible. The plots in Figure 4.10 indicate increases in frequencies at the chromatic blue to red transition at 100 ℃ on heating for pure poly-PCDA and around 120 ℃, 130 ℃ and 140 ℃, respectively, for poly-PCDA/ZnO composites with different ZnO concentrations. And on cooling process, the decreases in frequencies occur at 110 ℃, 120 ℃, 130 ℃ for each corresponding poly-PCDA/ZnO composite material, which corresponds to the intensity increase of COO^- suggested by ATR-FTIR spectra. Together with C≡C and C=C wavenumber as a function of ZnO concentration in both blue and red phase (Figure 4.11), it can be inferred that with the increase of ZnO concentration, the amount of chelation would be saturated once it reach certain point.

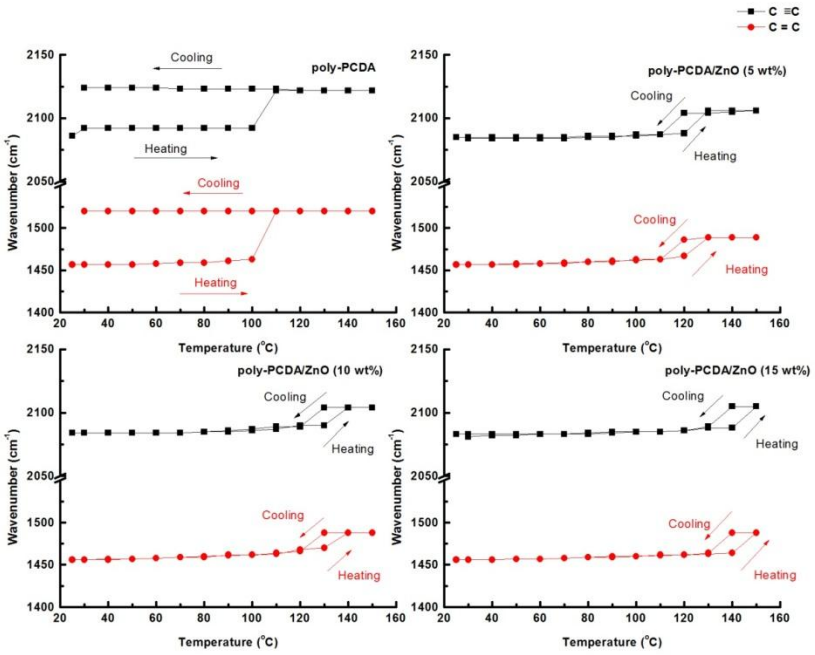

Figure 4.10 The polymer backbone C≡C and C=C stretching mode frequencies of poly-PCDA and poly-PCDA/ZnO composites with different ZnO content on heating and cooling.

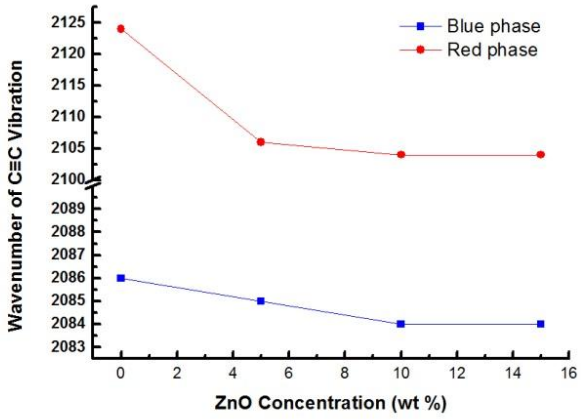

(a)

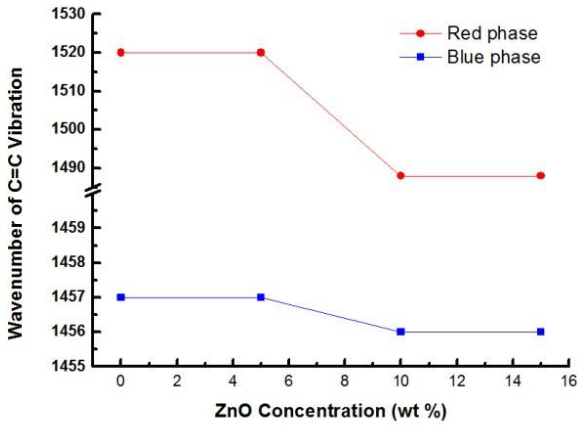

(b)

Figure 4.11 Wavenumber specific vibration peaks as a function of ZnO concentration (in blue phase and red phase of poly-PCDA/ZnO): (a) C≡C stretching mode; (b) C=C stretching mode.

4.3.3 Colorimetric Measurements

The colorimetric performance of poly-PCDA and poly-PCDA/ZnO composites were investigated from two aspects: (a) chromaticity as function of temperature, (b) the Red, Green and Blue (RGB) values of different inkjet printed indicators (5 layers inkjet printing, 5mm ×5mm square).

Chroma describes the dullness or vividness of a color, in other words, how close the color is to either gray or the pure hue. The changes in chromaticity as a function of temperature for poly-PCDA and poly-PCDA/ZnO composites are shown in Figure 4.12a. The rapid increase followed by a drop of the chromaticity of poly-PCDA is caused by the chromatic transition near 100 ℃. 5 wt% ZnO increases the chromatic transition to 120 ℃ consistent with the Raman data. The poly-PCDA/ZnO composites with 10 wt% and 15 wt% have almost the same correlation of chromaticity and temperature which indicates that most of the side chain head groups form chelate between PCDA and ZnO, the amount of chelate is reaching the maximum. Figure 4.12b shows fairly good reversibility in chromaticity as a function of number of cycles from 25 ℃ to 150 ℃ indicating that the nanocomposite can function as a very reproducible thermal sensor.

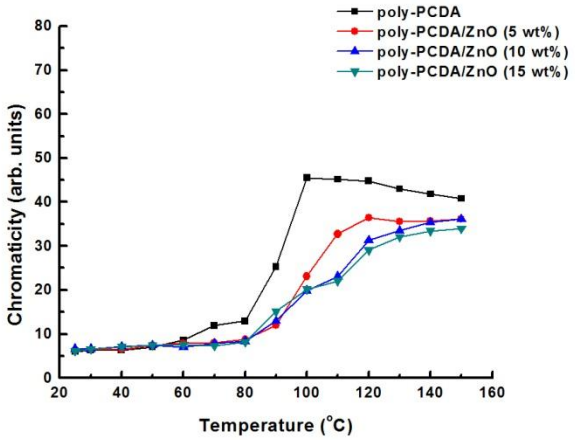

(a)

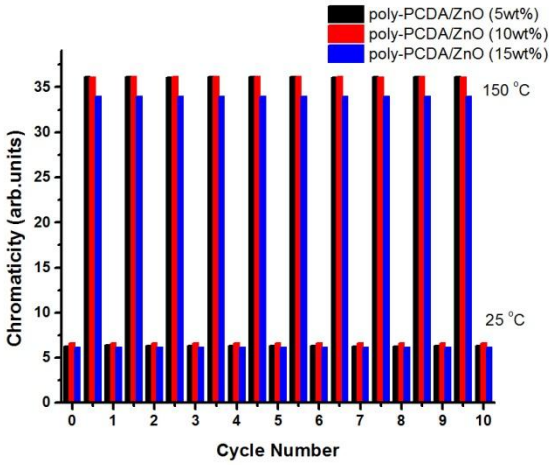

(b)

Figure 4.12 (a) Chromaticity versus temperature plots for poly-PCDA and poly-PCDA/ZnO composites of three different compositions; (b) Chromaticity of poly-PCDA/ZnO composites as a function of thermal cycle.

The photographic images of PCDA or PCDA/ZnO at specific temperature show vividly the color variation with the increase of ZnO concentration (Figure 4.13a). The color images of PCDA on conventional paper were quantitatively analyzed by photography processing software to obtain the RGB values, the histogram of RGB values shows a distinguishable color change with the increase of ZnO concentration (Figure 4.13b), which

justifies that the amount of strengthened blue phase poly-PCDA could affect the color of poly-PCDA. With the increase of ZnO concentration from 0~10 wt% the red value decreases, meanwhile blue value increases, this phenomena becomes more obvious at higher temperature. For the sample with 15 wt% ZnO, for the reason that the color is between red and black (by naked eye), so RGB values maintain at the same level.

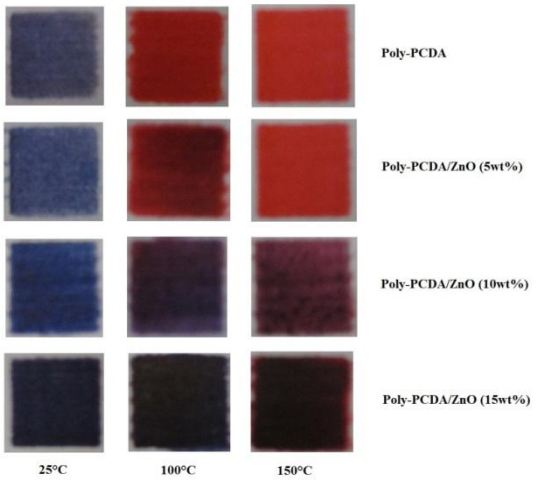

(a)

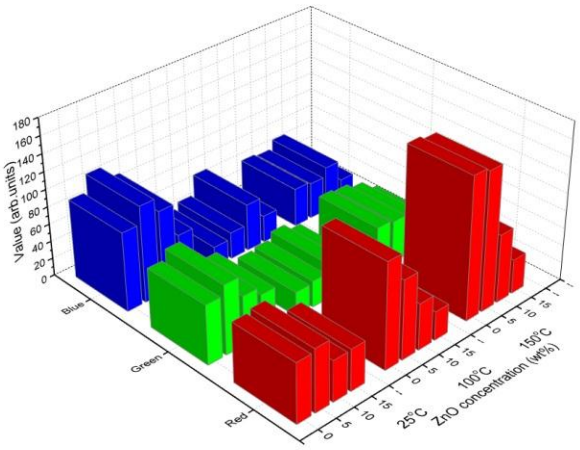

(b)

Figure 4.13 (a) Array of cropped photographic images of PCDA and PCDA/ZnO composites fabricated by inkjet printing on conventional paper at different temperatures; (b) Histogram of RGB values of the photographic images analyzed by software.

4.4 Conclusion

Raman, FTIR, and colorimetric measurements have been used to study the thermochromic reversibility of poly-PCDA/ZnO composites film fabricated by inkjet printing method. The ATR-FTIR results suggest that the surfactant SDS does not react with either poly-PCDA or poly-PCDA/ZnO, and SDS does not interfere with the chelate formation. Combined with temperature-dependent Raman spectra, the upshift temperature of the Raman-active υ(C≡C) and υ(C=C) vibration peaks increases with increasing ZnO content. From the Raman spectra of PCDA/ZnO samples, it can be seen that ZnO could enhance the formation of the blue poly-PCDA, meanwhile inhibiting the formation of red poly-PCDA. Colorimetric measurements demonstrate a distinguishable colorimetric discrepancy with the increase of ZnO concentration, and excellent color change reversibility for poly-PCDA/ZnO composites. Also, the success of inkjet printing poly-PCDA/ZnO composites film provides a fast and economic method to broad the application of PDAs on various substrates.

CHAPTER 5

EFFECT OF ALKYL CHAIN LENGTH ON CHEMICAL SENSING OF POLYDIACETYLENE AND POLYDIACETYLENE/ZINC OXIDE NANOCOMPOSITES

5.1 Introduction

As chromatic sensor materials, polydiacetylenes (PDAs) have drawn tremendous attention due to their unique blue to red colorimetric transition, which can be triggered by mechanical, temperature and chemical stimuli[1-6,130,131]. Also, the solid state topotactic photo-polymerization of diacetylene monomers by exposure to UV or γ-radiation makes the synthesis of the PDAs more convenient and widespread for use in applications [110,132]. Thermochromism in closely packed and uniformly ordered thin films of various PDAs are well known[97] and have been widely studied for temperature-sensing applications[71,133-136]. Recent studies on enhancing the electrical conductivity of PDAs have broadened electrochromic applicationsof PDAs[13,62,94]. However, little attention has been paid to a systematic study of the use of PDAs in chemical sensing. Most studies have been conducted on polymers obtained from PDA monomers with one carboxylic group on the side chain, such as in 10, 12-pentacosadiynoic acid (PCDA) and 10, 12-tricosadiynoic acid (TCDA)[71,130,133-135], however, PDA monomers with two carboxylic groups, such as 10,12-docosadiynedioic acid (DCDA), have not been investigated for chemical sensing.

Previous research on poly-PCDA/ZnO and poly-TCDA/ZnO nanocomposites provided a broad understanding of the changes in chromatic properties of the nanocomposites relative to those of the pure polymer[113,126]. In this chapter, further investigations have been carried out to study the phase transition of PDAs and PDA/ZnO

nanocomposites when exposed to different organics in the liquid phase. Raman spectroscopy was used to characterize the PDAs and PDAs/ZnO nanocomposites, together with ATR-FTIR studies at ambient temperature and density functional theory simulations to obtain a molecular level understanding of the colorimetric changes. In addition, colorimetric measurements were performed using photographic processing software to quantify the chromatic changes.

5.2 Experimental Section

5.2.1 Materials

TCDA, PCDA and DCDA were purchased from GFS Chemicals and nanocrystalline ZnO (<100 nm diameter) was purchased from Sigma-Aldrich. Analytical grade chloroform was purchased from Sigma-Aldrich and used without further purification.

5.2.2 Synthesis of PDA/ZnO Nanocomposites

PDA/ZnO suspensions were prepared by suspending 0.045 mMol equivalent of ZnO in 10 mM solution of the PDA monomer in chloroform. The suspension contained in a beaker was sonicated in a water bath at room temperature for 30 min and dried at 40 °C with magnetic stirring for 8 hours. The magnetic stirring was stopped after the liposome state was achieved. The pure PDA monomer and PDA monomer/ZnO composites were polymerized to the blue phase of PDA and PDA/ZnO composite by irradiating with a 254 nm wavelength UV source. Powders of the blue phase composite were obtained by scraping from the beaker and grinding into a fine powder. Red phase composite powders were similarly produced and suspended in different organic liquids.

5.2.3 Material Characterizations

Raman spectra were obtained using a Mesophotonics Raman spectrometer with 785 nm laser excitation. The spectrometer was calibrated using a silicon wafer and diamond powder standards to a frequency accuracy of 1 cm^{-1}. Thick films for the Raman measurements were prepared by mixing suspensions of PDA monomer with ZnO, using chloroform as the suspension medium. After drying and 254 nm uv-irradiation, Raman spectra from the dry powders of PDA and PDA/ZnO were measured on a silicon wafer. The effect of organic liquids on the PDAs were carried out by suspending the same molar amounts of PDA or PDA/ZnO in 4ml of the organic liquid, and measuring the Raman spectra after 5 minutes of bath sonication of the suspension.

Attentuated Total Reflection (ATR)-Fourier Transform Infrared (FTIR) was carried out using a Nicolet ThermoElectron FTIR 560 spectrometer with a MIRacle attenuated total reflectance (ATR) platform assembly and a Ge plate.

For precise colorimetric information, the photographic images of PDAs or PDA/ZnO composites in an organic liquid were quantitatively analyzed by photographic processing software to obtain the RGB values obtained from the combination of red, green and blue colors.

5.3 Results and Discussion

5.3.1 ATR-FTIR Spectroscopy

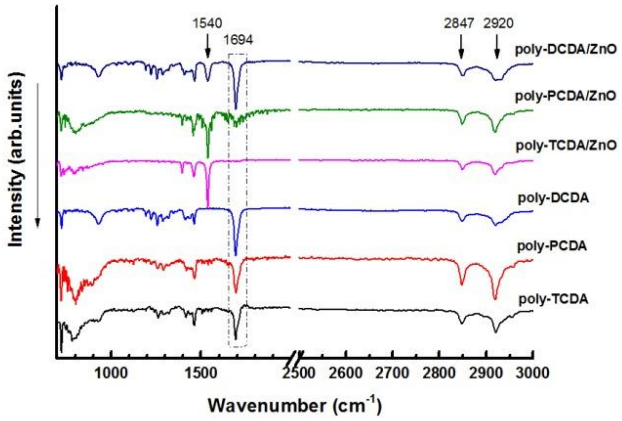

Figure 5.1 ATR-FTIR spectra at room temperature in the blue phase of poly-DCDA, poly-PCDA and poly-TCDA, and their corresponding ZnO composites.

Based on our previous studies[113,126], ATR-FTIR can provide information on chemical interactions between the PDA side chain in poly-PCDA/ZnO and poly-TCDA/ZnO. To confirm if poly-DCDA/ZnO shows similar behavior, FTIR spectroscopy was carried out on this nanocomposite and also, for comparison, on poly-PCDA/ZnO and poly-TCDA/ZnO. The effect of the side chain head group and ZnO interaction is reflected in the FTIR spectra shown in Figure 5.1 In the 700-3000 cm^{-1} spectral region, lines at 2920 and 2847cm^{-1} can be assigned to the asymmetric and symmetric stretching vibrations, respectively, of the CH_2 groups on the side chains, the lines at 1463 and 1417 cm^{-1} can be assigned to CH_2 scissoring modes, and the line at 1694 cm^{-1} can be attributed to the hydrogen-bonded carbonyl C=O stretching vibration. A relatively strong line appears at 1540 cm^{-1} in the spectra of PDA/ZnO composites together with a concomitant decrease in intensity of the C=O stretching line at 1694 cm^{-1}. This 1540

cm^{-1} line can be assigned to an asymmetric COO^- stretching vibration and its presence in the spectra together with the corresponding decrease in the intensity of the C=O stretching line can be attributed to the formation of a chelate between neighboring side chain -COOH head groups of the PDAs and Zn^{2+} ions from ZnO, in agreement with previous work[113,126]. However, comparing different PDA/ZnO composites under the same stoichiometric ratio of PDA to ZnO, even though chelate formation between PDA and ZnO are indicated in the ATR-FTIR spectra, the C=O line at 1694 cm^{-1} decreases in intensity to different degrees. For example, there is no evidence of the C=O line in the FTIR spectrum of poly-TCDA/ZnO. Also, the C=O line is very weak in poly-PCDA/ZnO, but remains relatively strong in poly-DCDA/ZnO (Figure 5.1). This suggests that chelation occurs only at one –COOH head group in poly-DCDA/ZnO, and at the one available –COOH head group present in both poly-TCDA and poly-PCDA.

5.3.2 Raman Spectroscopy

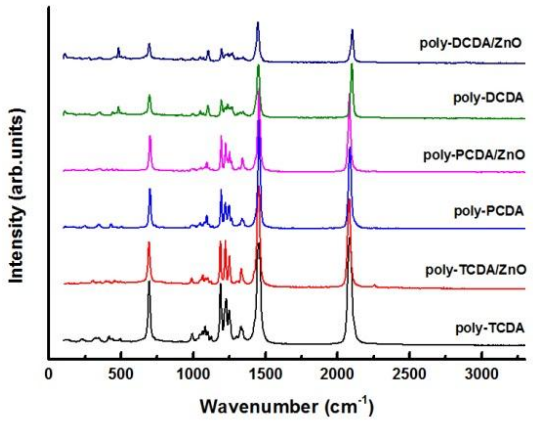

Figure 5.2 Raman spectra of poly-DCDA, poly-PCDA and poly-TCDA, and their corresponding ZnO nanocomposites in the blue phase at room temperature.

Raman scattering due to the molecular vibrational modes of the conjugated polymer backbone are expected to be primarily resonance-enhanced for excitation using 780 nm laser radiation. From the Raman spectra in Figure 5.2 for the pure PDAs in the blue phase, two intense lines near 2100 cm^{-1} and 1450 cm^{-1} are observed at room temperature in the blue phase, which can be definitively assigned to the C≡C and C=C stretching modes of the polymer backbone, respectively. However, there are small but measureable differences in the C≡C and C=C stretching mode frequencies for the different PDAs as summarized in Table 5.1. The C=C stretching mode frequencies for poly-TCDA and poly-PCDA are essentially the same within ±1 cm^{-1}, whereas the C≡C stretching mode frequencies shows a small 2 cm^{-1} upshift and the appearance of a shoulder at 2124 cm^{-1} in poly-PCDA that is most likely due to the presence of a red phase impurity in the sample.[113] The C≡C stretching mode frequency in poly-DCDA is, however, 16 and 18 cm^{-1} higher than that for poly-PCDA and poly-TCDA, respectively, indicating a higher strain on the polymer backbone in poly-DCDA associated with the presence of two –COOH head groups on its side chains. Chelate formation between PDA and ZnO in poly-TCDA/ZnO and poly-PCDA/ZnO results in a small frequency downshift for both the C≡C and C=C stretching modes relative to that of the pure polymer due to a small decrease in strain on the polymer backbone. By contrast, in poly-DCDA/ZnO there is a 4 cm^{-1} downshift in the C=C stretching mode frequency but a 2 cm^{-1} upshift in the C≡C stretching mode frequency, probably linked to the presence of two –COOH head groups in poly-DCDA (also see further discussion in section on density functional simulations).

In order to evaluate the use of the PDAs and PDA/ZnO nanocomposites as chromatic chemical sensors, Raman spectroscopy was carried out to study the effect of

organic liquids on the Raman spectra of the PDAs and PDA/ZnO nanocomposites. Methanol, ethanol, benzyl alcohol, octanol, diethyl ether, dimethylformamide (DMF), dichloromethane (DCM), tetrahydrofuran (THF) and acetone (analytical grade from Sigma-Aldrich) were selected as organic liquids to trigger a color change. The results are shown in Figures 5.3-5.5, and the observed C=C and C≡C stretching mode frequencies of the PDAs in the organics are listed in Table 5.1

Table 5.1 Polymer Backbone Raman Frequencies for Different PDAs and Corresponding PDA/ZnO Nanocomposites in the Blue Phase in the Presence of Organic Liquids

Organic liquid	Frequencies (cm^{-1})					
	C=C	C≡C	C=C	C≡C	C=C	C≡C
	poly-TCDA		poly-PCDA		poly-DCDA	
none	1456	2084	1457	2086/2124*	1452	2102
methanol	1458/1524	2084/2124	1457	2096/2124*	1446	2102
ethanol	1456/1524	2084/2124	1457/1522*	2090/2124*	1446	2102
benzyl alcohol	1456/1522	2082/2124	1457/1522	2086/2124*	1442	2098
octanol	1454/1518	2080/2120	1457/1522	2086/2122*	1444	2100
diethyl ether	1522/1456*	2126/2084*	1457/1522	2086/2124	1444	2100
DMF	1524	2124	1457*/1522	2086*/2126	1522/1444*	2120
DCM	1522	2126	1457/1520	2086/2126	1444	2100
THF	1522	2124	1524	2124	1520*/1446	2120*/2102
acetone	1524/1458	2126/2082	1457/1522	2090/2122*	1444	2102
	poly-TCDA/ZnO		poly-PCDA/ZnO		poly-DCDA/ZnO	
none	1454	2082	1456	2084	1448	2104
methanol	1458/1524*	2084/2118*	1456	2084	1446	2084/2104*
ethanol	1458/1524*	2086/2122*	1456/1522*	2084/2124*	1446	2080/2104*
benzyl alcohol	1458/1522*	2086/2124*	1456/1522*	2084	1444	2078
octanol	1454/1518*	2082/2118*	1456	2084	1446	2078
diethyl ether	1458/1522*	2086/2124*	1456/1522*	2084/2124*	1444	2100
DMF	1456/1520*	2082/2124*	1456/1522*	2084/2126*	1444	2076
DCM	1458/1522*	2086/2126*	1456/1520*	2086/2126*	1446	2080/2104*
THF	1456/1522*	2084/2118*	1456/1524*	2084/2124*	1446	2080
acetone	1456/1524*	2084/2124*	1456/1522*	2084/2122*	1444	2080/2104*

Symbol '*' represents a shoulder, DMF-dimethylformamide, DCM-dichloromethane, and THF-tetrahydrofuran

From Figure 5.3, it is evident that the C≡C and C=C stretching mode lines of poly-TCDA and poly-TCDA-ZnO are either split by the appearance of a line at higher frequency due to the partial conversion to the red phase or shift to higher frequencies due to complete conversion to the red phase, depending on the organic liquid added. Poly-TCDA showed a peak splitting in the C≡C and C=C stretching mode regions of the Raman spectrum due to partial formation of the red phase when alcohols and acetone are present,

while in DMF, DCM and THF, the C≡C and C=C Raman peaks increase in frequency to new values due to complete conversion of the blue to the red phase. In the presence of diethyl ether a small shoulder due to the blue phase remains at a lower frequency although conversion to the red phase is complete. For poly-TCDA/ZnO, only a high frequency shoulder is formed in the presence of all the selected organic liquids, indicating that conversion to the red phase is not complete. This is likely to be due to chelate formation between neighboring side chains in the nanocomposites which makes the blue phase more stable.

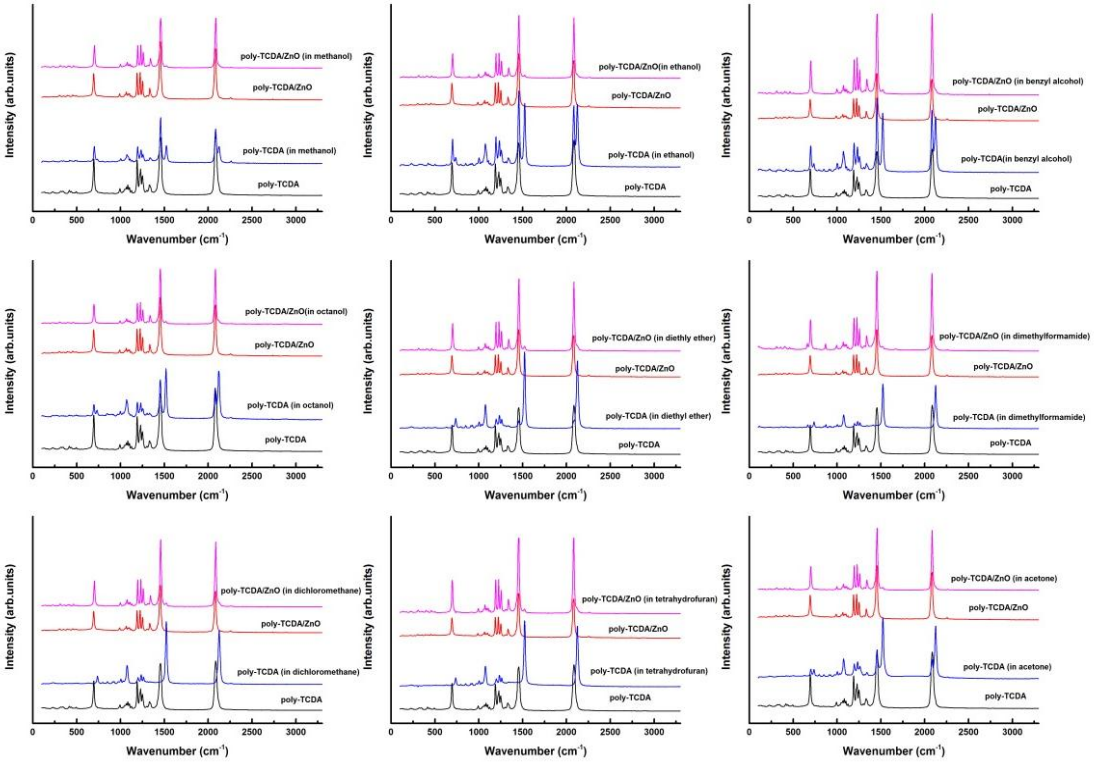

Figure 5.3 Raman spectra of poly-TCDA and poly TCDA/ZnO in the blue form and in different organic liquids.

The behavior of the Raman spectra of blue poly-PCDA and poly-PCDA/ZnO nanocomposite in different organic liquids is similar to that of poly-TCDA and its corresponding ZnO nanocomposite (Figure 5.4), except for the absence of red phase formation in methanol. For the other three alcohols, only weak red phase lines are observed.

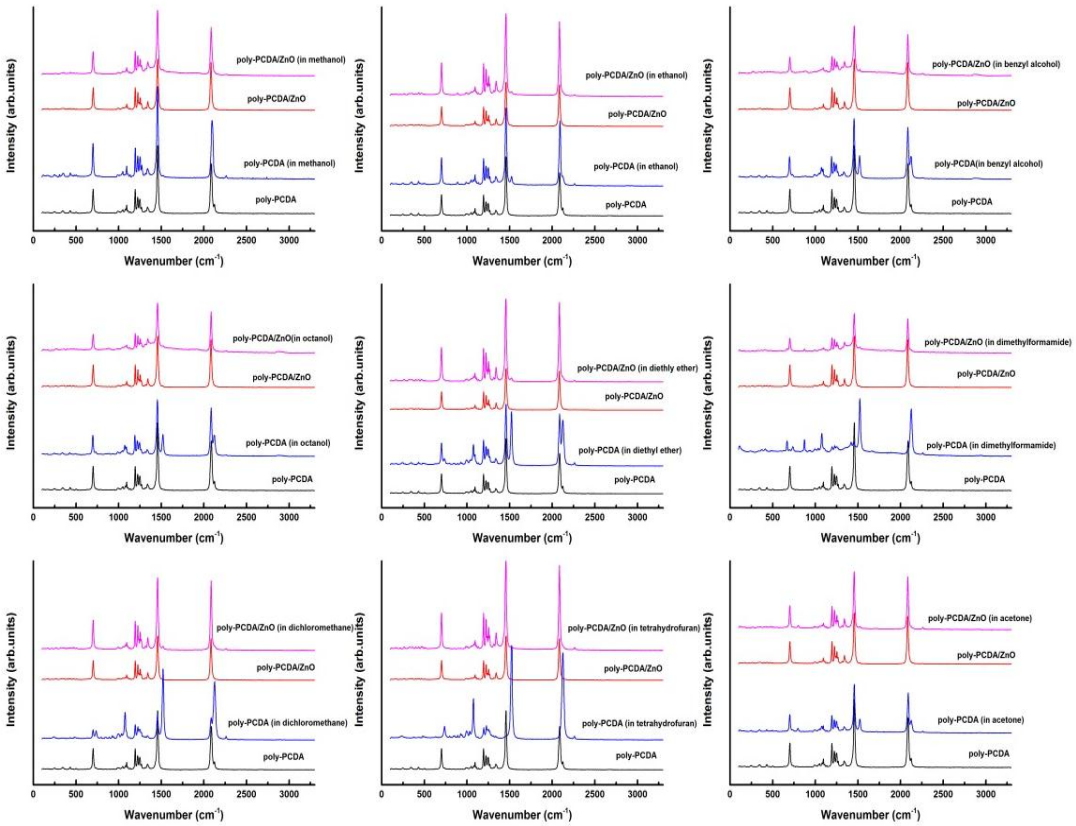

Figure 5.4 Raman spectra of poly-PCDA and poly PCDA/ZnO in the blue form and in different organic liquids.

The Raman spectra of poly-DCDA and poly-DCDA/ZnO in different organic liquids are shown in Figure 5.5. By contrast to the results of poly-TCDA and poly-PCDA, poly-DCDA shows a small downshift in the C=C stretching mode frequency in the presence of organic liquids possibly due to chemical interaction with the organics (except

in DMF and THF). For the C≡C stretching mode, the upshift due to red phase formation is only observed in DMF and THF, while in most other liquids, the C≡C stretching mode frequency either remains the same (as in methanol, ethanol and acetone) or downshifts slightly (as in benzyl alcohol, octanol, diethyl ether and DCM). Compared with poly-DCDA, the downshift of the C≡C peak frequencies for poly-DCDA/ZnO is much larger in the presence of the organic liquids (for example from 2104 cm^{-1} to about 2080 cm^{-1}), whereas the C=C peak frequency downshift is small (from 1448 cm^{-1} to about 1445 cm^{-1}).

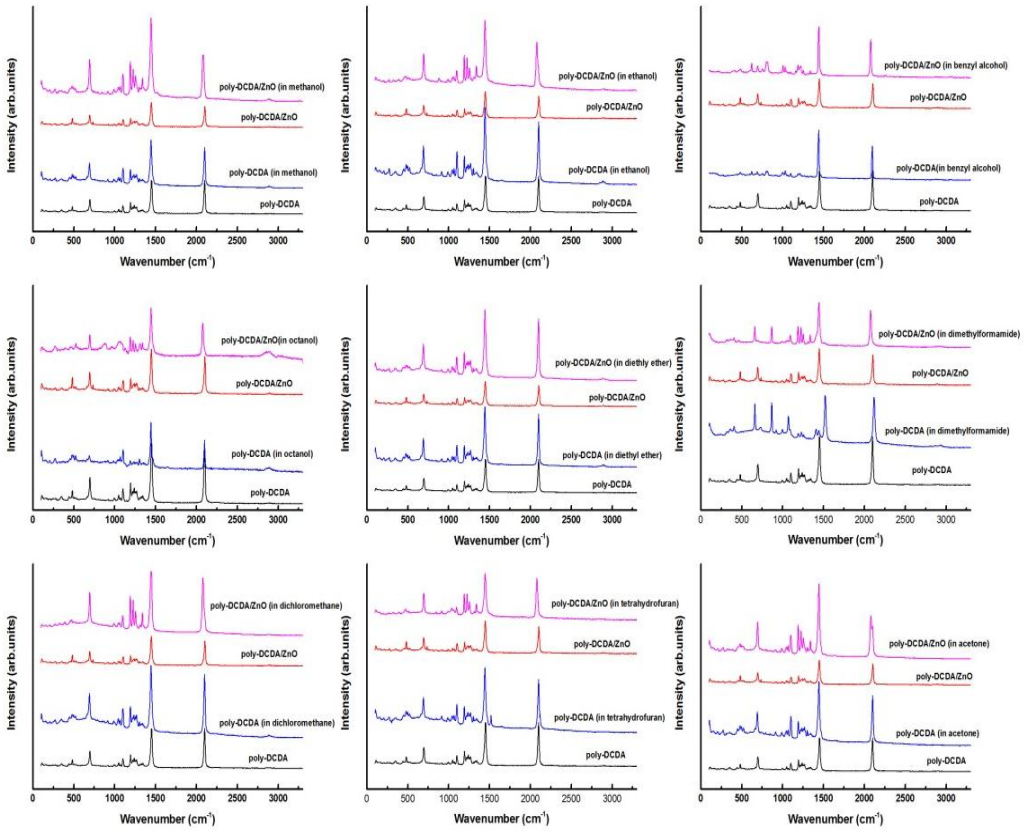

Figure 5.5 Raman spectra of poly-DCDA and poly DCDA/ZnO in the blue form and in different organic liquids.

From the Raman results, the kinetic mechanism of the chemochromism in PDA could be explained by the model suggested by Ajavakom et al[131]. An important feature worth noting is that the blue to red transition of PDAs induced by the organic liquids are all irreversible, but the organic liquid-induced transition for all three PDA/ZnO nanocomposites are reversible as shown by the Raman spectra (not shown here). This can be attributed to strong chelation interactions comparable to chemical bonding in the PDA/ZnO nanocomposites that provides greater stability to the blue relative to the red phase.

5.3.3 Density Functional Theory Simulations

Density functional theory (DFT) simulations were carried out to understand the interesting chemical sensing behaviors of the PDAs and PDA/ZnO composites in terms of their molecular structure properties. The simulations were carried out using Material Studio 4.3 (Accelrys Software Inc.) with B3LYP (DND basis set) function in DMol3 modules which is a counterpart of the 6-31G* basis set of Gaussian 3.0. On balancing between the accuracy and number of computations needed, a medium-accuracy level calculation was selected for the simulations.

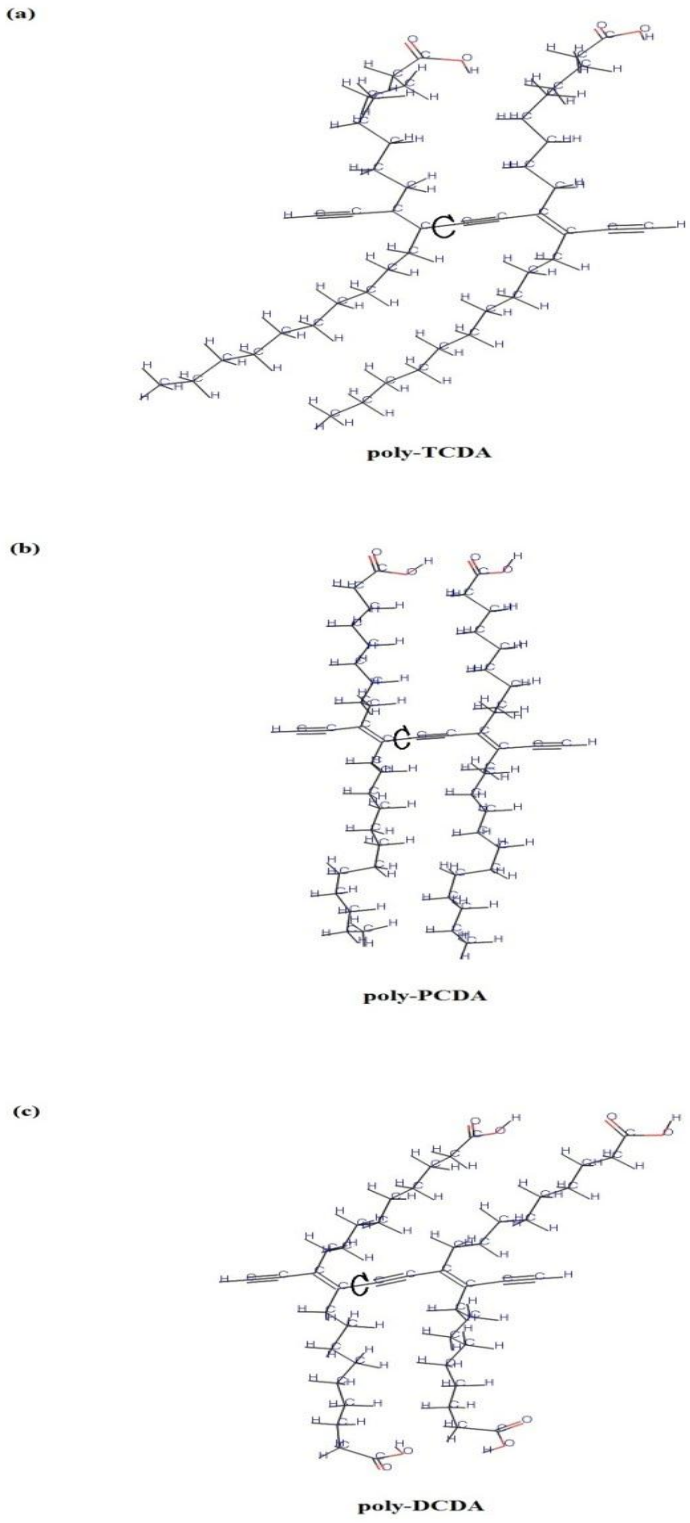

Figure 5.6 Structures of simulated PDA segments: a) Poly-TCDA, b) poly-PCDA, and c) poly-DCDA.

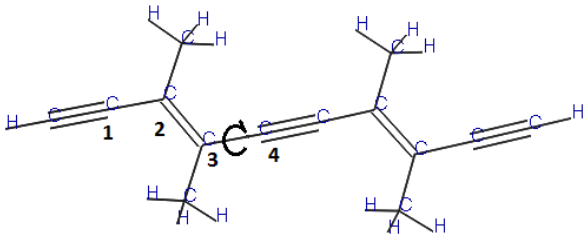

Figure 5.7 Structure of the PDA segment used for the C-C torsion angle study.

For construction of the molecular structure, consideration was given to the amount of computation needed and limitation of the Linux cluster available to carry out the simulations. Segments of the polymers shown in Figure 5.6, which are equivalent to molecules with a polymerization degree of 2, were used for this simulation. The main difference between the PDAs is the torsion angle of the single bond on the polymer backbone as indicated in Figure 5.7. This is probably due to the fact that the backbone carbon chain of the PDAs is in the zig-zag conformation with the possibility that torsion occurs on the carbon-carbon single bond. In order to clearly show the torsion angle of the carbon single bond for different PDAs, a *cis*-structured backbone is set as the 0 °reference point. Also, each PDA was constructed and simulated five times to make sure that the conformation of the side chains is in a random state. The results showed that the C-C bond torsion angles surprisingly fall within a certain small range from about 48^{o} to 50^{o} for TCDA, about 38^{o} to 40^{o} for PCDA and about 7 °to 8 °for DCDA as shown in Table 5.2.

Table 5.2 C-C Torsion Angle on the PDA Backbones

Trial Number	C-C Torsion Angle (°)		
	poly-TCDA	poly-PCDA	poly-DCDA
1	49.018	39.746	7.561
2	48.176	39.862	8.012
3	49.694	40.354	7.402
4	50.402	38.708	6.986
5	48.464	39.454	7.124

Due to the coincidence of C-C torsion angles in the simulations, it is obvious that the backbone structure of the PDAs is closely related to that of the side chain. In order to investigate the torsion on the backbone, the structure as shown in Figure 5.7 was adopted using a methyl group instead of the side chain. The basic idea was to determine how the torsion of the C-C bond affects the backbone structure; therefore, in this simulation the potential energy of this structure was considered as the criterion to evaluate the C-C bond torsion. The *trans*-structure was set as a reference potential energy point and the potential energy was calculated with the B3LYP/6-31G* function using C3-C4 torsions angles of 30 °, 60 °, 90 °, 120 °, 150 ° and 180 ° while other C-C torsion angles were restricted.

The results of the potential energy calculation are plotted in Figure 5.8, which shows that the maximum energy refers to a *cis*-structure which appears when θ=90°. This plot generally demonstrates how the C-C bond torsion angle affects the backbone system. It can also explain how PDAs with different side chains would exhibit different chromatic and spectroscopic changes discussed above (also see RGB section below). For example, the longer the C-C bond, the less stress is needed to induce a chromatic transition in the PDA, which is consistent with the fact that poly-TCDA is the most chromatically sensitive to the organic liquids evaluated.

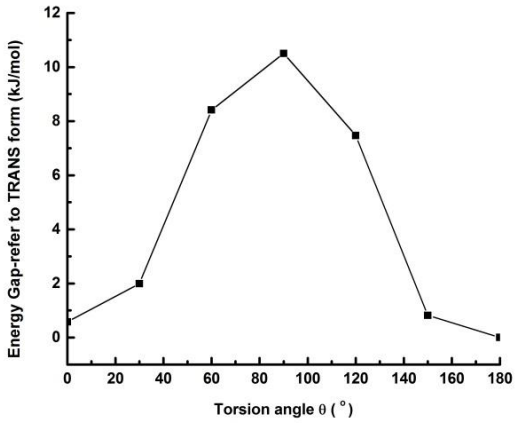

Figure 5.8 Potential energy curve as a function of torsion angle around the central C-C bond in *cis*-carbon with reoptimization of other geometrical parameters as discussed in the text.

5.3.4 RGB Measurements

To demonstrate the selective sensing capabilities of the PDAs, RGB measurements were conducted to quantitatively evaluate the color of the PDAs in the presence of selected organics. From Figure 5.9, it can be seen that poly-TCDA turned red on contacting an organic liquid corresponding to a higher red value than green and blue values. Similar phenomena were observed for poly-PCDA samples (except in methanol). However, poly-DCDA only shows a distinguishable red value when DMF and THF are present, indicating that the chemical recognition ability of PDAs is closely related to the chemical structure of the side chains on the PDA backbone.

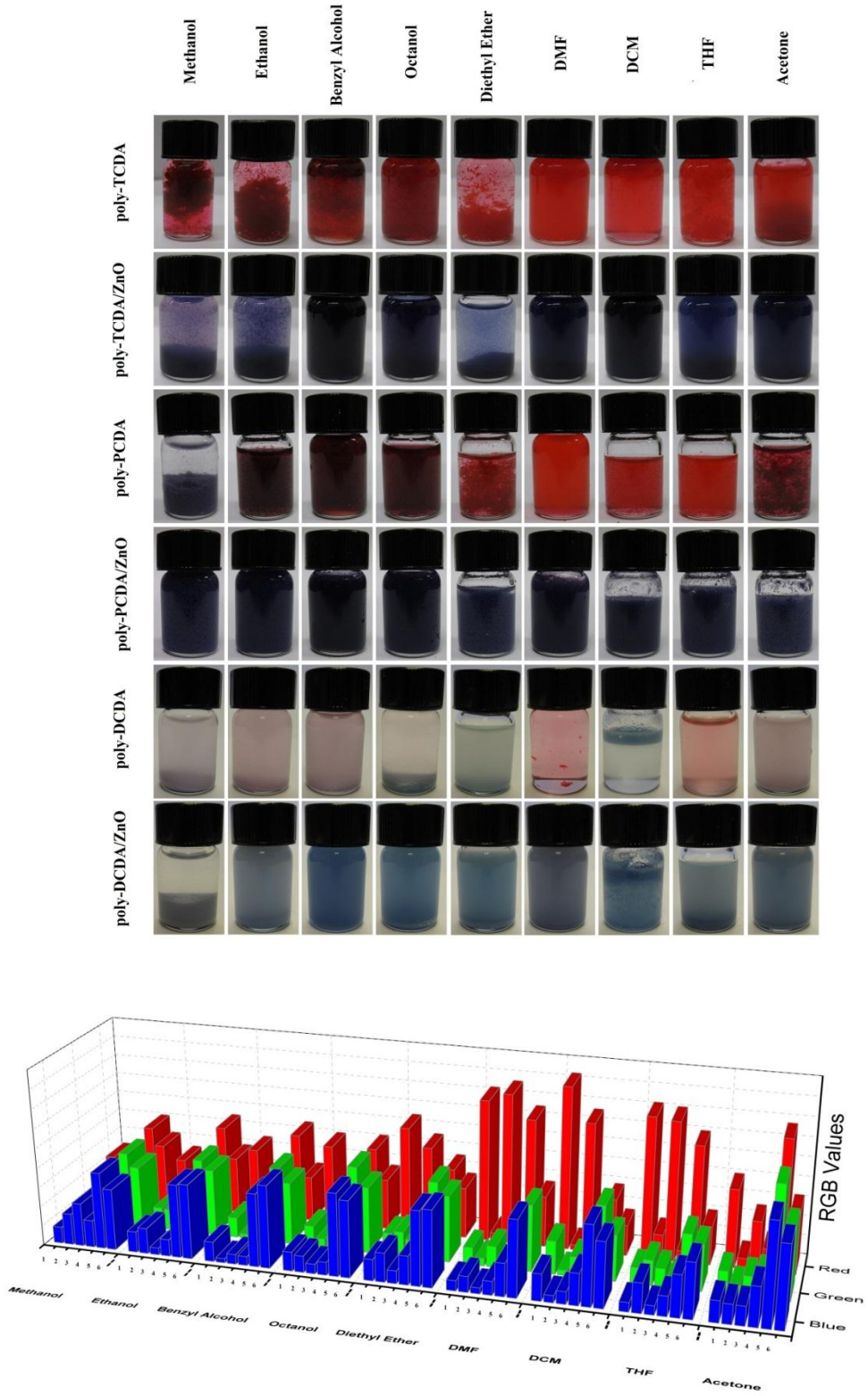

Figure 5.9 (Top panel) Array of cropped photographic images of PDAs and PDA/ZnO nanocomposites in selected organic liquids; and (Bottom panel) Histogram of RGB values of the photographic images analyzed by software.

It was also observed that all the PDA/ZnO nanocomposites show similar RGB values with different degrees of blue color in the presence of different organics. This indicates that the chelates formed in PDA/ZnO nanocomposites involve a strong chemical bond, and can therefore withstand chemical stress to maintain the blue phase (as shown by the Raman data) in the presence of the selected organic liquids.

5.4 Conclusions

PDAs based on the monomers 10,12-pentacosadiynoic acid (PCDA), 10,12-tricosadiynoic acid (TCDA) and 10,12-docosadiynedioic acid (DCDA), and their nanocomposites with ZnO were evaluated for potential use as chemical sensors for selected organics in liquid form. Chromatic sensitivity evaluated by Raman spectral data and quantitatively RGB analyses, were found to be associated with the interaction of the organics with the PDA side chain to give rise to the blue to red colorimetric transition. ATR-FTIR spectral data show that chelate formation occurs only on one of the two carboxylic head groups in poly-DCDA/ZnO. Due to strong chemical interactions between zinc and carboxylic ions during chelate formation that stabilize the blue phase, chromatic sensitivity to organic liquids is low for PDA/ZnO nanocomposites. Density functional theory (DFT) simulations indicate that the chromatic sensitivity of the PDAs to a particular organic depends on the C-C bond torsion angle of the PDA backbone. Future studies will focus on the limit of chromatic detection of organic species by the PDAs and their nanocomposites investigated here.

CHAPTER 6

DFT STUDY ON POLYDIACETYLENES AND THEIR DERIVATIVES

6.1 Introduction

Since polydiacetylene was first reported by Wegner in 1969 [36], researchers have focused on the potential sensing applications of this conjugated material by modification and functionalization. Although the π-π* transition of PDA backbone has been theoretically studied, with more and more successful synthesis of PDA derivatives, side chain (length and headgroup) effect are primarily subjected to experimental study and the theoretical studies on PDAs is quite scarce. Only the monomer and the cyclic trimer models of DAs were investigated by the valence effective Hamiltonian method [137].

In the present work, extensively theoretical calculations on the PDAs are performed. The geometries, vibrational frequencies, and electronic spectra of PDAs have been determined by density functional theory (DFT) and time-dependent-density functional theory (TD-DFT) calculations. The size dependence of excitation energy in PDA and the effect of the side chain properties on the conformation of backbone have been explored.

6.2 Computational Details

The equilibrium geometries and vibrational frequencies of PDAs and their derivatives in their ground states were calculated by the B3LYP functional with the 6-31G* basis set [138,139]. In previous studies[140-142], the B3LYP functional has been shown to be appropriate for the medium-sized heteroatom-containing carbon clusters. The vertical excitation energies of the π-π^* transition in the carbon chain were determined by TD-B3LYP [143-145].

For the extended-chain structure of PDA, the periodic boundary condition (PBC) calculation was conducted to determine its geometry and electronic property at the B3LYP/6-31G* level, where the repeat unit used in the PBC calculation is composed of four carbon atoms. All calculations in the present study were carried out with the Gaussian 03 and Material Studio 6.0 program package [146].

6.3 Results and Discussion

6.3.1 Structures and Stabilities of PDAs

The optimized bond lengths of PDAs with different chain length at ground state are listed in in Table 6.1. It can be seen that the carbon bond distance change bears an obvious alternating single bond, double bond and triple bond feature. For *cis*- and *trans*-forms of PDAs, the optimized C≡C, C=C, and C–C bond length are in the range of 1.201–1.215 Å, 1.324–1.357 Å, and 1.390–1.414 Å, respectively. Due to the conjugation effect, the length of carbon single bond (around 1.400Å) is shorter than the length it usually is (1.540Å), whereas the length of carbon triple bond (around 1.210Å) is longer than its usual number (1.200Å). Based on the bond distance data, it is clear that diene-structure could not exist in a stable ground state of alternating single, double and triple carbon bond system. No severe change of carbon bond length is observed with the length of carbon chain increase. It is noticeable that the C≡C bond is almost unchanged, and the bond length distribution is almost independent on the chain size and the terminal structure regardless of C≡C or C=C. As found in previous calculations[137], present calculations show that the acetylenic structure is more stable than a butatrienic structure, and no backbone transformation from acetylenic to butatrienic structure took place in full geometry optimization. The optimized C=C–C bond angles of *cis*- and *trans*-form isomers are about 124 °. These optimized structures of

PDAs indicate that the conjugated chains have the character of localized single, double, and triple bonds and these geometrical features are independent on the chain size, differing from other linear conjugated carbon chains [147,148].

To further verify the optimized structures are stable, the vibration frequency was calculated under B3LYP/6-31G*, and the calculated harmonic vibration frequencies are positive for all modes, which means the optimized structures are stable.

Table 6.1 *Cis*- and *Trans*-forms and the Optimized Bond Length (Å) of PDAs (*n* from 4 to 24)

n		C2C	C1C	C3C	C1C	C2C	C1C	C3C	C1C	C2C	C1C	C3C	C1C	C2C	C1C	C3C	C1C	C2C	C1C	C3C	C1C	C2C	C1C	C3C
4	cis	1.328	1.414	1.201																				
	trans	1.324	1.413	1.203																				
6	cis	1.332	1.409	1.208	1.411	1.333																		
	trans	1.331	1.409	1.208	1.409	1.332																		
8	cis	1.333	1.406	1.21	1.402	1.348	1.405	1.203																
	trans	1.333	1.404	1.21	1.399	1.347	1.408	1.203																
10	cis	1.334	1.405	1.209	1.398	1.35	1.398	1.209	1.405	1.333														
	trans	1.334	1.404	1.211	1.396	1.351	1.396	1.21	1.403	1.334														
12	cis	1.332	1.406	1.211	1.399	1.351	1.396	1.212	1.398	1.35	1.403	1.203												
	trans	1.333	1.405	1.211	1.396	1.355	1.398	1.212	1.399	1.352	1.404	1.202												
14	cis	1.334	1.406	1.211	1.399	1.351	1.395	1.213	1.397	1.352	1.395	1.21	1.405	1.335										
	trans	1.334	1.405	1.211	1.396	1.355	1.398	1.214	1.396	1.352	1.395	1.209	1.403	1.334										
16	cis	1.333	1.406	1.211	1.397	1.351	1.393	1.213	1.396	1.354	1.393	1.212	1.396	1.35	1.404	1.202								
	trans	1.332	1.406	1.211	1.396	1.354	1.394	1.213	1.395	1.353	1.395	1.212	1.395	1.348	1.404	1.202								
18	cis	1.334	1.403	1.209	1.395	1.353	1.393	1.212	1.394	1.355	1.394	1.213	1.394	1.353	1.397	1.21	1.404	1.334						
	trans	1.334	1.404	1.21	1.396	1.351	1.394	1.213	1.392	1.356	1.391	1.213	1.395	1.352	1.397	1.21	1.404	1.334						
20	cis	1.334	1.407	1.211	1.398	1.353	1.394	1.214	1.392	1.357	1.392	1.214	1.392	1.356	1.397	1.213	1.396	1.35	1.404	1.202				
	trans	1.333	1.406	1.211	1.396	1.354	1.395	1.214	1.392	1.355	1.392	1.213	1.392	1.355	1.393	1.213	1.396	1.349	1.407	1.203				
22	cis	1.336	1.404	1.21	1.393	1.355	1.393	1.214	1.392	1.354	1.394	1.214	1.394	1.354	1.392	1.213	1.393	1.355	1.394	1.211	1.404	1.336		
	trans	1.336	1.404	1.211	1.395	1.353	1.391	1.213	1.392	1.353	1.393	1.214	1.391	1.356	1.393	1.213	1.393	1.354	1.394	1.21	1.403	1.334		
24	cis	1.334	1.405	1.21	1.398	1.353	1.393	1.214	1.394	1.357	1.39	1.214	1.39	1.358	1.39	1.214	1.393	1.355	1.397	1.213	1.396	1.349	1.405	1.203
	trans	1.335	1.404	1.21	1.399	1.353	1.393	1.215	1.393	1.354	1.394	1.215	1.393	1.357	1.394	1.215	1.395	1.353	1.396	1.213	1.396	1.348	1.405	1.203

6.3.2 Electronic Transition Energy in PDA

The highest occupied molecular orbital (HOMO) and the lowest unoccupied molecular orbital (LUMO) of the repeated unit of four carbon atoms for the infinite PDA are depicted in Figure 6.1. HOMO is a bonding orbital, while LUMO is an anti-bonding orbital. The strongest adsorption for the infinite PDA is from the HOMO→LUMO transition. The HOMO–LUMO energy gaps (eV) for the *trans*-forms of PDAs as a function of the number of carbon atoms are depicted in Figure 6.2. As Figure 6.2 shows, the HOMO–LUMO energy gap decreases with the increase of the chain size, and the same behavior is also observed for *cis*-form isomers.

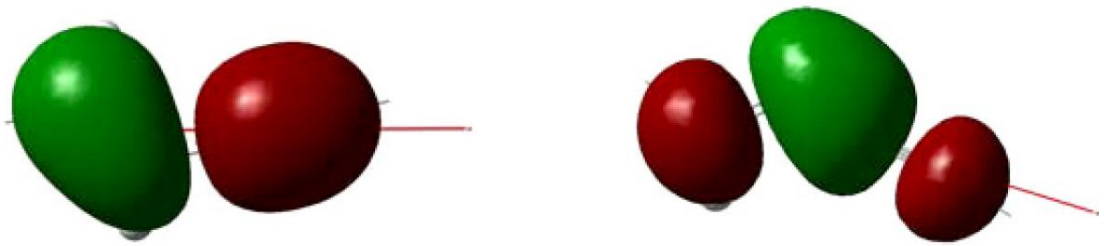

Figure 6.1 HOMO and LUMO orbitals of PDAs backbones.

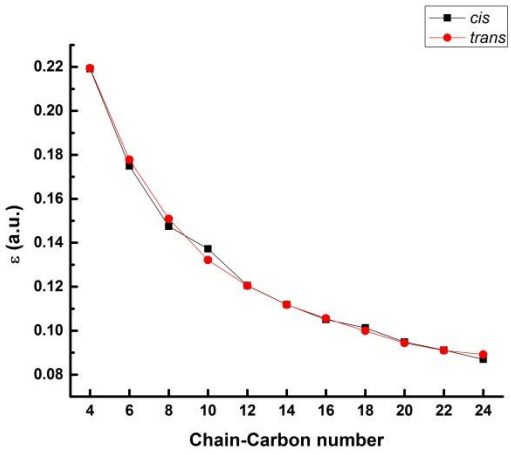

Figure 6.2 HOM-OLUMO energy gaps (eV) of the *cis*- and *trans*-form isomers vs the number of carbon atoms.

Based on the definition of Fermi level, one reasonable approximation is to define the middle of forbidden band as Fermi level[149], which could be expressed as $E_f = (E_H+E_L)/2$. The Fermi level vs chain length (N from 4 to 24) of polydiacetylenes (both *cis* and *trans*) is plotted in Figure 6.3. Based on the plotted figure, it is obvious that the Fermi levels exhibit a unique even-odd oscillation, in other words, the Fermi level of the chain of which carbon double bond number is equal to the number of carbon triple bond is lower than that of molecule of which carbon double bond number is more than the number of carbon triple bond. Meanwhile the Fermi level decreases with the increase of carbon chain length which could be due to the delocalization of the carbon chain.

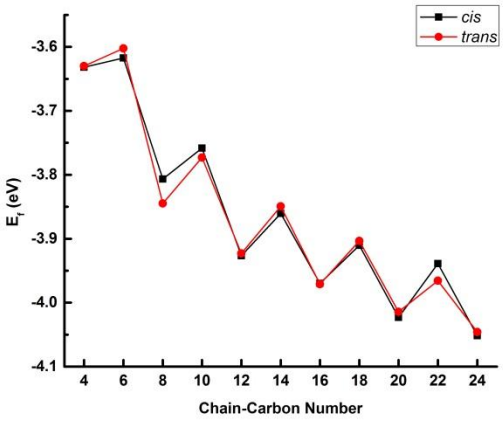

Figure 6.3 Fermi energy level of *cis*- and *trans*- carbon chain vs the number of carbon atoms.

Table 6.2 The Strongest Oscillator Strengths (*f*) and the Corresponding Vertical Transition Energies (λ) of *cis*- and *trans*-forms of PDAs

	cis			*trans*		
The number of C atoms	λ(nm)	*f*	ev	λ(nm)	*f*	ev
8	305	1.32257	4.1	305	1.25342	4.1
10	348	1.79294	3.6	347	1.64423	3.6
12	380	2.10411	3.3	380	1.95098	3.3
14	408	2.30056	3	411	2.13974	3
16	439	2.58981	2.8	439	2.6589	2.8
18	465	3.432	2.7	459	3.18355	2.7
20	488	3.57951	2.5	479	3.18298	2.6
22	502	3.61147	2.5	506	3.30491	2.5
24	527	3.83984	2.4	518	3.77881	2.4

Table 6.2 presents the vertical transition energies and oscillator strengths for the $\pi \rightarrow \pi^*$ transition in *cis*- and *trans*-form isomers by TD-B3LYP/6-31G*. As Table 6.2 shows, the transition energy for the strongest adsorption gradually decreases, while the intensity increases as the chain size (*n*) increases. Such properties of electronic excitation are consistent with HOMO–LUMO gaps shown in Figure 6.2. The PBC calculations indicate that the energy levels of HOMO and LUMO are −0.181 and −0.118 au,

respectively, and this suggests that the strongest HOMO→LUMO adsorption for the infinite PDA appears at 723 nm. By plotting the maximum absorption wavelength as a function of chain carbon length, the nonlinear relationship is shown in Figure 6.4. To further precisely illustrate the relationship, curves could be fitted according to the expression

$$\lambda = \frac{1240.6}{2+\sqrt{3n+6}-\sqrt{3n+3}}(A - B/C^n)^{150} \quad (6.1)$$

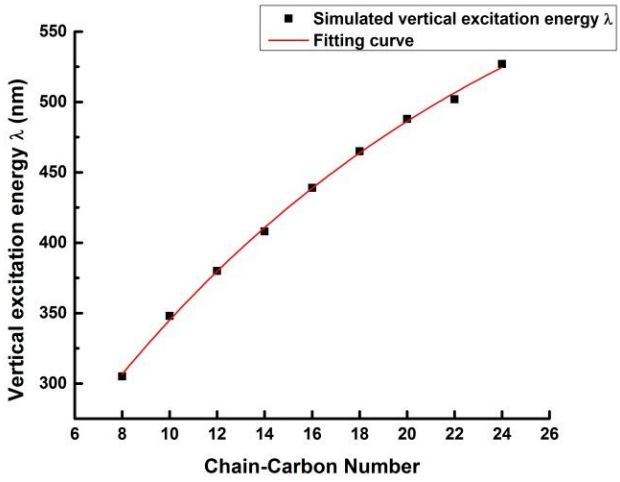

(a)

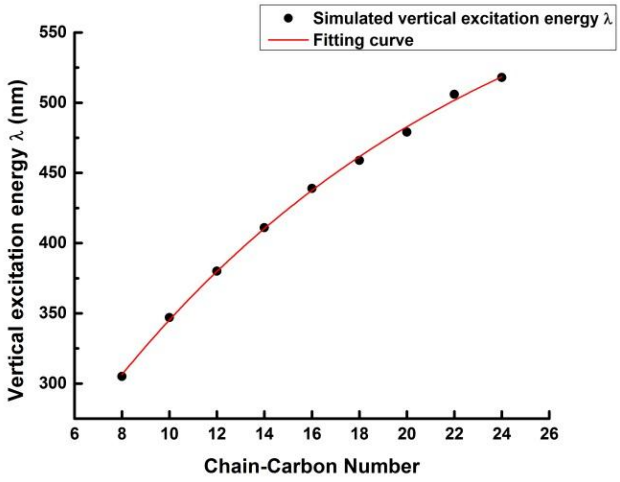

(b)

Figure 6.4 Vertical transition energy vs Chain carbon number of polydiacetylene: (a) *cis*-form carbon chain; (b) *trans*-form carbon chain.

On the basis Equation (1), the fitting results for both cis form polydiacetylene are A=1.160, B=0.937, C=1.058, while for the *trans* form polydiacetylene A=1.101, B=0.896, C=1.066. When n→∞, the λ equals to 720nm and 683 nm for *cis* and *trans* form polydiacetylene, respectively, which match the PBC-predicted value of 723nm for the infinite PDA very well.

In the PDAs system, we found that the TD-DFT calculation data is something different from the experimental data. Unfortunately, there is not any experimental value on small conjugate systems absorption available. However, this optical absorption characteristic is similar to that $HC_{2n}H$ system[151], which is also caused by the excitation of π electrons in the extended linear backbone. In the $HC_{2n}H$ system, it usually takes Eq. (2) to rectify the calculation data. By Equation (2), we obtained the theoretical value of 638 nm, which is in good agreement with experimental value 640 nm.

$$\lambda_1 = 0.8 \times (\lambda_0 + 70)^{151} \tag{6.2}$$

6.3.3 The Carbon Chain Conformation

The electronic structure properties of PDA are closely related to both the backbone and side chain, which are closely related to the conformation. In last charpter, for the reason that the primary feature of the backbone of PDA is the Zig-Zag conformation, the C-C torsion effect on backbone was investigated and discussed. More attention has been given to side chain aspect in the following discussion, because, for the derivatives of PDA, the side chain could result in the change of electronic structure of PDAs' backbones, which could attribute to variation of sensing abilities.

The basic structure used for the side chain effect refers to Figure 5.7. First, define the plane which chain carbons lie in as the XY plane, then use methyl group as R group for

the starting structure. The C3-C4 torsion was calculated under B3LYP/6-31G*. The first series of calculations is to investigate the effect of alkyl chain length on the conformation of PDA's backbone. The structure was changed accordingly by substituting the four R groups with different alkyl chains (number of carbon from 1 to 12). In order to increase the practical value of DFT simulation and further verify the assumption of C-C torsion effect on the sensing abilities, the second series of calculation is to investigate the C-C torsion by substituting two affinitive $–CH_3$ groups with –COOH groups. Figure 6.5 shows an example of the structure used for the two series calculations.

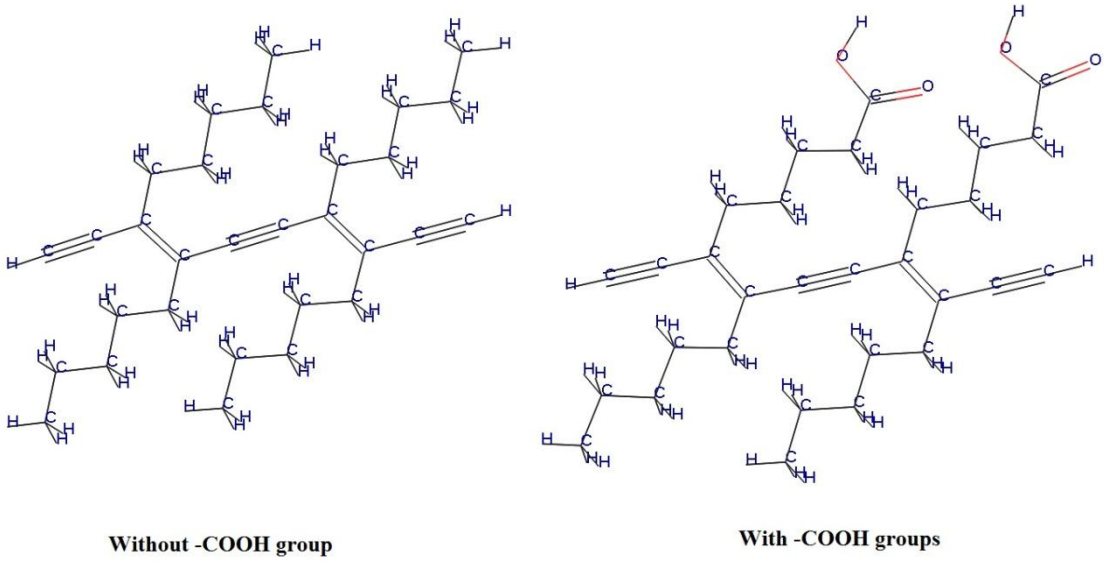

Figure 6.5 Snap shot of structures for the simulations in series1 and series 2 (side chain with five carbon atoms).

The C-C torsions as a function of side chain length of series 1 and series 2 are plotted in Figure 6.6. It is obvious that for side chain with only alkyl structure, the C3-C4 torsion increases with the side chain length, which could be due to the fact that the interactions between side chains becomes stronger with the increase of side chain length.

However, for the side chain with two headgroups substituted with carboxylic groups, the torsion angle increases at the beginning, after the side chain length reaches 8C, the torsion angle decreases. Also, compared with series 1, the torsion angles are much bigger than that of series 2, which is most likely caused by the interactions between the –COOH groups. Thus, in series 2, both the side chain length effect and interaction between carboxylic groups are acting on the overall C3-C4 torsion. Before side chain length reaching 8C, probably, the effect of interaction between the carboxylic groups is more dominant, in order to maintain the system at a stable state, the C-C torsion has to take place. This is why the changes of the C3-C4 torsion angle is more obvious that of series 1. However, when the side chain is longer than 8C, due to the flexibility and rearrangement of the side chain where the carboxylic groups locate in, the torsion caused by the headgroups interaction could be compensated by the side chain re-conformation. Thus, a decrease of torsion shows at the range of side chain length from 8C to 12C.

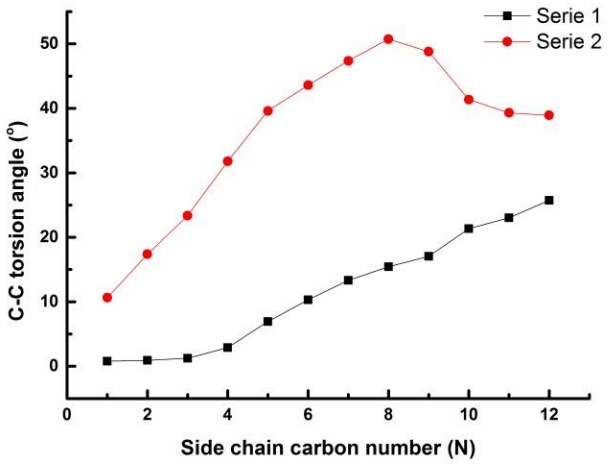

Figure 6.6 Torsion angle of C-C on the backbone of PDA vs side chain length.

6.4 Conclusions

A theoretical study of PDAs has been carried out by B3LYP and TD-B3LYP calculations with the DMol3/6-31G* basis sets. For the infinite PDA, PBC calculations were used to estimate the limits of structural and electronic transition energies. Calculations show that PDAs have remarkable character of localized single, double, and triple bonds and such structural features are independent of the chain size and the substitution of terminal atom. The alkyl side chain length and the carboxylic head group in PDAs can significantly modify their structural and electronic properties.

The explicit analytical expression for the electronic excitation energy and the PBC calculation predict that the strongest adsorption for the infinite chain of PDA appears at 723 nm, and the $\pi \rightarrow \pi^*$ excitation in the carbon backbone is responsible for this strong electronic transition. Present results provide a basis for further experimental and theoretical exploration of these conjugated carbon chains. Also, by using DFT simulation, the C-C torsion, an important factor reflecting the thermo- or chemo- sensing ability, could be visually predicted.

CHAPTER 7

SUMMARY

From the thermochromism and chemochromism study of PDAs and PDA/ZnO composites, it is clear that thermal and chemical triggers would result in the structural changes of PDA backbones. The primary changes are double bonds and triple bonds of PDA backbones, which could be observed via Raman spectroscopy. On the presence of ZnO nano particles, chelation between the carboxylic groups and the zinc ions could take place which could be observed via ATR-FTIR. The chelate could enhance the recovering ability of the structural changes caused by thermal and chemical triggers, in other words, it will lead to reversible color change.

The studies of fabrication PDA thin films by inkjet printing show that both chloroform and water based DA or DA/ZnO inks could be ink jetted. The water based inks win over the organic system inks due to the fact that they are environmentally friendly, have long shelf life and adjustable ZnO concentration features. By adjusting ZnO concentration, the PDA/ZnO can provide different chromatic properties. The main advantage of fabrication of PDA or PDA/ZnO films by the inkjet printing method is that PDA or PDA/ZnO films can be deposited on various substrates.

The DFT study of PDA structures further indicates the connection between the side chains and the PDA backbone structures. From the simulation results, it is obvious that the carbon single bond is more sensitive to the side chain structures. And the torsion angle could be an important index of the sensing ability of PDA or PDA derivatives.

REFERENCES

(1) Champaiboon, T.; Tumcharern, G.; Potisatityuenyong, A.; Wacharasindhu, S.; Sukwattanasinitt, M. A Polydiacetylene Multilayer Film for Naked Eye Detection of Aromatic Compounds. *Sens. Actuators, B* **2009**, *139*, 532-537.

(2) Lu, Y.; Yang, Y.; Sellinger, A.; Lu, M.; Huang, J.; Fan, H.; Haddad, R.; Lopez, G.; Burns, A. R.; Sasaki, D. Y.et al. Self-assembly of Mesoscopically Ordered Chromatic Polydiacetylene/silica Nanocomposites. *Nature* **2001**, *410*, 913-917.

(3) Rakow, N. A.; Suslick, K. S. A Colorimetric Sensor Array for Odour Visualization. *Nature* **2000**, *406*, 710-713.

(4) Janzen, M. C.; Ponder, J. B.; Bailey, D. P.; Ingison, C. K.; Suslick, K. S. Colorimetric Sensor Arrays for Volatile Organic Compounds. *Anal. Chem.* **2006**, *78*, 3591-3600.

(5) Muro, M. L.; Daws, C. A.; Castellano, F. N. Microarray Pattern Recognition Based on PtII Terpyridyl Chloride Complexes: Vapochromic and Vapoluminescent Response. *Chem. Commun.* **2008**, 6134-6136.

(6) Descalzo, A. B.; Dolores Marcos, M.; Monte, C.; Martinez-Manez, R.; Rurack, K. Mesoporous Silica Materials with Covalently Anchored Phenoxazinone Dyes as Fluorescent Hybrid Materials for Vapour Sensing. *J. Mater. Chem.* **2007**, *17*, 4716-4723.

(7) Yoon, J.; Chae, S. K.; Kim, J.-M. Colorimetric Sensors for Volatile Organic Compounds (VOCs) Based on Conjugated Polymer-Embedded Electrospun Fibers. *J. Am. Chem. Soc.* **2007**, *129*, 3038-3039.

(8) Jung, Y. K.; Kim, T. W.; Kim, J.; Kim, J.-M.; Park, H. G. Universal Colorimetric Detection of Nucleic Acids Based on Polydiacetylene (PDA) Liposomes. *Adv. Funct. Mater.* **2008**, *18*, 701-708.

(9) Ma, G.; Müller, A. M.; Bardeen, C. J.; Cheng, Q. Self-Assembly Combined with Photopolymerization for the Fabrication of Fluorescence "Turn-On" Vesicle Sensors with Reversible "On–Off" Switching Properties. *Adv. Mater.* **2006**, *18*, 55-60.

(10) Pires, A. C. d. S.; Soares, N. d. F. F.; da Silva, L. H. M.; da Silva, M. d. C. H.; De Almeida, M. V.; Le Hyaric, M.; Andrade, N. J. d.; Soares, R. F.; Mageste, A. B.; Reis, S. G. A Colorimetric Biosensor for the Detection of Foodborne Bacteria. *Sens. Actuators, B* **2011**, *153*, 17-23.

(11) Yokoyama, T.; Masuhara, A.; Onodera, T.; Kasai, H.; Oikawa, H. Development of Fabrication Process for Ag/Polydiacetylene (core/shell) Hybridized Nanocrystals. *Synth. Met.* **2009**, *159*, 897-899.

(12) Su, Y. Preparation of Polydiacetylene/Silica Nanocomposite for Use as a Chemosensor. *React. Funct. Polym.* **2006**, *66*, 967-973.

(13) Peng, H.; Sun, X.; Cai, F.; Chen, X.; Zhu, Y.; Liao, G.; Chen, D.; Li, Q.; Lu, Y.; Zhu, Y.et al. Electrochromatic Carbon Nanotube/Polydiacetylene Nanocomposite Fibres. *Nat Nano* **2009**, *4*, 738-741.

(14) Ahn, D. J.; Kim, J.-M. Fluorogenic Polydiacetylene Supramolecules: Immobilization, Micropatterning, and Application to Label-Free Chemosensors. *Acc. Chem. Res.* **2008**, *41*, 805-816.

(15) Yoon, B.; Lee, S.; Kim, J.-M. Recent Conceptual and Technological Advances in Polydiacetylene-Based Supramolecular Chemosensors. *Chem. Soc. Rev.* **2009**, *38*, 1958-1968.

(16) Sun, X.; Chen, T.; Huang, S.; Li, L.; Peng, H. Chromatic Polydiacetylene with Novel Sensitivity. *Chem. Soc. Rev.* **2010**, *39*, 4244-4257.

(17) Kolusheva, S.; Kafri, R.; Katz, M.; Jelinek, R. Rapid Colorimetric Detection of Antibody−Epitope Recognition at a Biomimetic Membrane Interface. *J. Am. Chem. Soc.* **2000**, *123*, 417-422.

(18) Kolusheva, S.; Shahal, T.; Jelinek, R. Cation-Selective Color Sensors Composed of Ionophore−Phospholipid−Polydiacetylene Mixed Vesicles. *J. Am. Chem. Soc.* **2000**, *122*, 776-780.

(19) Su, Y.; Li, J.; Jiang, L. Chromatic Immunoassay Based on Polydiacetylene Vesicles. *Colloids Surf., B* **2004**, *38*, 29-33.

(20) Potisatityuenyong, A.; Tumcharern, G.; Dubas, S. T.; Sukwattanasinitt, M. Layer-By-Layer Assembly of Intact Polydiacetylene Vesicles with Retained Chromic Properties. *J. Colloid Interface Sci.* **2006**, *304*, 45-51.

(21) Lee, K.; Povlich, L. K.; Kim, J. Recent Advances in Fluorescent and Colorimetric Conjugated Polymer-Based Biosensors. *Analyst* **2010**, *135*, 2179-2189.

(22) Reppy, M. A.; Pindzola, B. A. Biosensing with Polydiacetylene Materials: Structures, Optical Properties and Applications. *Chem. Commun.* **2007**, 4317-4338.

(23) Langer, R.; Tirrell, D. A. Designing Materials for Biology and Medicine. *Nature* **2004**, *428*, 487-492.

(24) Storhoff, J. J.; Mirkin, C. A. Programmed Materials Synthesis with DNA. *Chem. Rev.* **1999**, *99*, 1849-1862.

(25) Sanghvi, A. B.; Miller, K. P. H.; Belcher, A. M.; Schmidt, C. E. Biomaterials Functionalization Using a Novel Peptide That Selectively Binds to a Conducting Polymer. *Nat Mater* **2005**, *4*, 496-502.

(26) Wang, S.; Gaylord, B. S.; Bazan, G. C. Fluorescein Provides a Resonance Gate for FRET from Conjugated Polymers to DNA Intercalated Dyes. *J. Am. Chem. Soc.* **2004**, *126*, 5446-5451.

(27) Lee, K.; Rouillard, J.-M.; Pham, T.; Gulari, E.; Kim, J. Signal-Amplifying Conjugated Polymer–DNA Hybrid Chips. *Angew. Chem. Int. Ed.* **2007**, *46*, 4667-4670.

(28) Wang, S.; Gaylord, B. S.; Bazan, G. C. Collective Optical Behavior of Cationic Water-Soluble Dendrimers. *Adv. Mater.* **2004**, *16*, 2127-2132.

(29) Cassagneau, T.; Caruso, F. Inverse Opals for Optical Affinity Biosensing. *Adv. Mater.* **2002**, *14*, 1629-1633.

(30) Huang, J.; Virji, S.; Weiller, B. H.; Kaner, R. B. Polyaniline Nanofibers: Facile Synthesis and Chemical Sensors. *J. Am. Chem. Soc.* **2002**, *125*, 314-315.

(31) Korri-Youssoufi, H.; Yassar, A. Electrochemical Probing of DNA Based on Oligonucleotide-Functionalized Polypyrrole. *Biomacromolecules* **2001**, *2*, 58-64.

(32) Pinto, M. R.; Kristal, B. M.; Schanze, K. S. A Water-Soluble Poly(phenylene ethynylene) with Pendant Phosphonate Groups. Synthesis, Photophysics, and Layer-by-Layer Self-Assembled Films. *Langmuir* **2003**, *19*, 6523-6533.

(33) Wang, B.; Wasielewski, M. R. Design and Synthesis of Metal ion-recognition-induced Conjugated Polymers: An Approach to Metal Ion Sensory Materials. *J. Am. Chem. Soc.* **1997**, *119*, 12-21.

(34) Liu, Y.; Mills, R. C.; Boncella, J. M.; Schanze, K. S. Fluorescent Polyacetylene Thin Film Sensor for Nitroaromatics. *Langmuir* **2001**, *17*, 7452-7455.

(35) Okada, S. Y.; Jelinek, R.; Charych, D. Induced Color Change of Conjugated Polymeric Vesicles by Interfacial Catalysis of Phospholipase A2. *Angew. Chem. Int. Ed.* **1999**, *38*, 655-659.

(36) Wegner, G. Topochemical Reactions of Monomers with Conjugated Triple Bonds. I. Polymerization of 2.4-Hexadiyn-1.6-Diols Deivatives in Crystalline State. *Z. Naturforsch. B* **1969**, 24, 824.

(37) Wegner, G. Topochemical reactions of monomers with conjugated triple-bonds. IV. Polymerization of Bis-(p-toluene sulfonate) of 2.4-Hexadiin-1.6-Diol. *Macromol. Chem. Phys.* **1971**, *145*, 85-94.

(38) Tieke, B.; Graf, H. J.; Wegner, G.; Naegele, B.; Ringsdorf, H.; Banerjie, A.; Day, D.; Lando, J. B. Polymerization of Mono- and Multilayer Forming Diacetylenes. *Colloid. Polym. Sci.* **1977**, *255*, 521-531.

(39) Tieke, B.; Wegner, G.; Naegele, D.; Ringsdorf, H. Polymerization of Tricosa-10,12-diynoic Acid in Multilayers. *Angew. Chem. Int. Ed.* **1976**, *15*, 764-765.

(40) Patel, G. N.; Miller, G. G. Structure-Property Relationships of Diacetylenes and Their Polymers. *J. Macromol. Sci., B* **1981**, *20*, 111-131.

(41) Chance, R. R. Chromism in Polydiacetylene Solutions and Crystals. *Macromolecules* **1980**, *13*, 396-398.

(42) Baughman, R. H.; Chance, R. R. Comments on the Optical Properties of Fully Conjugated Polymers: Analogy between Polyenes and Polydiacetylenes. *J. Polym. Sci., Part B: Polym. Phys.* **1976**, *14*, 2037-2045.

(43) Olmsted, J.; Strand, M. Fluorescence of Polymerized Diacetylene Bilayer Films. *The J. Phys. Chem.* **1983**, *87*, 4790-4792.

(44) Bubeck, C.; Tieke, B.; Wegner, G. Selfsensitization of the Photopolymerization of Diacetylenes Studied in Multilayers. *Ber. Bunsen-Ges. Phys. Chem.* **1982**, *86*, 495-498.

(45) Ringsdorf, H.; Schlarb, B.; Venzmer, J. Molecular Architecture and Function of Polymeric Oriented Systems: Models for the Study of Organization, Surface Recognition, and Dynamics of Biomembranes. *Angew. Chem. Int. Ed.* **1988**, *27*, 113-158.

(46) Charych, D.; Nagy, J.; Spevak, W.; Bednarski, M. Direct Colorimetric Detection of a Receptor-ligand Interaction by a Polymerized Bilayer Assembly. *Science* **1993**, *261*, 585-588.

(47) Chen, Y. J.; Carter, G. M.; Tripathy, S. K. Study of Langmuir-Blodgett Polydiacetylene Polymer Films by Surface Enhanced Raman Scattering. *Solid State Commun.* **1985**, *54*, 19-22.

(48) Vincett, P. S.; Roberts, G. G. Electrical and Photoelectrical Transport Properties of Langmuir-Blodgett Films and a Discussion of Possible Device Applications. *Thin Solid Films* **1980**, *68*, 135-171.

(49) Carpick, R. W.; Sasaki, D. Y.; Marcus, M. S.; Eriksson, M.; Burns, A. R. Polydiacetylene Films: A Review of Recent Investigations into Chromogenic Transitions and Nanomechanical Properties. *J. Phys.: Condens. Matter* **2004**, *16*, R679.

(50) Spevak, W.; Nagy, J. O.; Charych, D. H. Molecular Assemblies of Functionalized Polydiacetylenes. *Adv. Mater.* **1995**, *7*, 85-89.

(51) Chance, R. R.; Patel, G. N.; Witt, J. D. Thermal Effects on the Optical Properties of Single Crystals and Solution-cast Films of Urethane Substituted Polydiacetylenes. *J. Chem. Phys.* **1979**, *71*, 206-211.

(52) Baughman, R. H.; Chance, R. R. Fully Conjugated Polymer Crystals: Solid-state Synthesis and Properties of the Polydiacetylenes*. *Ann. N.Y. Acad. Sci.* **1978**, *313*, 705-724.

(53) Filhol, J.-S.; Deschamps, J.; Dutremez, S. G.; Boury, B.; Barisien, T.; Legrand, L.; Schott, M. Polymorphs and Colors of Polydiacetylenes: A First Principles Study. *J. Am. Chem. Soc.* **2009**, *131*, 6976-6988.

(54) Peng, H.; Tang, J.; Yang, L.; Pang, J.; Ashbaugh, H. S.; Brinker, C. J.; Yang, Z.; Lu, Y. Responsive Periodic Mesoporous Polydiacetylene/Silica Nanocomposites. *J. Am. Chem. Soc.* **2006**, *128*, 5304-5305.

(55) Tong, L.; Cheng, B.; Liu, Z.; Wang, Y. Fabrication, Structural Characterization and Sensing Properties of Polydiacetylene Nanofibers Templated from Anodized Aluminum Oxide. *Sens. Actuators, B* **2011**, *155*, 584-591.

(56) Kolusheva, S.; Yossef, R.; Kugel, A.; Katz, M.; Volinsky, R.; Welt, M.; Hadad, U.; Drory, V.; Kliger, M.; Rubin, E.et al. Array-Based Disease Diagnostics Using Lipid/Polydiacetylene Vesicles Encapsulated in a Sol–Gel Matrix. *Anal. Chem.* **2012**, *84*, 5925-5931.

(57) Chae, S. K.; Park, H.; Yoon, J.; Lee, C. H.; Ahn, D. J.; Kim, J. M. Polydiacetylene Supramolecules in Electrospun Microfibers: Fabrication, Micropatterning, and Sensor Applications. *Adv. Mater.* **2007**, *19*, 521-524.

(58) Kim, J. M.; Lee, Y. B.; Chae, S. K.; Ahn, D. J. Patterned Color and Fluorescent Images with Polydiacetylene Supramolecules Embedded in Poly(vinyl alcohol) Films. *Adv. Funct. Mater.* **2006**, *16*, 2103-2109.

(59) Orynbayeva, Z.; Kolusheva, S.; Livneh, E.; Lichtenshtein, A.; Nathan, I.; Jelinek, R. Visualization of Membrane Processes in Living Cells by Surface-Attached Chromatic Polymer Patches. *Angew. Chem. Int. Ed.* **2005**, *44*, 1092-1096.

(60) Chance, R. R.; Baughman, R. H.; Müller, H.; Eckhardt, C. J. Thermochromism in a Polydiacetylene Crystal. *J.Chem. Phys.* **1977**, *67*, 3616-3618.

(61) Eckhardt, H.; Boudreaux, D. S.; Chance, R. R. Effects of Substituent-induced Strain on the Electronic Structure of Polydiacetylenes. *J. Chem. Phys.* **1986**, *85*, 4116-4119.

(62) Gatebe, E.; Herron, H.; Zakeri, R.; Ramiah Rajasekaran, P.; Aouadi, S.; Kohli, P. Synthesis and Characterization of Polydiacetylene Films and Nanotubes. *Langmuir* **2008**, *24*, 11947-11954.

(63) Jun, B.-H.; Baek, J.; Kang, H.; Park, Y. J.; Jeong, D. H.; Lee, Y.-S. Preparation of Polydiacetylene Immobilized Optically Encoded Beads. *J. Colloid Interface Sci.* **2011**, *355*, 29-34.

(64) Wang, C.; Ma, Z. Colorimetric Detection of Oligonucleotides Using a Polydiacetylene Vesicle Sensor. *Anal. Bioanal. Chem.* **2005**, *382*, 1708-1710.

(65) Ahn, D. J.; Chae, E.-H.; Lee, G. S.; Shim, H.-Y.; Chang, T.-E.; Ahn, K.-D.; Kim, J.-M. Colorimetric Reversibility of Polydiacetylene Supramolecules Having Enhanced Hydrogen-Bonding under Thermal and pH Stimuli. *J. Am. Chem. Soc.* **2003**, *125*, 8976-8977.

(66) Jonas, U.; Shah, K.; Norvez, S.; Charych, D. H. Reversible Color Switching and Unusual Solution Polymerization of Hydrazide-Modified Diacetylene Lipids. *J. Am. Chem. Soc.* **1999**, *121*, 4580-4588.

(67) Day, D.; Ringsdorf, H. Polymerization of Diacetylene Carbonic Acid Monolayers at the Gas-water Interface. *J. Polym. Sci.: Polym. Lett. Ed.* **1978**, *16*, 205-210.

(68) Diegelmann, S. R.; Hartman, N.; Markovic, N.; Tovar, J. D. Synthesis and Alignment of Discrete Polydiacetylene-Peptide Nanostructures. *J. Am. Chem. Soc.* **2012**, *134*, 2028-2031.

(69) Yuan, Z.; Hanks, T. W. A Reversible Colorimetric and Fluorescent Polydiacetylene Vesicle Sensor Platform. *Polymer* **2008**, *49*, 5023-5026.

(70) Lee, J.; Yarimaga, O.; Lee, C. H.; Choi, Y.-K.; Kim, J.-M. Network Polydiacetylene Films: Preparation, Patterning, and Sensor Applications. *Adv. Funct. Mater.* **2011**, *21*, 1032-1039.

(71) Traiphol, N.; Rungruangviriya, N.; Potai, R.; Traiphol, R. Stable Polydiacetylene/ZnO Nanocomposites with Two-steps Reversible and Irreversible Thermochromism: The Influence of Strong Surface Anchoring. *J. Colloid Interface Sci.* **2011**, *356*, 481-489.

(72) Wu, J.; Zawistowski, A.; Ehrmann, M.; Yi, T.; Schmuck, C. Peptide Functionalized Polydiacetylene Liposomes Act as a Fluorescent Turn-on Sensor for Bacterial Lipopolysaccharide. *J. Am. Chem. Soc.* **2011**, *133*, 9720-9723.

(73) Morrison, D. C.; Jacobs, D. M. Binding of Polymyxin B to the Lipid A Portion of Bacterial Lipopolysaccharides. *Immunochemistry* **1976**, *13*, 813-818.

(74) Xu, Y.; Smith, M. D.; Geer, M. F.; Pellechia, P. J.; Brown, J. C.; Wibowo, A. C.; Shimizu, L. S. Thermal Reaction of a Columnar Assembled Diacetylene Macrocycle. *J. Am. Chem. Soc.* **2010**, *132*, 5334-5335.

(75) Xu, R.; Schweizer, W. B.; Frauenrath, H. Soluble Poly(diacetylene)s Using the Perfluorophenyl−Phenyl Motif as a Supramolecular Synthon. *J. Am. Chem. Soc.* **2008**, *130*, 11437-11445.

(76) Enkelmann, V. In *Polydiacetylenes*. Springer Berlin Heidelberg: **1984**, 63, 91-136.

(77) Huo, Q.; Russell, K. C.; Leblanc, R. M. Chromatic Studies of a Polymerizable Diacetylene Hydrogen Bonding Self-Assembly: A "Self-Folding" Process To Explain the Chromatic Changes of Polydiacetylenes. *Langmuir* **1999**, *15*, 3972-3980.

(78) Chen, X.; Yoon, J. A Thermally Reversible Temperature Sensor Based on Polydiacetylene: Synthesis and Thermochromic Properties. *Dyes Pigm.* **2011**, *89*, 194-198.

(79) Yoon, J.; Jung, Y.-S.; Kim, J.-M. A Combinatorial Approach for Colorimetric Differentiation of Organic Solvents Based on Conjugated Polymer-Embedded Electrospun Fibers. *Adv. Funct. Mater.* **2009**, *19*, 209-214.

(80) Wu, S.; Shi, F.; Zhang, Q.; Bubeck, C. Stable Hydrogen-Bonding Complexes of Poly(4-vinylpyridine) and Polydiacetylenes for Photolithography and Sensing. *Macromolecules* **2009**, *42*, 4110-4117.

(81) Lee, S. B.; Koepsel, R. R.; Russell, A. J. Surface Dispersion and Hardening of Self-Assembled Diacetylene Nanotubes. *Nano Lett.* **2005**, *5*, 2202-2206.

(82) Dei, S.; Shimogaki, T.; Matsumoto, A. Thermochromism of Polydiacetylenes Containing Robust 2D Hydrogen Bond Network of Naphthylmethylammonium Carboxylates. *Macromolecules* **2008**, *41*, 6055-6065.

(83) Dei, S.; Matsumoto, A.; Matsumoto, A. Thermochromism of Polydiacetylenes in the Solid State and in Solution by the Self-Organization of Polymer Chains Containing No Polar Group. *Macromolecules* **2008**, *41*, 2467-2473.

(84) Gu, Y.; Cao, W.; Zhu, L.; Chen, D.; Jiang, M. Polymer Mortar Assisted Self-assembly of Nanocrystalline Polydiacetylene Bricks Showing Reversible Thermochromism. *Macromolecules* **2008**, *41*, 2299-2303.

(85) Thauvin, C.; Rickling, S.; Schultz, P.; Celia, H.; Meunier, S.; Mioskowski, C. Carbon Nanotubes as Templates for Polymerized Lipid Assemblies. *Nat Nano* **2008**, *3*, 743-748.

(86) Yang, K. S.; Yun, J. S.; Kim, J. C.; Min, J.; Park, T. J.; Ahn, J. K.; Kim, D. H. Polydiacetylene Single-Walled Carbon Nanotubes Nano-hybrid for Cellular Imaging Applications. *J. Nanosci. Nanotechnol.* **2012**, *12*, 377-385.

(87) Lefebvre, J.; Finnie, P. Photoluminescence and Förster Resonance Energy Transfer in Elemental Bundles of Single-Walled Carbon Nanotubes. *J. Phys. Chem. C* **2009**, *113*, 7536-7540.

(88) Chen, X.; Li, L.; Sun, X.; Liu, Y.; Luo, B.; Wang, C.; Bao, Y.; Xu, H.; Peng, H. Magnetochromatic Polydiacetylene by Incorporation of Fe3O4 Nanoparticles. *Angew. Chem. Int. Ed.* **2011**, *50*, 5486-5489.

(89) Chen, S.; Chen, G.; Yang, T. Plasma Passivation of Siloxane-Based Low-k Polymeric Films Comparison of Single and Mixed (O 2/N 2/H 2) Gas Sources. *J. Electrochem. Soc.* **2003**, *150*, F194-F199.

(90) Gravel, E.; Ogier, J.; Arnauld, T.; Mackiewicz, N.; Ducongé, F.; Doris, E. Drug Delivery and Imaging with Polydiacetylene Micelles. *Chem. –Eur. J.* **2012**, *18*, 400-408.

(91) van Osch, T. H. J.; Perelaer, J.; de Laat, A. W. M.; Schubert, U. S. Inkjet Printing of Narrow Conductive Tracks on Untreated Polymeric Substrates. *Adv. Mater.* **2008**, *20*, 343-345.

(92) Oh, Y.; Kim, J.; Yoon, Y. J.; Kim, H.; Yoon, H. G.; Lee, S.-N.; Kim, J. Inkjet Printing of Al2O3 Dots, Lines, and Films: From Uniform Dots to Uniform Films. *Curr. Appl. Phys.* **2011**, *11*, S359-S363.

(93) Lee, J. K.; Lee, U. J.; Kim, M.-K.; Lee, S. H.; Kang, K.-T. Direct Writing of Semiconducting Polythiophene and Fullerene Derivatives Composite from Bulk Heterojunction Solar Cell by Inkjet Printing. *Thin Solid Films* **2011**, *519*, 5649-5653.

(94) Yoon, B.; Ham, D.-Y.; Yarimaga, O.; An, H.; Lee, C. W.; Kim, J.-M. Inkjet Printing of Conjugated Polymer Precursors on Paper Substrates for Colorimetric Sensing and Flexible Electrothermochromic Display. *Adv. Mater.* **2011**, *23*, 5492-5497.

(95) Zschieschang, U.; Yamamoto, T.; Takimiya, K.; Kuwabara, H.; Ikeda, M.; Sekitani, T.; Someya, T.; Klauk, H. Organic Electronics on Banknotes. *Adv. Mater.* **2011**, *23*, 654-658.

(96) Champaiboon, T.; Tumcharern, G.; Potisatityuenyong, A.; Wacharasindhu, S.; Sukwattanasinitt, M. A Polydiacetylene Multilayer Film for Naked Eye Detection of Aromatic Compounds. *Sens. Actuators B: Chem* **2009**, *139*, 532-537.

(97) Robert, W. C.; Darryl, Y. S.; Matthew, S. M.; Eriksson, M. A.; Alan, R. B. Polydiacetylene Films: A Review of Recent Investigations into Chromogenic Transitions and Nanomechanical Properties. *J. Phys.: Condens. Matter* **2004**, *16*, R679-R697.

(98) Yuan, W.; Jiang, G.; Song, Y.; Jiang, L. Micropatterning of Polydiacetylene Based on a Photoinduced Chromatic Transition and Mechanism Study. *J. Appl. Polym. Sci.* **2007**, *103*, 942-946.

(99) Hammond, P. T.; Rubner, M. F. Thermochromism in Liquid Crystalline Polydiacetylenes. *Macromolecules* **1997**, *30*, 5773-5782.

(100) Huang, X.; Jiang, S.; Liu, M. Metal Ion Modulated Organization and Function of the Langmuir−Blodgett Films of Amphiphilic Diacetylene: Photopolymerization, Thermochromism, and Supramolecular Chirality. *J. Phys. Chem. B* **2004**, *109*, 114-119.

(101) Peng, H.; Tang, J.; Pang, J.; Chen, D.; Yang, L.; Ashbaugh, H. S.; Brinker, C. J.; Yang, Z.; Lu, Y. Polydiacetylene/Silica Nanocomposites with Tunable Mesostructure and Thermochromatism from Diacetylenic Assembling Molecules. *J. Am. Chem. Soc.* **2005**, *127*, 12782-12783.

(102) Ahn, D. J.; Chae, E. H.; Lee, G. S.; Shim, H. Y.; Chang, T. E.; Ahn, K. D.; Kim, J. M. Colorimetric Reversibility of Polydiacetylene Supramolecules Having Enhanced Hydrogen-Bonding under Thermal and pH Stimuli. *J. Am. Chem. Soc.* **2003**, *125*, 8976-8977.

(103) Kim, J.; Lee, J.; Choi, H.; Sohn, D.; Ahn, D. J. Rational Design and in-Situ FTIR Analyses of Colorimetrically Reversibe Polydiacetylene Supramolecules. *Macromolecules* **2005**, *38*, 9366-9376.

(104) Lee, S.; Kim, J. M. Alpha-Cyclodextrin: A Molecule for Testing Colorimetric Reversibility of Polydiacetylene Supramolecules. *Macromolecules* **2007**, *40*, 9201-9204.

(105) Park, H.; Lee, J. S.; Choi, H.; Ahn, D. J.; Kim, J. M. Rational Design of Supramolecular Conjugated Polymers Displaying Unusual Colorimetric Stability upon Thermal Stress. *Adv. Funct. Mater.* **2007**, *17*, 3447-3455.

(106) Yuan, Z.; Lee, C. W.; Lee, S. H. Reversible Thermochromism in Hydrogen-Bonded Polymers Containing Polydiacetylenes. *Angew. Chem.* **2004**, *116*, 4293-4296.

(107) Song, J.; Cisar, J. S.; Bertozzi, C. R. Functional Self-Assembling Bolaamphiphilic Polydiacetylenes as Colorimetric Sensor Scaffolds. *J. Am. Chem. Soc.* **2004**, *126*, 8459-8465.

(108) Li, L. S.; Stupp, S. I. Two-Dimensional Supramolecular Assemblies of a Polydiacetylene. 2. Morphology, Structure, and Chromic Transitions. *Macromolecules* **1997**, *30*, 5313-5320.

(109) Yang, Y.; Lu, Y.; Lu, M.; Huang, J.; Haddad, R.; Xomeritakis, G.; Liu, N.; Malanoski, A. P.; Sturmayr, D.; Fan, H.et al. Functional Nanocomposites Prepared by Self-assembly and Polymerization of Diacetylene Surfactants and Silicic Acid. *J. Am. Chem. Soc.* **2003**, *125*, 1269-1277.

(110) Baughman, R. H. Solid-State Polymerization of Diacetylenes. *J. Appl. Phys.* **1972**, *43*, 4362-4370.

(111) Lim, K. C.; Heeger, A. J. Spectroscopic and Light Scattering Studies of the Conformational (Rod-to-Coil) Transition of Poly(diacetylene) in Solution. *J. Chem. Phys.* **1985**, *82*, 522-530.

(112) Chance, R. R.; Baughman, R. H.; Muller, H.; Eckhardt, C. J. Thermochromism in A Polydiacetylene Crystal. *J. Chem. Phys.* **1977**, *67*, 3616-3618.

(113) Patlolla, A.; Zunino, J.; Frenkel, A. I.; Iqbal, Z. Thermochromism in Polydiacetylene-Metal Oxide Nanocomposites. *J. Mater. Chem.* **2012**, *22*, 7028-7035.

(114) Lim, C.; Sandman, D. J.; Sukwattanasinitt, M. Topological Polymerization of tert-Butylcalix[4]arenes Containing Diynes. *Macromolecules* **2007**, *41*, 675-681.

(115) Tobjörk, D.; Österbacka, R. Paper Electronics. *Adv. Mater.* **2011**, *23*, 1935-1961.

(116) Nyholm, L.; Nyström, G.; Mihranyan, A.; Strømme, M. Toward Flexible Polymer and Paper-Based Energy Storage Devices. *Adv. Mater.* **2011**, *23*, 3751-3769.

(117) Siegel, A. C.; Phillips, S. T.; Dickey, M. D.; Lu, N.; Suo, Z.; Whitesides, G. M. Printable Electronics: Foldable Printed Circuit Boards on Paper Substrates *Adv. Funct. Mater.* **2010**, *20*, 28-35.

(118) Russo, A.; Ahn, B. Y.; Adams, J. J.; Duoss, E. B.; Bernhard, J. T.; Lewis, J. A. Pen-on-paper Flexible Electronics. *Adv. Mater.* **2011**, *23*, 3426-3430.

(119) Barr, M. C.; Rowehl, J. A.; Lunt, R. R.; Xu, J.; Wang, A.; Boyce, C. M.; Im, S. G.; Bulović, V.; Gleason, K. K. Direct Monolithic Integration of Organic Photovoltaic Circuits on Unmodified Paper. *Adv. Mater.* **2011**, *23*, 3500-3505.

(120) Jang, J.; Ha, J.; Cho, J. Fabrication of Water-Dispersible Polyaniline-Poly(4-styrenesulfonate) Nanoparticles For Inkjet-Printed Chemical-Sensor Applications. *Adv. Mater.* **2007**, *19*, 1772-1775.

(121) Kang, J.-H.; Xu, Z.; Paek, S.-M.; Wang, F.; Hwang, S.-J.; Yoon, J.; Choy, J.-H. A Dual-Polymer Electrochromic Device with High Coloration Efficiency and Fast Response Time: Poly(3,4-(1,4-butylene-(2-ene)dioxy)thiophene)–polyaniline ECD. *Chem. –Asian J.* **2011**, *6*, 2123-2129.

(122) de Gans, B. J.; Duineveld, P. C.; Schubert, U. S. Inkjet Printing of Polymers: State of the Art and Future Developments. *Adv. Mater.* **2004**, *16*, 203-213.

(123) Robert, W. C.; Darryl, Y. S.; Matthew, S. M.; Eriksson, M. A.; Alan, R. B. Polydiacetylene Films: A Review of Recent Investigations into Chromogenic Transitions and Nanomechanical Properties. *J. Phys.: Condens. Matter* **2004**, *16*, R679.

(124) Lim, K. C.; Heeger, A. J. Spectroscopic and Light Scattering Studies of the Conformational (rod-to-coil) Transition of Poly(diacetylene) in Solution. *J. Chem. Phys.* **1985**, *82*, 522-530.

(125) Chance, R. R.; Baughman, R. H.; Muller, H.; Eckhardt, C. J. Thermochromism in a Polydiacetylene Crystal. *J. Chem. Phys.* **1977**, *67*, 3616-3618.

(126) Wu, A.; Beck, C.; Ying, Y.; Federici, J.; Iqbal, Z. Thermochromism in Polydiacetylene–ZnO Nanocomposites. *J. Phys. Chem. C* **2013**, *117*, 19593-19600.

(127) Chuang, J.; Hu, Y.; Ko, H. A Novel Secret Sharing Technique Using QR Code. *Int. J. Image Proc.* **2010**, *4*, 468-475.

(128) Okada, S.; Peng, S.; Spevak, W.; Charych, D. Color and Chromism of Polydiacetylene Vesicles. *Acc. Chem. Res.* **1998**, *31*, 229-239.

(129) Wenzel, M.; Atkinson, G. H. Chromatic Properties of Polydiacetylene Films. *J. Am. Chem. Soc.* **1989**, *111*, 6123-6127.

(130) Jiang, H.; Wang, Y.; Ye, Q.; Zou, G.; Su, W.; Zhang, Q. Polydiacetylene-based Colorimetric Sensor Microarray for Volatile Organic Compounds. *Sens. Actuators, B* **2010**, *143*, 789-794.

(131) Pumtang, S.; Siripornnoppakhun, W.; Sukwattanasinitt, M.; Ajavakom, A. Solvent Colorimetric Paper-based Polydiacetylene Sensors from Diacetylene Lipids. *J. Colloid Interface Sci.* **2011**, *364*, 366-372.

(132) Batchelder, D. N.; Evans, S. D.; Freeman, T. L.; Haeussling, L.; Ringsdorf, H.; Wolf, H. Self-Assembled Monolayers Containing Polydiacetylenes. *J. Am. Chem. Soc.* **1994**, *116*, 1050-1053.

(133) Chanakul, A.; Traiphol, N.; Traiphol, R. Controlling the Reversible Thermochromism of Polydiacetylene/ZnO Nanocomposites by Varying Alkyl Chain Length. *J. Colloid Interface Sci.* **2013**, *389*, 106-114.

(134) Charoenthai, N.; Pattanatornchai, T.; Wacharasindhu, S.; Sukwattanasinitt, M.; Traiphol, R. Roles of Head Group Architecture and Side Chain Length on Colorimetric Response of Polydiacetylene Vesicles to Temperature, Ethanol and pH. *J. Colloid Interface Sci.* **2011**, *360*, 565-573.

(135) Gou, M.; Guo, G.; Zhang, J.; Men, K.; Song, J.; Luo, F.; Zhao, X.; Qian, Z.; Wei, Y. Time–temperature Chromatic Sensor Based on Polydiacetylene (PDA) Vesicle and Amphiphilic Copolymer. *Sens. Actuators B* **2010**, *150*, 406-411.

(136) Ryu, S.; Yoo, I.; Song, S.; Yoon, B.; Kim, J.-M. A Thermoresponsive Fluorogenic Conjugated Polymer for a Temperature Sensor in Microfluidic Devices. *J. Am. Chem. Soc.* **2009**, *131*, 3800-3801.

(137) Orchard, B. J.; Tripathy, S. K. Molecular Structure and Electronic Property Modification of Poly(diacetylenes). *Macromolecules* **1986**, *19*, 1844-1850.

(138) Becke, A. D. Density Functional Calculations of Molecular Bond Energies. *The J. Chem. Phys.* **1986**, *84*, 4524-4529.

(139) Becke, A. D. Density-Functional Exchange-energy Approximation with Correct Asymptotic Behavior. *Phys. Rev. A* **1988**, *38*, 3098.

(140) Chuchev, K.; BelBruno, J. J. Density Functional Theory Study of the Isomers of CnB and CnB2. *J. Phys. Chem. A* **2004**, *108*, 5226-5233.

(141) Redondo, P.; Barrientos, C.; Cimas, A.; Largo, A. Structure and Stability of Small NaC n, NaC n+, and NaC n- Clusters: A Theoretical Study. *J. Phys. Chem. A* **2004**, *108*, 212-224.

(142) Pascoli, G.; Lavendy, H. Structures and energies of CnS ($1 \leq n \leq 20$) sulphur carbide clusters. *Int. J. Mass Spectrom.* **1998**, *181*, 11-25.

(143) Bauernschmitt, R.; Ahlrichs, R. Chem Phys Lett 256: 454 (b) Straman RE. *Scuseria GE, Frisch MJ (1998) J. Chem. Phys.* **1996**, *109*, 8218.

(144) Stratmann, R. E.; Scuseria, G. E.; Frisch, M. J. An Efficient Implementation of Time-Dependent Density-functional Theory for the Calculation of Excitation Energies of Large Molecules. *J. Chem. Phys.* **1998**, *109*, 8218-8224.

(145) Casida, M. E.; Jamorski, C.; Casida, K. C.; Salahub, D. R. Molecular Excitation Energies to High-lying Bound States From Time-Dependent Density-functional Response Theory: Characterization and Correction of the Time-dependent Local Density Approximation Ionization Threshold. *J. Chem. Phys.* **1998**, *108*, 4439-4449.

(146) Frisch, M.; Trucks, G.; Schlegel, H.; Scuseria, G.; Robb, M.; Cheeseman, J.; Montgomery Jr, J.; Vreven, T.; Kudin, K.; Burant, J. Gaussian 03, revision c. 02; Gaussian. *Inc., Wallingford, CT* **2004**, *4*.

(147) Zhang, C.; Xu, X.; Wu, H.; Zhang, Q. Geometry Optimization of Cn (n=2–30) with Genetic Algorithm. *Chem. Phys. Lett.* **2002**, *364*, 213-219.

(148) Burnin, A.; BelBruno, J. J. SCnS Linear Chain Production by Direct Laser Ablation. *J. Phys Chem A* **2003**, *107*, 9547-9553.

(149) Li, H.-H.; Li, Y.-D.; Wang, C.-K. First-principles Study of the Interaction Between Molecules and a Gold Surface. *Acta Phys. Sin.* **2002**, *51*, 1239-1243.

(150) Li, X.; Paldus, J. Size Dependence of the X1Ag→11Bu Excitation Energy in Linear Polyenes. *Int. J. Quantum Chem.* **1999**, *74*, 177-192.

(151) Pino, T.; Ding, H.; Güthe, F.; Maier, J. P. Electronic Spectra of the Chains HC2nH (n=8–13) in the Gas Phase. *J. Chem. Phys.* **2001**, *114*.